Processing and analysis of rotational motions around vertical and horizontal axes recorded by ring lasers in Christchurch, New Zealand

Susanne Lehndorfer

12th March 2008

Geophysics
Department of Earth and Environmental Sciences
Ludwig-Maximilians-University Munich

For Elli

Prof. Heiner Igel

Geophysics

Department of Earth and Environmental Sciences

Ludwigs-Maximilians-University Munich, Germany

Prof. Ulrich Schreiber

Geodesy

Forschungseinrichtung für Satellitengeodäsie

Technical University Munich, Germany

Dr. Robert Hurst

Physics

Department of Physics and Astronomy

University fo Canterbury, Christchurch, NZ

Abstract

Rotational ground motions have become a promising new observable in seismology. With the ring laser gyroscope, a reliable instrument sensitive enough to study even weak teleseismic signals of rotation was found. In this study the focus is laid on rotational as well as translational motions recorded by three ring lasers and a standard seismometer in an underground observatory of the Canterbury University in Christchurch, New Zealand in 2003 and 2004. In addition to observations of rotational motions around vertical axes, one of the instruments offers the possibility to record rotations around a horizontal axis of rotation. Latter motions are of special interest as they are equal to tilt at the Earth's surface. We have found good correlations of up to 99% between transverse acceleration and vertical rotation rate in phase for teleseismic events. For local events these values drop significantly, although a good match in time onset can be reported. The horizontal rotation rate data was compared with tilt rate derived from translations applying the Li-Method for Rayleigh waves. Good correlations of the two signals in phase but not in amplitude for a given phase velocity for distant earthquakes could be observed. These main results imply that the ring lasers deliver good quality data. Nevertheless, technical improvements are needed to increase the performance of the instruments.

Key words: rotational seismology, rotational motions, ring laser, horizontal axis, tilt.

Zusammenfassung

Rotationsbewegungen des Untergrundes stellen eine viel versprechende, neue Messgrösse im Bereich der Seismologie dar. Mit dem Ringlaser Gyroskop fand man ein zuverlässiges Instrument, empfindlich genug, um sogar schwache teleseismische Rotationssignale zu untersuchen. Die folgende Arbeit stützt sich auf Rotations- und Translationsdaten, die von drei Ringlasern und einem Standard Seismometer in einem Untergrundlabor der Canterbury University in Christchurch, Neuseeland in den Jahren 2003 und 2004 aufgenommen wurden. Eines dieser Instrumente macht es möglich, zusätzlich zu den Untersuchungen von Rotationsbewegungen um vertikale Achsen, auch Rotationen um eine horizontale Achse aufzuzeichnen. Letztere Grösse ist von besonderem Interesse, da diese Bewegung an der Erdoberfläche mit Tilt gleichzusetzen ist. Gute Übereinstimmungen von bis zu 99% zwischen transversaler Beschleunigung und Rotationsrate in Phase wurden für teleseismische Erdbeben beobachtet. Lokale Ereignisse hingegen zeigen eine deutliche Abnahme der Korrelations-Faktoren, obwohl eine gute zeitliche Übereinstimmung der Ersteinsätze zu erkennen ist. Die Li-Methode ermöglicht uns den Vergleich zwischen horizontaler Rotationsrate und Tiltrate, abgeleitet von Translationsbewegungen. Für teleseismische Ereignisse zeigen sich, bei einheitlicher Phasengeschwindigkeit, gute Übereinstimmungen zwischen den beiden Signalen in Phase, jedoch nicht in Amplitude. Diese Hauptergebnisse unterstreichen die hohe Qualität der Ringlaserdaten. Jedoch sind technische Verbesserungen unumgänglich, um die Leistung der Instrumente weiter zu erhöhen.

Motivation

Seismology opens a unique window into the Earth, its structure and physical processes. The seismic waves generated in and travelling through our planet allow scientist to gather information about places, where no direct observations are possible. The suitable instrument for measuring and recording these vibrations of the Earth is the seismometer.

In the late nineteenth century instruments were designed that recorded earthquake ground motion as a continuous function of time. This development resulted in seismograms as we know them today. But it was a long way from simple analogue recorders back then to present-day, complex instruments with Analogue to Digital Converters (ADCs), automatic data acquisition, near real time internet presentation, automated traveltime and magnitude calculation and many additional processing tools all focused on one jointly goal: filtering out the information about the physics of the Earth hidden in the seismograms.

Nowadays, seismometers and their acquisition systems are highly sophisticated instruments. There have been great innovations since the beginning of instrumental seismology, especially during the advent of computer technology in the 1960s. With all these improvements new and valuable information was gained.

However, to fully describe the complete motion of a point caused by an earthquake, three components of translation, six components of strain and another three components of rotation are needed (Aki and Richards, 2002). A seismometer is only capable of recording translations, while a strainmeter - whose technical evolution is comparable to the seismometer ones - provides the six components of strain. For years the missing three rotational components of motions were neglected in seismology. On the

one hand, because they were assumed to be too insignificant (Bouchon and Aki, 1982) and on the other hand, because there was no suitable instrument available to record these very small additional components.

By now, there are several instruments available measuring seismic induced rotational motions based on different physical or chemical processes. Some of the instruments suitable for seismic investigations are:

- A ring laser gyroscope is an active optical interferometer exploiting the Sagnac effect for measuring rotations (Schreiber, 2000; Stedman, 2001; Igel et al., 2005).

- A parallel seismograph is based on two antiparallel pendulum seismometers (TAPS) situated at a common vertical axis (Teisseyre et al., 2003; Solarz et al., 2004).

- A FOG (Fibre-Optic Gyro) is a passive rotation sensor, whose measurements are also based on the Sagnac effect (Jaroszewicz et al., 2006).

- The array technique - not an instrument in itself, but one of the most common methods - offers to derive rotational motions from data recorded by an array of seismometers (Spudich et al., 1995; Huang, 2003; Suryanto et al., 2006).

- A solid state sensor provides six-degree-of-freedom measurements based on the Coriolis forces (Nigbor, 1994; Takeo, 1998).

Ring lasers provide high resolution for angular velocities in a wide band of frequencies and epicentral distances. Compared to other rotational sensors, they offer optimal sensitivity, long time stability, wide dynamic range and allow point measurements. But the utilisation of ring lasers in geosciences is still at the beginning. In 1995 Stedman et al. (1995) started to use ring lasers for fundamental geoscientific measurements. Since then there have been major improvements not only in instrument technology, but also towards broader acceptance of this method for seismological use. The evolution history of the seismometer stretches over more than a hundred years. Hence, the question rises: what can we expect from the ring laser if its applicability for seismology progresses with a similar pace?

Fundamental research has been carried out by Igel et al. (2005), Schreiber et al. (2006), Cochard et al. (2006) and Suryanto et al. (2006), the latter conducted the first direct

comparison between ring laser observations and rotations derived from array measurements. All these investigations show the increasing importance of ring laser seismology and offer further investigations to break new ground. The aim of this thesis is to continue the research in this new field of seismology with rotational data from the Christchurch observatory by giving answers to the following questions:

- How do the observations vary with epicentral distance and magnitude?

- What do collocated ring lasers tell us about the quality of the recorded data?

- Are the recorded translations and rotations comparable in phase and amplitude as previous studies indicate?

- Can we derive phase velocities from our observations?

- To what extent are the horizontal rotations comparable to tilt derived from translations?

Thesis context and overview

The research carried out in this study concerns ring laser seismology in Christchurch, New Zealand, based on Igel et al. (2007) and their investigations of the ring laser 'G' in Wettzell, Germany.

The thesis is divided into two main parts with two chapters each. Part I represents a general introduction to the theory of rotational motions and operation of ring lasers in the Christchurch observatory, while in Part II the focus is laid on the recorded data and the corresponding analysis. It can be outlined as follows:

Chapter 1 (*Introduction*) represents an overview about theoretical basics of rotational seismology and ring laser technology in general.

Chapter 2 (*Instrumentation*) gives a brief general introduction to the history behind ring lasers in Christchurch and to the instruments that provide the data for this study.

Chapter 3 (*Data set*) focusses on the data acquisition processes and the description of the final data format.

Chapter 4 (*Data analysis*) offers the results of our investigations based on the theory discussed in detail in Chapter 1. Special attention is paid to the rotational data from the worlds only ring laser with a horizontal axis of rotation.

Chapter 5 (*Conclusion*) rounds of the thesis with a comprehensive resume of the four preceding chapters and an outlook on future projects.

Additionally, each chapter ends with a summary highlighting the main statements for

an easy access to the subsequent chapters. To provide further assistance, a list of abbreviations and symbols is attached right before the Appendix, followed by a list of figures and a list of tables. In the seven chapters of the Appendix one can find ring laser instrument specifications (Appendix A) and further information about all relevant earthquakes of 2003 and 2004 (Appendix B) in tabular form plus all discussed plots (Appendix C to Appendix F). On the supplementary CD a digital version of this thesis plus all codes used for generating the figures can be found.

Contents

Part I.

Chapter 1.

Introduction to ring laser seismology

Rotational motions recorded on the Earth's surface have many different origins. Rotation rates induced by earthquake waves vary from 10^{-13} to 10^{-2} rad/s (Flaws, 2003) and are of main interest for seismology. Latter motions can be recorded by rotation sensors with a sufficiently high sensitivity, like a ring laser gyroscope. Worldwide there are four ring laser observatories with altogether six ring lasers used for geoscientific research (in chronological order):

- Cashmere Cavern in Christchurch, New Zealand,

- Hendrix College in Arkansas, USA,

- Fundamentalstation Wettzell in Germany and

- Piñon Flat Observatory in California , USA.

While other rotation sensors are only capable of measuring nearfield events (Takeo, 1998) (which can lead to immense destruction on buildings and permanent displacement, but which are also shedding light on the rupturing fault planes), the signals recorded by ring lasers can vary from very weak teleseismic signals (Stedman et al., 1995; Pancha et al., 2000; Igel et al., 2005), penetrating deep into the Earth and therefore giving additional information about the Earth's interior and physical behaviour, to relatively strong regional motions. Though, it should be mentioned that by now no rotation sensor can provide the full range of amplitudes induced by earthquakes, mentioned above.

So, there is no longer the question why we should measure rotational motions, but rather, what kind of new opportunities do the new signals offer us. Therefore, a basic introduction to the therory of rotational motions is inevitable.

1.1. Rotational motions

Rotations have been of great interest in other sciences for a long time, while representing a relatively new observable in seismology. In the subsequent sections the focus is laid on the basic theory behind rotations before giving detailed information about ring laser technology and its applicability for seismic investigations.

1.1.1. Rotations in seismology

Theory of rotational motion is an inevitable basis for the interpretation of rotational seismograms. Assuming the Earth acts like an elastic material, the displacement $\mathbf{u}$ of a point $\mathbf{x}$ - caused by infinitesimal deformations - can be described according to the classical elastic theory (Aki and Richards, 2002; Cochard et al., 2006) with the vector

$$
\begin{aligned}
\mathbf{u}\left(\mathbf{x}+\delta\mathbf{x}\right) &= \mathbf{u}(\mathbf{x}) + G\delta\mathbf{x} \\
&= \mathbf{u}(\mathbf{x}) + \epsilon\delta\mathbf{x} + \Omega\delta\mathbf{x} \\
&= \mathbf{u}(\mathbf{x}) + \epsilon\delta\mathbf{x} + \omega \times \delta\mathbf{x}
\end{aligned}
\tag{1.1}
$$

where $\mathbf{x}+\delta\mathbf{x}$ represents the new point next to $\mathbf{x}$, G is the deformation gradient, ϵ the strain tensor and Ω the rotation tensor. Derived from this, the angle of the rigid body rotation ω in rad can be expressed with:

$$
\omega = \frac{1}{2}\nabla \times \mathbf{u}.
\tag{1.2}
$$

In other words, the rotation is half the curl ($\nabla\times$) of the wave field.
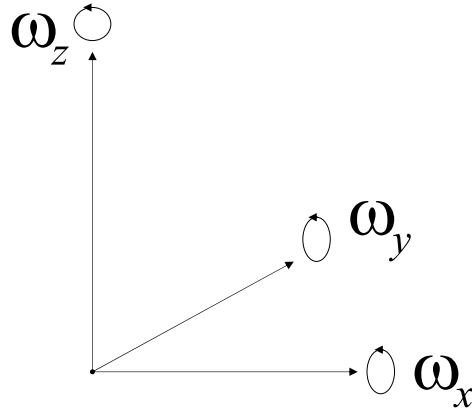
Figure 1.1: The three axes of rotation with the corresponding components of rotational motion (ω_x, ω_y and ω_z).

According to Equation (1.2), the three components of rotation are:

$$\omega_x = \frac{1}{2} \times \left(\frac{\delta u_z}{\delta y} - \frac{\delta u_y}{\delta z}\right)$$
$$\omega_y = \frac{1}{2} \times \left(\frac{\delta u_x}{\delta z} - \frac{\delta u_z}{\delta x}\right) \tag{1.3}$$
$$\omega_z = \frac{1}{2} \times \left(\frac{\delta u_y}{\delta x} - \frac{\delta u_x}{\delta y}\right)$$

This illustrates that the full description of distortion near the point **x** requires three components of rotation (Figure 1.1) in addition to three components of translation and six components of strain.

While ω_x and ω_y are caused by vertically polarised S waves (SV) and Rayleigh waves, ω_z is induced by horizontally polarised S waves (SH) and Love waves. P waves do not induce rotations, except when there is P to S wave conversion caused e.g. by layering in the Earth near the receiver. Thus, a rotational seismogram consists of rotational signals induced by body as well as surface waves.

Vertical rotation rate and transverse acceleration   are related via Equation (1.2). For a transversely polarised plane wave propagating in x direction the displacement is

$$\mathbf{u} = (0, u_y(t - x/c), 0) \tag{1.4}$$

where c is the horizontal phase velocity. Thus, the vector of rotation is given as:

$$\frac{1}{2}\nabla \times \mathbf{u} = (0, 0, -\frac{1}{2c}\dot{u}_y(t - x/c)) \tag{1.5}$$

with the corresponding z-component of rotation rate being

$$\Omega_z(x, t) = -\frac{1}{2c}\ddot{u}_y(t - x/c). \tag{1.6}$$

Hence, we will receive the relation:

$$\frac{\ddot{u}_y(x, t)}{\Omega_z(x, t)} = -2c \tag{1.7}$$

$$\Omega_z(x, t) = -\frac{\ddot{u}_y(x, t)}{2c}. \tag{1.8}$$

As a result, transverse acceleration and vertical rotation rate are identical in phase, assuming plane wave propagation and transverse polarisation. Additionally, the ratio between their amplitudes is proportional to the horizontal phase velocity c according to Equation (1.8). These two statements are valid for earthquakes with large epicentral distances.

Rotation rate and surface wave phase velocity   are linked through Equation (1.8). According to this formula we can derive the phase velocity from rotational and collocated translational measurements like this:

$$c = -\frac{1}{2}\frac{\ddot{u}}{\Omega_z}. \tag{1.9}$$

Rotational measurements around a vertical axis of rotation deliver the Love wave phase velocity.

Rotation rate and surface wave magnitude are connected with each other through the definition of the surface wave magnitude Ms (Shearer, 1999):

$$Ms = log_{10}\frac{A}{T} + 1.66log_{10}d + 3.3. \tag{1.10}$$

Because of the relationship between displacement and rotation rate the z-component of rotation rate can be described by the following formula (Igel et al., 2007):

$$\Omega_z = 2\frac{\pi^2}{cT^2}A(Ms, d) \tag{1.11}$$

$$= 2\frac{\pi^2}{cT^2}10^{Ms-1.66log_{10}d-9.3} \tag{1.12}$$

where A is the surface wave amplitude in 10^{-6} m, T the period in s, d represents the epicentral distance in degrees and c_L the Love wave phase velocity in m/s. Ms is only applicable within an epicentral distance of 20° to 160°. Now a direct comparison between observed peak rotation rate and theoretically predicted, distance- and period-dependent peak rotation rate of Ω_z is possible.

Horizontal rotation rate and tilt correspond to each other due to the zero traction condition at the Earth's free surface (Cochard et al., 2006):

$$\sigma_{iz} = 0(i = x, y, z). \tag{1.13}$$

In combination with Hooke's law in homogeneous, isotropic medium (describing the elastic behaviour of a rigid body) stating:

$$\sigma_{ij} = \lambda\epsilon_{kk}\delta_{ij} + 2\mu\epsilon_{ij}, \tag{1.14}$$

this leads to:

$$\begin{aligned}
\frac{\delta u_x}{\delta x_z} &= -\frac{\delta u_z}{\delta x_x}, \\
\frac{\delta u_y}{\delta x_z} &= -\frac{\delta u_z}{\delta x_y} \quad and \\
\frac{\delta u_z}{\delta x_z} &= -\frac{\lambda}{\lambda + 2\mu}\left(\frac{\delta u_x}{\delta x_x} + \frac{\delta u_y}{\delta x_z}\right).
\end{aligned} \tag{1.15}$$

7

with σ being the stress and ϵ the strain tensor. λ and μ are the Lamé parameters. The application of Equation (1.15) on Equation (1.2) leads to the horizontal components of rotation ω_x and ω_y formulated as:

$$\omega_x = \frac{\delta u_z}{\delta x_y} \quad and \tag{1.16}$$

$$\omega_y = -\frac{\delta u_z}{\delta x_x}. \tag{1.17}$$

This states that rotational motion around a horizontal axis is equal to tilt at the Earth's free surface. Given that seismometers are not only sensitive to translations, but also to tilt (Graizer, 2006), the measurement of ω_x and ω_y could provide a new way of correcting seismograms for disturbing tilt signals. This tilt effect is small but - especially in strong-motion earthquakes - not negligible. Conventional tiltmeters, normally used for correction, only offer long period measurements and have the disadvantage of being sensitive to translations.

1.1.2. Rotations in other disciplines

Rotational motions in seismology are a very new field of interest, but for years rotations have been measured and analysed in other disciplines by different instruments. Also here, the ring lasers' wide band of applications can be found. With information gained throughout the years the implementation of ring laser technology to seismology was eased immensely. Nevertheless, there were many improvements to be made to fit the demands of geosciences.

In physics rotational motions have always been important observables, whether it was in large scale mechanics or connected with the spin of electrons in quantum mechanics. Only if the three components of rotation additionally to the components of translation and strain are known, a full description of motion is possible.

Already in the middle of the 19th century devices to measure rotational motions were developed, so called gyrometers. With these instruments the first measurements of rotation and its variation were accomplished. Later, the gyroscope - one example of a gyrometer - was developed, based on the laws of conservation of angular momentum. Classical devices consist of a spinning wheel or disk.

In aviation and nautics these gyroscopes have been used as compasses for years, so called gyrocompasses. By finding the direction of Earth's rotational axis, they provide 'true north', while magnetic compasses only show 'magnetic north'. Here all three components of rotation (one around a vertical and two around a horizontal axis) called pitch, hive and roll are measured with gyroscopes. Ring lasers as a part of gyrocompasses are very small and therefore especially suitable for aircraft and submarine navigation as well as for space science. They have been developed to a commercial level and offer high technical standards.

In geodesy and astrometry Earth's rotation rate and its variation present two of the main quantities to be measured. Normally VLBI (Very Long Baseline Interferometry), SLR (Satellite Laser Ranging), LLR (Lunar Laser Ranging), GPS measurements are used to determine these rotational motions. In contrast to the latter methods ring laser recordings are independent of the local reference system. In geosciences measuring Earth's rotation was the first application for ring lasers (Höling, 1990). By now, also other effects like tidal motions (Schreiber et al., 2003) and polar motions (Schreiber et al., 2004) can be measured with ring lasers. A minimum effective area of 1 m² is the precondition for the use of ring lasers in geodesy.

In civil engineering rotational motions in building structures are mainly observed and analysed with FOGs. While translational motions from surface waves are generally the most destructive, some structures like high buildings, bridges or piplines are also particularly vulnerable to rotations (Hart et al., 1975). In civil engineering rotations are called rocking motion, spin, vorticity or drift. In terms of earthquake stability of buildings civil engineering and seismology are very closely linked.

1.2. Ring laser

The importance of rotational motions not only is seismology, but also in physics and engineering, led to an intense search for suitable instruments. As already mentioned, geodesy was the first geoscience to discover the gain of ring laser technology for their research. By now, these ring lasers also present a powerful tool to measure rotational motions induced by earthquakes. How they operate and what they measure is the topic of the following section.

1.2.1. Theory and operation

Based on his fundamental interferometry experiments, G. Sagnac proved the link between optical frequencies and rotational motions as early as in 1913. Ring laser gyroscopes - as optic interferometers - measure rotations exploiting exactly this Sagnac Effect by detecting the resulting frequency difference, the so called Sagnac beat frequency δf:

$$\delta f = \frac{4A_R}{\lambda P} \cdot \mathbf{n} \cdot \Omega \qquad (1.18)$$

with A_R being the area, P the perimeter of the ring laser, λ the wavelength of the laser and Ω the rotation rate. This signal is directly proportional to the rotation rate Ω of the whole system around the surface normal $\mathbf{n}$. Equation (1.18) represents the Sagnac formula.

In this thesis the relevant rotational data has been recorded by three separate ring lasers ('C-II', 'UG-1' and 'G0') in an observatory near Christchurch, New Zealand. The instruments referred to are equipped with an enclosed square-shaped cavity (see Figure 1.2). After being evacuated by a turbomolecular pump, this cavity is filled with a Helium-Neon gas mixture. Two laser beams are generated in a gain tube situated in-between two corner boxes. From there they are travelling in opposite direction through the cavity until they are redirected by high reflecting supermirrors (reflectivity of 99.9965 %) at each corner, allowing the counter-rotating beams to travel on a quasi circular path. The counter-rotating beams define a standing wave pattern enclosing the area A_R of the ring laser.

A beamsplitter allows the beams to interfere, while a Photomultiplier Tube (PMT) detects the outcoming signal. When the system is rotated, the travel path for one beam is shortened, while the other one is elongated. This leads to a change in frequency, because the number of modes for both beams is constant. Hence, the Sagnac Effect creates a phaseshift expressed by a frequency difference, the already mentioned Sagnac frequency δf.

The Sagnac frequency depends on the scale factor $\dfrac{4A_R}{\lambda P}$ (in other words on the instrument specifications), the orientation of the surface normal $\mathbf{n}$ and, most importantly,
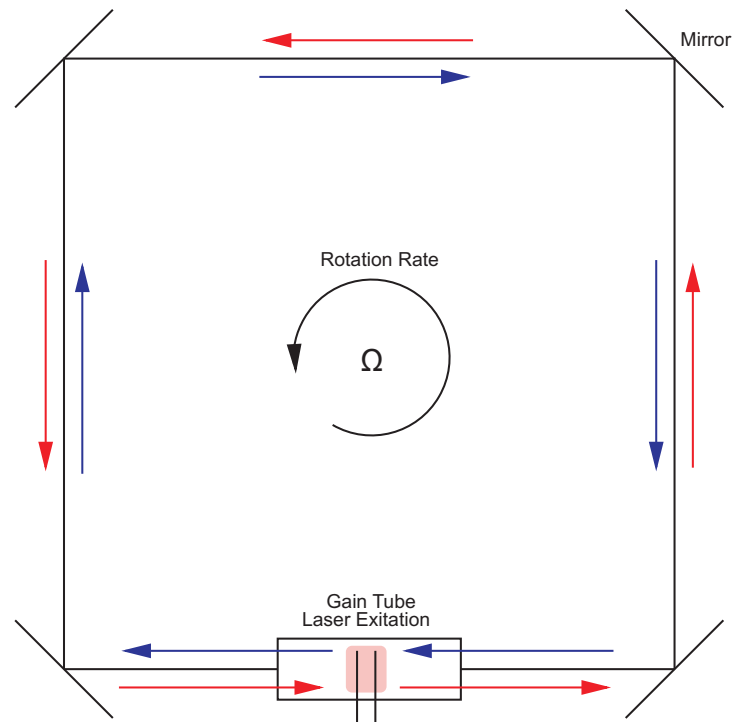
Figure 1.2: Sketch of a ring laser gyroscope. The two counter-propagating laser beams (red and blue) are both generated in a gain tube. At each corner a super mirror redirects them about 90°. When the ring laser is rotated with Ω a characteristic beat frequency is created.

on the rotation rate Ω. The ring laser needs to be made mechanically as rigid as possible to keep the scale factor constant and to avoid variations in orientation. Thus, the employment of Zerodur® (a glass ceramic by Schott AG with an extremely low thermal expansion coefficient between 0.01 and 0.02 $\cdot 10^{-6}$ 1/K) blocks as part of the ring laser body guarantees minimal changes in cavity length. Other external disturbing factors like pressure and humidity changes are taken into account as well, by creating appropriate instrument housings.

By assuring constant scale factors and orientation, the final δf signal represents a significant rotational measurement quantity, resulting in rotational seismograms comparable to standard translational time series. We want to stress that ring lasers are only sensitive to rotations assuming perfectly rigid installation, while a seismometer is polluted by rotational and a strainmeter by translational components. However, tilting of the ring laser plane and the resulting change of orientation of **n** needs to be considered mainly for nearfield events.

1.2.2. Ring laser in seismology

The rotation rate Ω is composed of different rotational components: Earth's rotation rate Ω_{Earth}, seismically induced rotational rate $\Omega_{Seismic}$ and other variations (Table 1.1). They all vary strongly in period as well as in amplitude. Since in seismology we are only interested in the seismic component $\delta f_{Seismic}$, we need to subtract at least the most dominant component from the observed Sagnac frequency δf: Earth's rotational signal δf_{Earth}. As a result, the desired component can be obtained according to Equation (1.18) with:

$$
\begin{aligned}
\delta f_{Seismic} &= \delta f - \delta f_{Earth} \\
&= \delta f - (\frac{4A_R}{\lambda P} \cdot \mathbf{n} \cdot \Omega_{Earth}).
\end{aligned}
\tag{1.19}
$$

For every instrument the required latitude dependent δf_{Earth} can be easily assessed based on the corresponding observatory location and the scale factor.

Table 1.1: Some periods of rotational motion detectable by a ring laser (Schreiber, 2000).

Source	Period
moon and iceage	≥ 100 years
core	10-30 years
tropical winds	every two years
	once a year
	twice a year
tides (sun, moon)	50 days
	27 days
atmosphere	14 days
	≤ 1 day
Earth's rotation	24 hours

As an example, we calculate the Earth's induced Sagnac frequency for the ring laser 'C-II' (specifications see Table A.1) in Christchurch, New Zealand (172.62328 E and 43.57475 S). Earth's rotation rate Ω_{Earth} of one rotation per day is:

$$
\frac{1}{23.94h} = \frac{2\pi}{23.94 \cdot 60 \cdot 60} rad/s = 7.29 \times 10^-5 rad/s.
\tag{1.20}
$$

Thus, we obtain

$$
\begin{aligned}
\delta f_{Earth} &= \frac{4A_R}{\lambda P} \cdot sin(latitude) \cdot \Omega_{Earth} \\
&= 1.58 \times 10^6 \cdot sin(43.57475) \cdot 7.29 \times 10^-5 rad/s \\
&= 79.4 Hz
\end{aligned}
\tag{1.21}
$$

as the Earth's induced Sagnac beat frequency. If the same instrument would be situated elsewhere, this frequency would vary according to its latitude from 0 Hz at the equator to maximal 115.2 Hz at one of the poles. The latitude dependence is also clearly visible in Figure 1.3. Here the Sagnac frequency caused by the Earth's rotation is plotted against latitude for three ring lasers installed in Christchurch, stressing that a small change in orientation of the surface normal **n** - in this case caused by a variation of latitude - has an immense effect on the outcoming frequency signal.
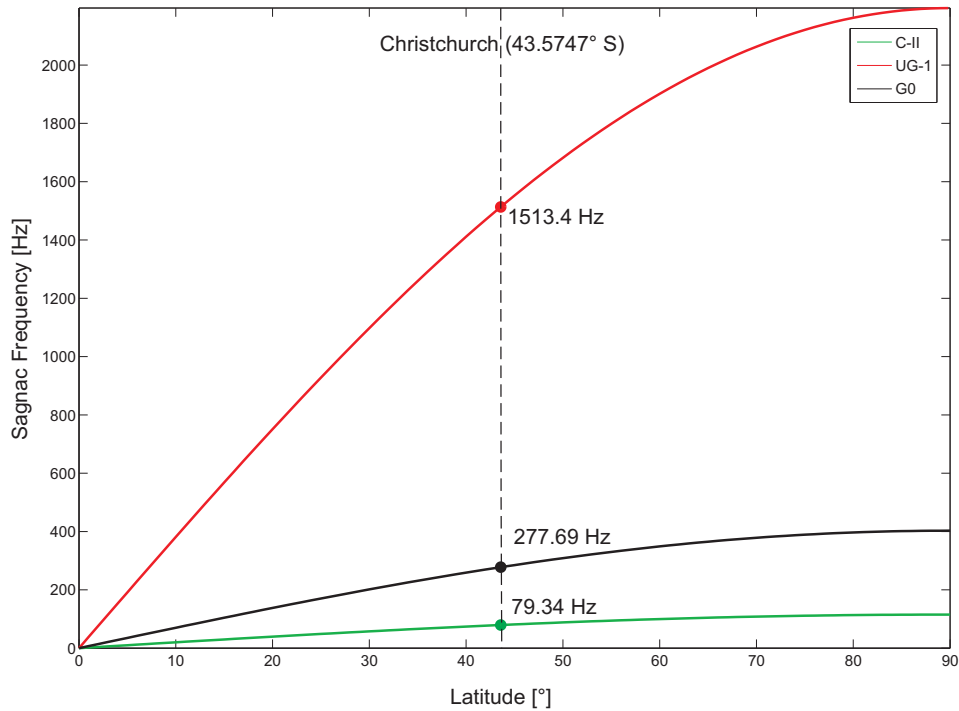
Figure 1.3: Latitude dependence of the Earth-induced Sagnac frequency δf_{Earth} for 0 to $\pm 90°$. According to the different scale factors each ring laser has a different frequency at the same latitude, here marked for the three ring lasers 'C-II' (green), 'UG-1' (red) and 'G0' (black) in Christchurch (43.57475° S).

Removing the Earth's induced component leads to the Sagnac formula in the following form used for seismological purposes:

$$\delta f_{Seismic} \;\; = \;\; \frac{4A}{\lambda P} \cdot \Omega_{Seismic}. \tag{1.22}$$

1.3. Summary

A full description of motion requires additionally three components of rotation. They are of great interest for physics, navigation, geodesy and recently for seismology. Alongside with translations, earthquake waves generate rotational motion as well. Theory implies that:

- rotations are equal to the curl of the wavefield,

- vertical rotation rate and transverse acceleration are comparable in phase,

- the ratio between their amplitudes is proportional to the phase velocity,

- peak rotation rates can be estimated from Ms and

- horizontal rotation rate is equal to tilt at the free surface.

The required measurements can be carried out by several instruments. However, only ring lasers offer high sensitivity, good running stability, a high level of development and the possibility of point measurements. At the moment there are four ring laser observatories worldwide with their instruments capable of recording small rotations caused by earthquakes. The corresponding output signal is the Sagnac beat frequency $\delta f_{Seismic}$, which is proportional to the induced rotation rate $\Omega_{Seismic}$. Most importantly, the ring laser is only sensitive to rotation. However, tilt changes the orientation of the surface normal and thus the signal itself, making nearfield application difficult.

With measurements of rotational motions induced by earthquakes information about fault plane geometry, and hence constrains of the rupture histories, source processes, permanent displacement and P to S wave conversion ratio can be obtained. Additionally, tilt correction of seismometers could be made possible by ring laser recordings around horizontal axes.

Chapter 2.

Instrumentation in Christchurch

In this thesis the main focus is laid on rotational motion recorded by three He-Ne ring lasers in Christchurch, New Zealand:

'C-II', 'UG-1' and 'G0' (Figures 2.4 to 2.6).

The provided data covers the years 2003 and 2004. At that time 'C-II', 'UG-1' and 'G0' were simultaneously operated. The following sections will describe the above mentioned instruments including the corresponding seismometer and the observatory in detail and will give additional information about secondary ring lasers.

2.1. Location

Before concentrating on technical specifications of the individual instruments, we will at first focus on the location and give a short introduction to the seismic situation around the observatory, given that it is situated in one of the most geologically active countries in the world. This serves as important background information for the succeeding data interpretation.

New Zealand's position on the active plate boundaries between the Pacific and the Australian Plate leads to extensive volcanism and frequently occurring earthquakes. The tectonic setting of New Zealand (Figure 2.1) can be differentiated as follows: While the North Island is located atop of the Pacific Plate subducting underneath the Australian Plate, the South Island is dominated by a transform fault. Further south a second subduction zone is caused, this time by the Australian Plate submerging under the Pacific Plate. These plate motions release every so often enormous energy in form
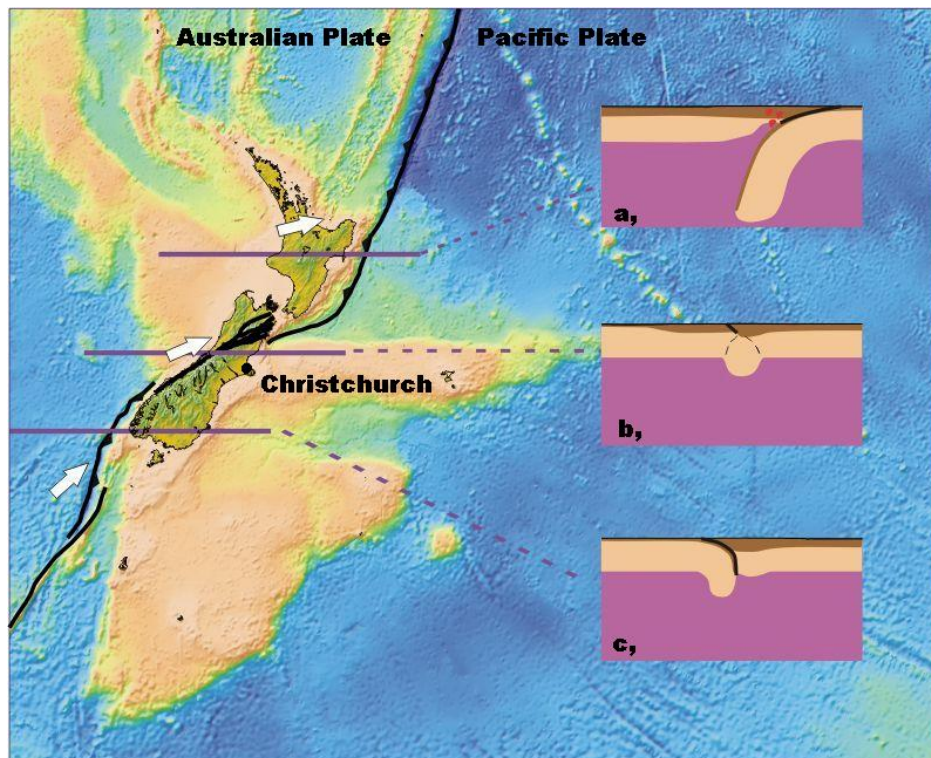
Figure 2.1: Map of New Zealand with an overview of the tectonic settings. Cross-sections of the three main regions are shown on the right: a and c: subduction zones and b: transform fault. The plate boundaries between the Pacific Plate and the Australian Plate are marked black. After GNS (2007), modified.

of earthquakes, whose distribution can be extracted from the New Zealand seismicity map (Figure 2.2). In terms of seismology, New Zealand therefore ranks among the most active countries on earth. According to the GNS (Institute of Geological and Nuclear Sciences), there are about 14,000 earthquakes larger than magnitude 3 occurring each year in New Zealand. However, only about 100 to 150 of these events are big enough to be felt.

Being part of the circum pacific 'Chain of Fire' and therefore its proximity to other seismic active regions - like the Kermadec Trench, Papua New Guinea or Japan - makes New Zealand an interesting place to study local as well as teleseismic events. In addition, New Zealand offers an excellent seismic network provided by the GNS. The instruments for this study are located in an observatory on the east coast of New Zealand's South island in the city of Christchurch.
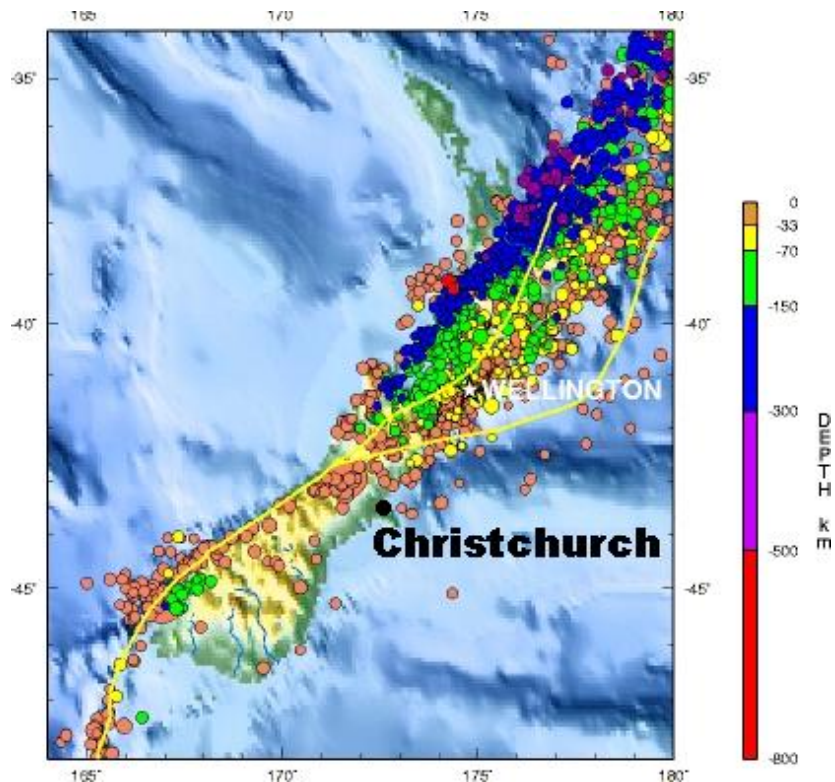
Figure 2.2: Seismicity map of New Zealand (1990-2000) showing the plate boundaries (yellow lines), the location of Christchurch and the earthquakes in different colours according to their depth. After USGS (2007), modified.

The observatory is situated in the Cashmere Cavern, an unfinished World War II bunker 30 m below the southern outskirts of Christchurch, which now provides a basis for an underground laboratory (Figure 2.3) for the Physics Department of the Canterbury University. The coordinates are:

$$43.57475° \text{ South,}$$
$$172.62328° \text{ East.}$$

With a size of over 20 m by 40 m it is able to host four ring lasers, a seismometer and a small laboratory. The cavern was blast into the remnants of the Banks Volcano, which form the peninsula adjoining Christchurch in the south. Only parts of the floor, walls and ceiling are covered with concrete. All instruments are mounted on concrete or massive granite blocks directly attached to the solid lava rock, offering an optimal signal transmission. There are no records of earthquakes in the direct proximity (closer than 10 km) of Christchurch. This is an advantage, because ring lasers are very sensitive

instruments that would easily be misaligned by extreme large ground motions induced by a nearby event.
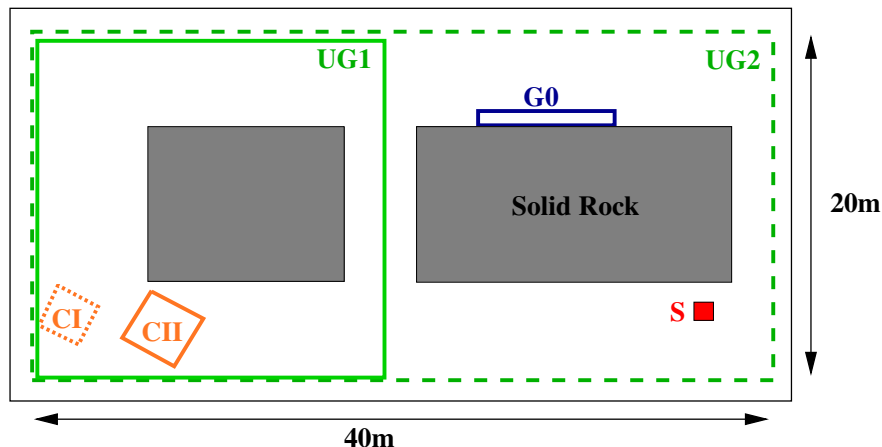
Figure 2.3: Horizontal projection of the Cashmere Cavern (not to scale) with the locations of all ring lasers and the seismometer (red). Note that 'UG-1' was replaced by 'UG-2' in 2005.

2.2. Ring laser with a vertical axis of rotation

As we already discussed the general structure and operating mode of a ring laser in Chapter 1, we will now provide extra information about each individual instrument and stress its special features. Thereby, we start with the ones being mounted on the cavern floor. Hence, they have a vertical axis of rotation, making it possible to record ω_z caused by Love waves and SH waves. A resume of the most important parameters of the ring laser can be found in the summary in Table 2.1.

2.2.1. 'C-I' and 'C-II'

According to the chronological order the description starts with 'C-I'. Even though 'C-I's data is not used for this study, we will nevertheless mention it due to its enormous importance to ring laser development in general. In this study the focus is laid on data recorded - amongst others - by 'C-II'.

'C-I' - Canterbury Ring I was the first large[1] ring laser in Christchurch. As a proto-type 'C-I' was built to test if large ring lasers can be used as sagnac interferomters at all. 'C-I' encloses an area of 0.7547 m^2 and was build between 1987-1997 by the Canterbury University and the Oklahoma State University. Its mirror holders are placed on a 1.2 m× 1.2 m × 25 mm Zerodur$^®$ plate (Subsection 1.2.1), that is attached to a 700 kg granite block, anchored to the surrounding volcanic rock. Due to its mechanical instability it is unfortunately not usable for geoscientific observations. However, it proved that large ring lasers are technically feasible and served as a kind of template for all following ring laser projects for the last decades. According to 'C-I's scale factor the Earths rotation generates a Sagnac frequency of 68.95 Hz.

'C-II' - Canterbury Ring II is, with a size of 1 m^2, the smallest of all Christchurch ring lasers suitable for geoscientific observations. It was constructed in Germany in 1995 and 1996 by Carl Zeiss as a cooperation project of the Technical University Munich, the FESG and the Canterbury University. In 1997 it was installed in the Cashmere Cavern. Its body is made of a monolithic Zerodur$^®$ block (1.2 m× 1.2 m × 18 cm) attached to a cubic granite block and therefore its signal quality is less vulnerable towards thermal expansion. The laser cavity was drilled into the ceramic material and operated with ultra-high vacuum technology, offering a far better stability than 'C-I'. In addition, 'C-II' is encased by a separate pressure controlled chamber. The beat frequency induced by the rotation of the Earth accounts to 79.4 Hz. 'C-II' as well represents a prototype for even bigger geoscientific rotational sensors. 'C-II's' noise level is still high compared to the ones of the larger, but less sophisticated ring lasers 'UG-1' or 'UG-2'. This can be explained by a factor of 20 difference in the corresponding scale factors (Subsection 1.2.1). The scale factor varies for each instrument according to its input parameters.

2.2.2. 'UG-1' and 'UG-2'

After the great success of the smaller ring lasers, the need for bigger instruments with higher sensibility and better resolution emerged. After 'G0' was successfully put into operation, another even larger ring laser was installed in the Cashmere Cavern rounding off the observatory. Table 2.1 offers all ring laser parameters relevant for this thesis.

---

[1]The term 'large' refers to ring lasers with a perimeter of more than 0.6 m. Standard instruments have smaller sizes (Subsection 1.1.2), but are not applicable for geoscientific research.

'UG-1' - Ultra Grossring[2] 1   was built in 2001 by the Canterbury University. In contrast to 'C-II' its body is not made of Zerodur®, but of mechanically relatively unstable steel pipes and mirror boxes attached to concrete blocks at the corners. For a large instrument like 'UG-1' with a size of 366.86 m^2 the use of this expensive material would have not been economical acceptable. The beat frequency caused by the Earths rotation is 1512 Hz, making it very hard to find a proper recording system. Most of the commercial systems offer a sampling frequency of up to 1000 Hz. Respecting the Nyquist frequency being half of the sampling frequency (Scherbaum, 1996), this leads to a maximum recordable incoming signal of 500 Hz. 'UG-1's signal with over 1500 Hz clearly exceeds this value. Hence, an individual recording system needed to be developed. One of the big advantages of a second ring laser suitable for geoscientific research is that now we are able to compare its measurements directly to the collocated smaller 'CII's. Until early 2005 'UG-1' was the biggest ring laser in Christchurch delivering excellent data also used in this study. It was then enhanced to its present-day size and renamed to 'UG-2'.

'UG-2' - Ultra Grossring 2   is 'UG-1's successor, based on a similar construction technique, but with an even bigger enclosed area of 834.12 m^2. A further increase in size would not be possible, because 'UG-2' already meets the limit of space provided by the cave. As one can derive from the Sagnac formula (Equation (4.1.5)) the instruments sensitivity increases with its the size. Though, also problems like gas leakage, temperature and mechanical instability accumulate and contribute to an increase in noise level. Nevertheless, the increase in dimension of 'UG-2' compensates these obstacles and results in an improvement of the resolution. Due to its size 'UG-2' has a high Earth-induced Sagnac beat frequency of 2177 Hz.

2.3. Ring laser with horizontal axis of rotation

There is only one ring laser in Christchurch with a horizontal axis of rotation. In contrast to all other instruments this one is mounted on one of the cavern walls with a 10° west of north axis orientation. With its help the detection of ω_y caused by Rayleigh waves and SV waves is possible.

---

[2]The term Grossring is a German expression meaning large ring. The ring laser actually called Grossring is located in Wettzell, Germany.

'G0' - Grossring 0   was build in 2000 as a test version for 'UG-1' concerning dimension (but not orientation). It reaches a size of 12.25 m^2 and distinguishes itself from the other ring lasers through its very simple technique. There was no Zerodur$^®$ used in the construction. Originally 'G0' was not planned as one of the recording instruments. But soon after the first tests, it became clear that despite its simple construction and mechanical instability, seismic data was recorded in sufficient quality. The Sagnac frequency accounts to 288 Hz. 'G0' turned out to be the most reliable of all ring lasers in terms of running stability over time. The information gained through 'G0' served as a guideline for all subsequent ring lasers including future six-component sensors (three translations and three rotations).

Table 2.1: Ring laser parameters required by the Sagnac formula (Equation (1.22)).

Ring Laser	Wavelength [nm]	Perimeter [m]	Area [m^2]	$\delta f_{\textbf{Earth}}$ [Hz]
C-II	632.99	4.00	1.00	79.40
UG-1	632.99	76.93	366.86	1512.85
G0	632.99	14.00	12.25	288.00

2.4. Seismometer

Collocated with the four ring lasers, a CMG-3ESP broadband seismometer (Figure 2.7) from Güralp Systems Limeted Limited can be found in the cavern (for location see Figure 2.3). The instrument is part of the NZ-Seismometer Net (http://www.geonet.org.nz/), representing a three-component seismometer that samples at 1000 Hz and that is able to record signals with frequencies ranging from 0.003 Hz to 50 Hz. There is no exact documentation of the instrument deployment available. Hence, it should be mentioned that proper documentation is crucial and helps avoiding additional time delays during data analysis.

Further specifications, including information required for an instrument correction are listed in Table 3.1.

2.5. Summary

The instruments of the observatory in Christchurch allow the recording of rotational and translational motions of regional as well as teleseismic events. Its position 30 meter underground insulates even large ring lasers from high noise signals. This in combination with its excellent temperature, humidity (less than 1 mK/h) and seismic stability turns the Cashmere Cavern into an excellent location to study rotations. Its enormous size of more than 20 by 40 m allows to host all ring lasers, additional instrumentation and a laboratory in one place. The three ring lasers whose data is used in this study deliver data around a vertical ('C-II' and 'UG-1') and a horizontal axis ('G0'). Some of the instruments' characteristic parameters are shown in Table 2.1 and more detailed in Appendix A.

For further details of the New Zealand ring lasers, their evolution and construction units see Schreiber (2000) or Stedman (2001). More detailed information about technical aspects of the ring laser technology and other instruments worldwide can be found in Velikoseltsev and Schreiber (2005), Schreiber et al. (2006) and on the official homepage of the Fundamentalstation Wettzel (http://www.wettzell.ifag.de).

Figure 2.4: Picture of 'C-II' without pressure case, thus the Zerodur® block (orange) is clearly visible (FESG, 2007).

Figure 2.5: Picture of one of 'UG-1's corner boxes (marked by the red helmet) with the laboratory entrance in the background.

Figure 2.6: Picture of 'G0' mounted to the concrete wall during construction (UC, 2007).
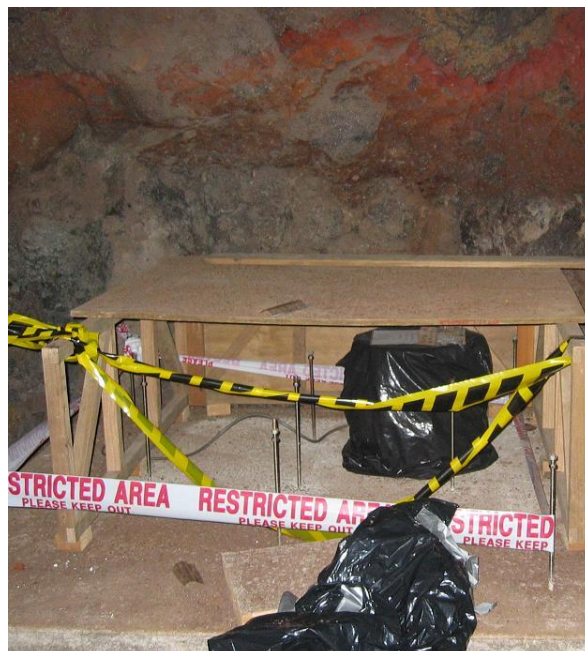
Figure 2.7: Picture of the Güralp CMG-3ESP broadband seismometer during reconstruction.

Part II.

Chapter 3.

Data set

The instruments of the Christchurch observatory recorded rotational and translational motions in the course of 2003 and 2004. In the following sections we will describe the required acquisition processes, focus on the basic conversions and corrections applied to the data and also specify their final format.

3.1. Data acquisition

Data acquisition is one of the most complex and important features of every data delivering system. It is not enough to record useful data, but also to guarantee that it is properly stored and made accessible to further processing. For seismometers there are many well established standards assuring this demand, but for an instrument like the ring laser, those standards needed to be developed and tested first. In this section the main LabView based acquisition features are described. LabView (Laboratory Virtual Instrumentation Engineering Workbench) is a graphical development environment by National Instruments.

3.1.1. Main acquisition

Once the ring laser generates an optical signal (described in Subsection 1.2.1), it is transformed by a PMT to a voltage output. This analogue signal is then sampled by an ADC with a sampling rate of 1000 Hz (800 Hz until 2003) and thereby brought to a digital form. The rotational data in Hz of the ring lasers is saved continuously, but due to limited storage capacity the seismometer signal in counts is exclusively stored during an earthquake. The saving process for the seismic data is triggered by the crossing of

a certain threshold, previously defined well above the average noise level. If this is the case, the seven channels (three rotational signals, three seismometer components plus a time channel) are stored as a 30 min binary file with a filename according to the record start time. These files were locally saved and later stored on DVDs, as a direct connection to a server at the Physics Department was not possible. Figure 3.1 gives a compact overview of the acquisition system's main components. The LabView Pre-processing tool mentioned therein will be discussed in the next subsection.
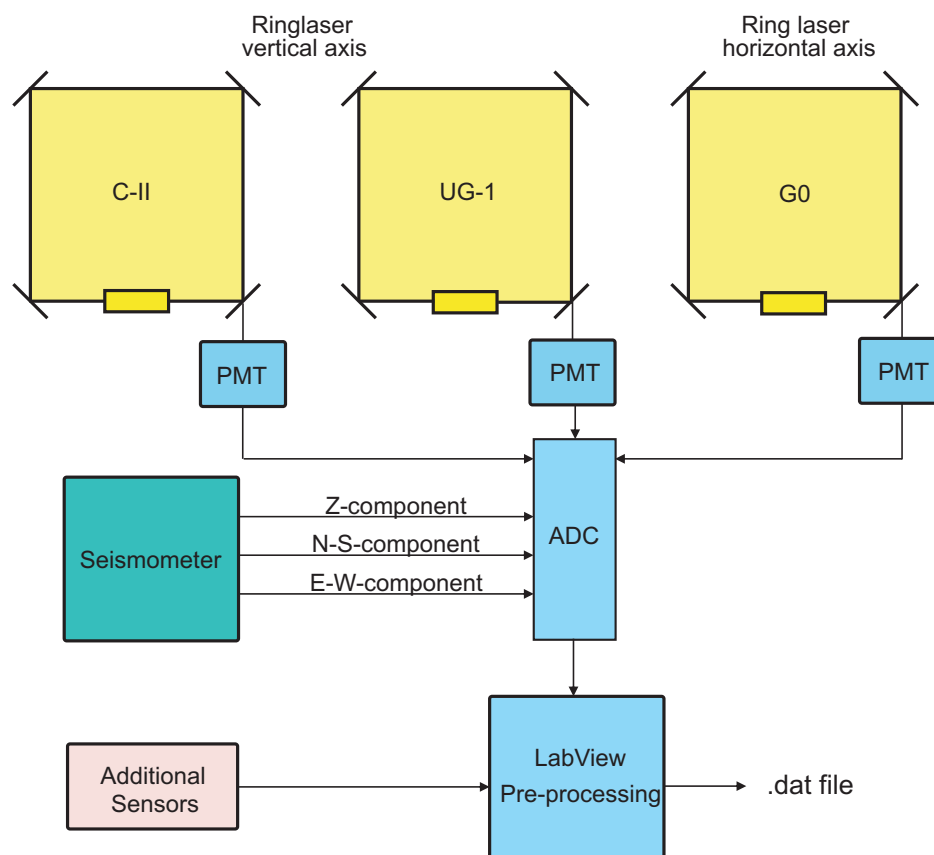
Figure 3.1: Simplified sketch of the acquisition system (blue) in Christchurch with the main data delivering components. The three ring lasers are shown in yellow, their optical signals are transformed into a voltage by a PMT. Together with the three components of the seismometer (green) they are converted from analogue to digital signals by the ADC. Additional data of a thermometer and barometer (pink) are included by the LabView Pre-Processing tool.

Due to a sampling rate of 1000 Hz, each 30 min data file covers seven channels with 1.8 million samples respectively. Each sample is 2 bytes long. Together with the header (88 bytes) and tailer (64 bytes) this results in a 25200152 bytes file length. Until 2003 a sampling rate of 800 Hz was used, creating 20160125 bytes long files. Every variation of these two values exposes an invalid file. These rarely occurring files were caused by conversion problems between the two different system softwares of the cavern and the Physics Department.

Another important disadvantage of this storing process was the 8 s time gap created between every consecutive 30 min files. This loss of data was caused by the acquisition programme closing and storing the old file before opening the new one. In total this took 8 s, a period in which no data could be recorded. In addition, the sampling rate was triggered by a GPS clock using UTC (Coordinated Universal Time), while the time stamping of the seven channels relied on an internal computer clock, because GPS time was not compatible with the regulatory acquisition system. An offset between UTC and internal time of up to 13 s has been reported. Hence, a direct comparison in time of the data with other seismograms is not possible. The installation of a standardised data acquisition unit by Refraction Technology Inc. in early 2008 solved all those problems at once.

3.1.2. LabView pre-processing

After the data has been successfully stored, a specially designed LabView programme (ReadRawdata.vi) transforms the binary files to a format, that can easily be further processed by seismic tools. The LabView programme includes the following steps:

- Transformation of the binary data to ASCII code data.

- Subtraction of the Earth's induced Sagnac frequency δf_{Earth} for each ring laser trace.

- Downsampling of the data from 1000 Hz or 800 Hz to 20 Hz (standard frequency in seismology). Figure 3.2 shows the corresponding part of the ReadRawdata.vi programme.

- Visualising and picking of the most promising events.

The names of the new ASCII files is composed of the recording start time in sidereal time and the file ending .dat for data. As an example, a file recorded at 07:28:05 (0.31178 of the day) on March, 11th 2003 (70th day of 2003) results in: 2003-70-31178.dat. Later the filenames of the most important events were again renamed, including the date and source region:

$$2003.03.11\_papua.dat. \tag{3.1}$$

For each earthquake file there is also an information file generated called for our example: 2003-70-31178.inf. Additional data like start time and end time of the files (both in sidereal time), number of samples taken, temperature and barometric pressure in the cavern can be found there.
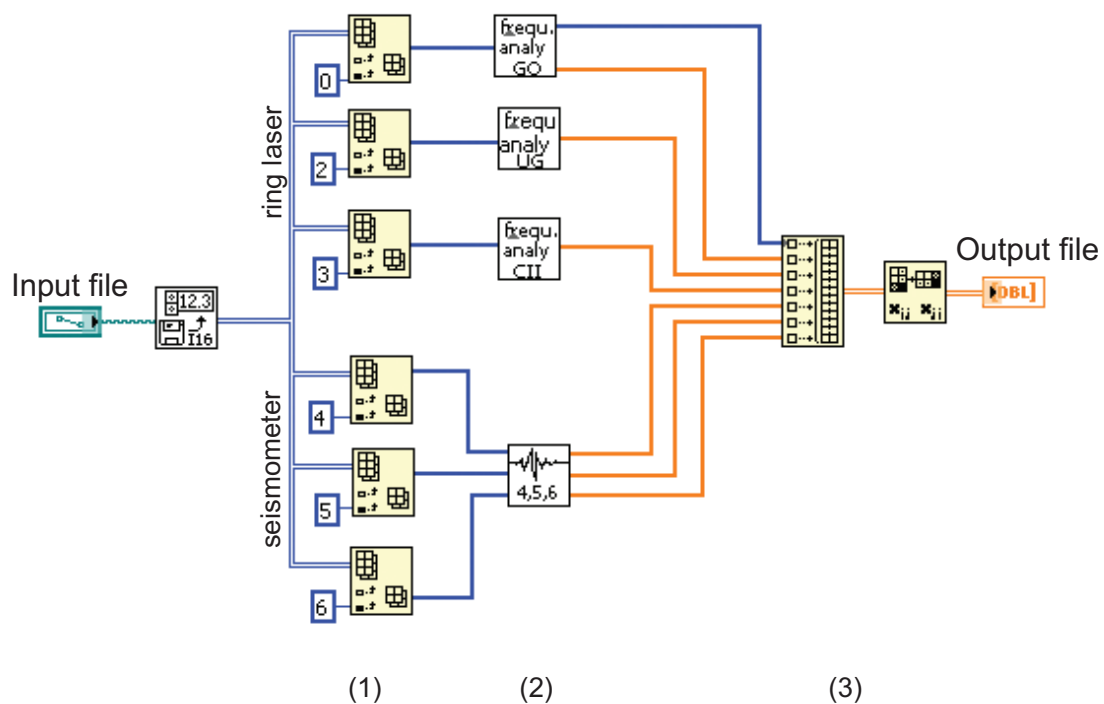
Figure 3.2: Part of the ReadRawdata.vi coded in LabView. In (1) the data is split into three ring laser channels and three seismometer channels, (2) is the frequency analysis - one for each ring laser and one for all three seismic channels sampling the data down from 1000 Hz or 800 Hz to 20 Hz. In the end, these six components (orange) plus the time channel (blue) are concatenated (3) to form a new output file in ASCII format.

3.2. Data conversion and correction

The processes described in the preceding section deliver three rotational and three seismic data channels. However, prior to further analysis the data needs to be corrected. For ring laser as well as for seismic data there are some adjustments inevitable. Here, we discuss the corrections and stress the ring lasers advantage as an optical instrument. After these final pre-processing the data is available in its final form and a direct comparison between rotational and translational data is possible.

3.2.1. Ring laser

The first step is to convert the rotational signal from a beat frequency δf in Hz to a rotation rate Ω in rad/s. This is done according to the Sagnac formula (Equation (1.22)) with

$$\Omega_{Seismic} = \frac{\lambda P}{4 A_R} \cdot \delta f_{Seismic} \tag{3.2}$$

where $\dfrac{\lambda P}{4 A_R}$ depends on each ring laser's particular parameters shown in Table 2.1 or Appendix A. It should be stressed, that this simple conversion executed by a Matlab script is the only correction applied to the ring laser raw data before further analysis. A ring laser is an optical instrument only sensitive to rotations, relying on no moving mechanical parts and hence - in contrast to a seismometer - is totally independent of mass inertia and has a uniform transform function.

3.2.2. Seismometer

Unit Conversion is the first step towards a standardised event dataset consisting of three rotational and tree translational seismograms. During the data acquisition process the seismic data is recorded in voltage and then converted by the ADC to counts. To achieve a signal in nm/s, we convert the count signal for each seismometer component (Z, N-S and E-W) according to the following formula (Scherbaum, 1996):

$$Signal[nm/s] = Signal[counts]/\frac{LSBvalue}{Sensitivity} \tag{3.3}$$

The LSBvalue (Least Significant Bit value) is defined as:

$$LSBvalue = \frac{FullScaleVoltage}{2^{n-1}} \tag{3.4}$$

with a n-bit resolution of the ADC (16 bit in our case). For the CMG-3ESP Seismometer used in this study - input parameters for Equation (3.3) and (3.4) can be found in Table 3.1 - the LSBvalue accounts to 6.1035×10^{-4} V/count, which finally needs to be divided by the sensor sensibility for each component to accomplish a unit conversion for the seismic data.

Table 3.1: Extract from the seismometer calibration sheet.

Güralp CMG-3ESP		
Poles	-23.56 $\times 10^- 3$ ° j 23.35 $\times 10^- 3$	[Hz]
	-50° j 32.2	"
Zeros	0	"
	0	"
	138° j 144	"
Full Scale Voltage	20	[V]
Sensitivity	2 × 996.77 (Z)	$[V/\frac{m}{s}]$
	2 × 1007.69 (N-S)	$[V/\frac{m}{s}]$
	2 × 1000.70 (E-W)	$[V/\frac{m}{s}]$

Instrument Response is a problem only related to instruments relying on inertial masses to record signals, like seismometers. In a simplified form a seismometer consists of a spring, a damping mechanism and and a mass. And exactly this mass affects the signal depending on the incoming frequencies and the natural frequency of the instrument itself. This influence is called instrument response. Therefore, a seismometer as part of the seismic recording system acts - like the Earth - as a filter to the incoming signal (Figure 3.3). However, in Seismology we are interested in seismic source processes and the filter function of the Earth, but not in the recording system itself. Hence, the instrument response needs to be eliminated. Otherwise, it can cause changes in phase as well as in amplitude resulting in the signal no longer representing the actual ground motion. This correction is required for all seismometer recordings not only in this thesis but in every study relying on seismic data.
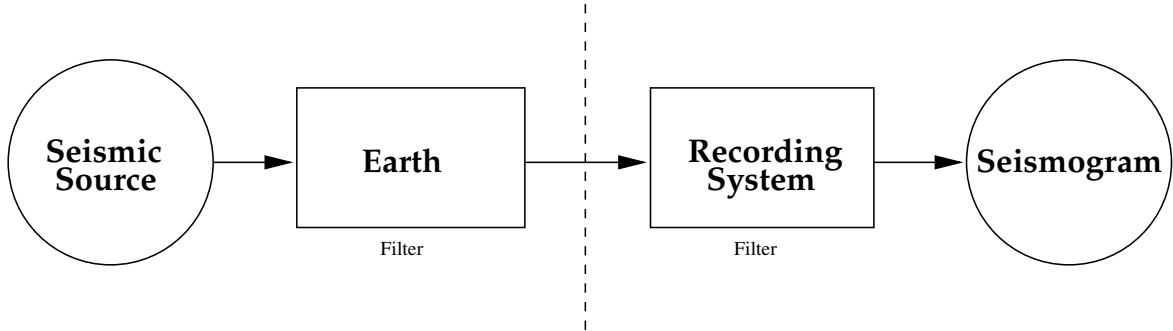
Figure 3.3: System diagram of the generation of a seismogram, after Scherbaum (1996) modified. Both, the Earth and the recording system act as a filter to the signal generated by the source.

Conducting of the seismic corrections can be achieved with several seismic processing tools suitable to perform both tasks - unit conversion and elimination of the instrument response. In this study we chose PITSA Version 5.0. The programme is demanding a calibration file, which needs to be written for each seismometer trace individually. Here the LSBvalue and other required input parameters (Table 3.1) are inserted. For briefness reasons we will only give a short summary of further steps involved with the conversion and correction:

- Generation of a calibration file for each seismometer component including all information needed for the unit conversion (Paragraph 3.2.2).

- Uploading of the relevant seismometer trace in PITSA.

- Seismometer simulation for each component (Z, N-S and E-W). Therefore, the corresponding calibration file is required.

- Now, the damping constant h and the natural frequency ω_0 of the seismometer are entered (in our case h = 0.707 and ω_0 = 0.0125 1/s).

- PITSA then creates the signal trace in nm/s without the instrument response of the simulated seismometer.

- Finally, the signals for each component are stored and later integrated in the new ASCII file.

The new files are named according to their date and source region. Our example file (3.1) is now called:

$$2003.03.11\_papua.asc \qquad (3.5)$$

The effect of the instrument response can be seen in Figure 3.4 illustrating the superposition of the Z-component before (blue) and after (black) the elimination of the instrument response for two selected earthquakes with different frequency contents. At first, the effect appears rather small for both events, but by zooming into parts of the Z-component we can detect a clear change in amplitude and phase between the two signals. Depending on the frequency content of an event a correction for the instrument response is not always required, because the eigenfrequency of the instrument might not interfere with the incoming signal itself. However, there can always be small, unobvious differences. This fact demands that every event needs to be corrected for its instrument response to avoid unintentional defects of the data.
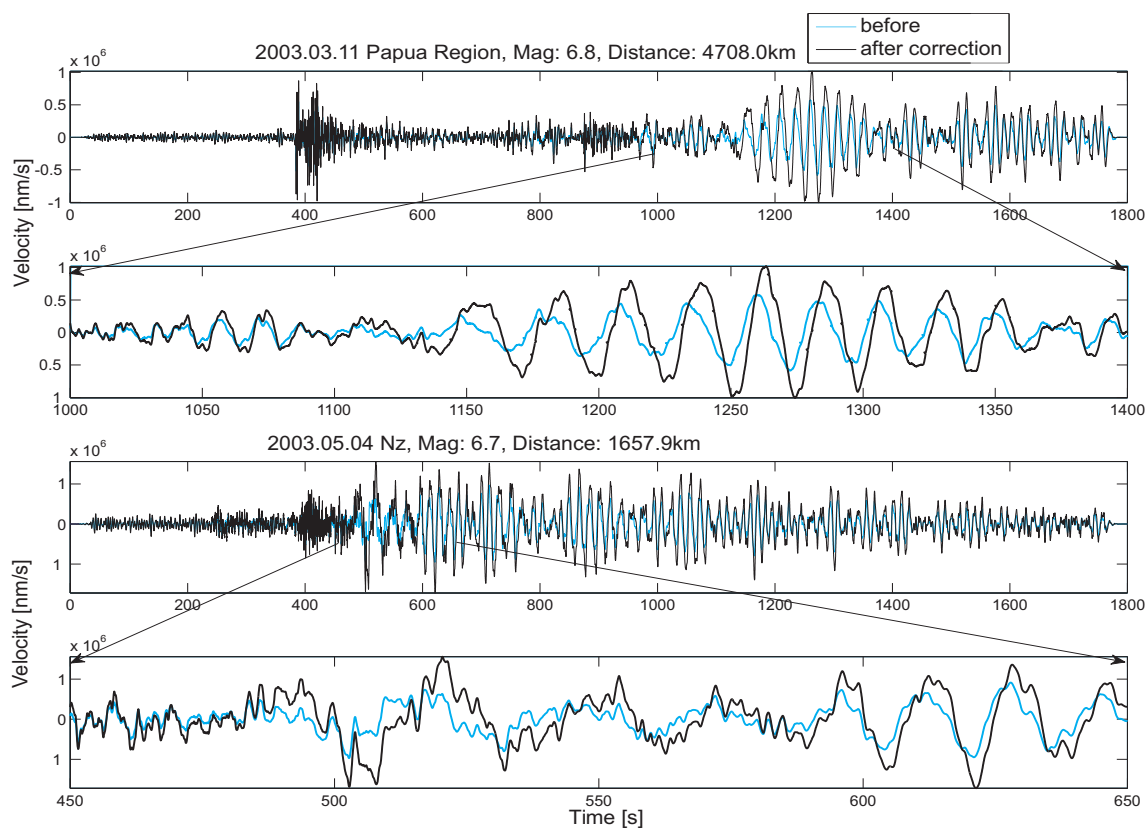
Figure 3.4: Superposition of the Z-component of translation before and after the correction of instrument response for two selected events with different frequency contents. Note the changes in phase as well as amplitude particularly well visible in the zoomed-in section.

3.3. Resulting data files

The final format of the obtained ring laser and seismometer data will be described here in detail, starting with its basic sectioning. Each 30 min long file is stored in ASCII format consisting of seven channels:

1	Time	[s]
2	'G0' data	[rad/s]
3	'UG-1' data	[rad/s]
4	'C-II' data	[rad/s]
5	Seismometer Z component	[nm/s]
6	Seismometer N-S component	[nm/s]
7	Seismometer E-W component	[nm/s]

Between the consecutive file there is a gap of 8 s. The effect on the data can be seen in Figure 3.5 showing one ring laser component - in this case 'G0' - and the corresponding three seismometer components. This M 8.1 2004.12.23, New Zealand event was cut in half, making it worthless for further analysis, because of the data missing between the two files. In addition, this event shows that due to the magnitude the seismometer traces were clipped, while the ring laser still was able to record properly.

Problems like this reduced the number of suitable events significantly. There was also hardly any period of time, when all three ringlasers were operating and delivering data simultaneously. The main reasons for the resulting lack of data are: maintenance work on one or more ring lasers, the ring laser being in split mode (one laser beam changes mode or one changes more than the other) and the occurrence of mode jumps (both beams change mode). Latter complications are caused by thermal expansion or deformation of the ring laser.

Employing the LabView pre-processing programme, we were able to search through the database of the years 2003 and 2004 picking all relevant earthquakes (Table B.1). For the year 2003 we could find 10 valid events and for 2004 the number accounts to 11. In this thesis we refer to "valid" data as datafiles with all three seismometer channels available and at least one useful ring laser component.
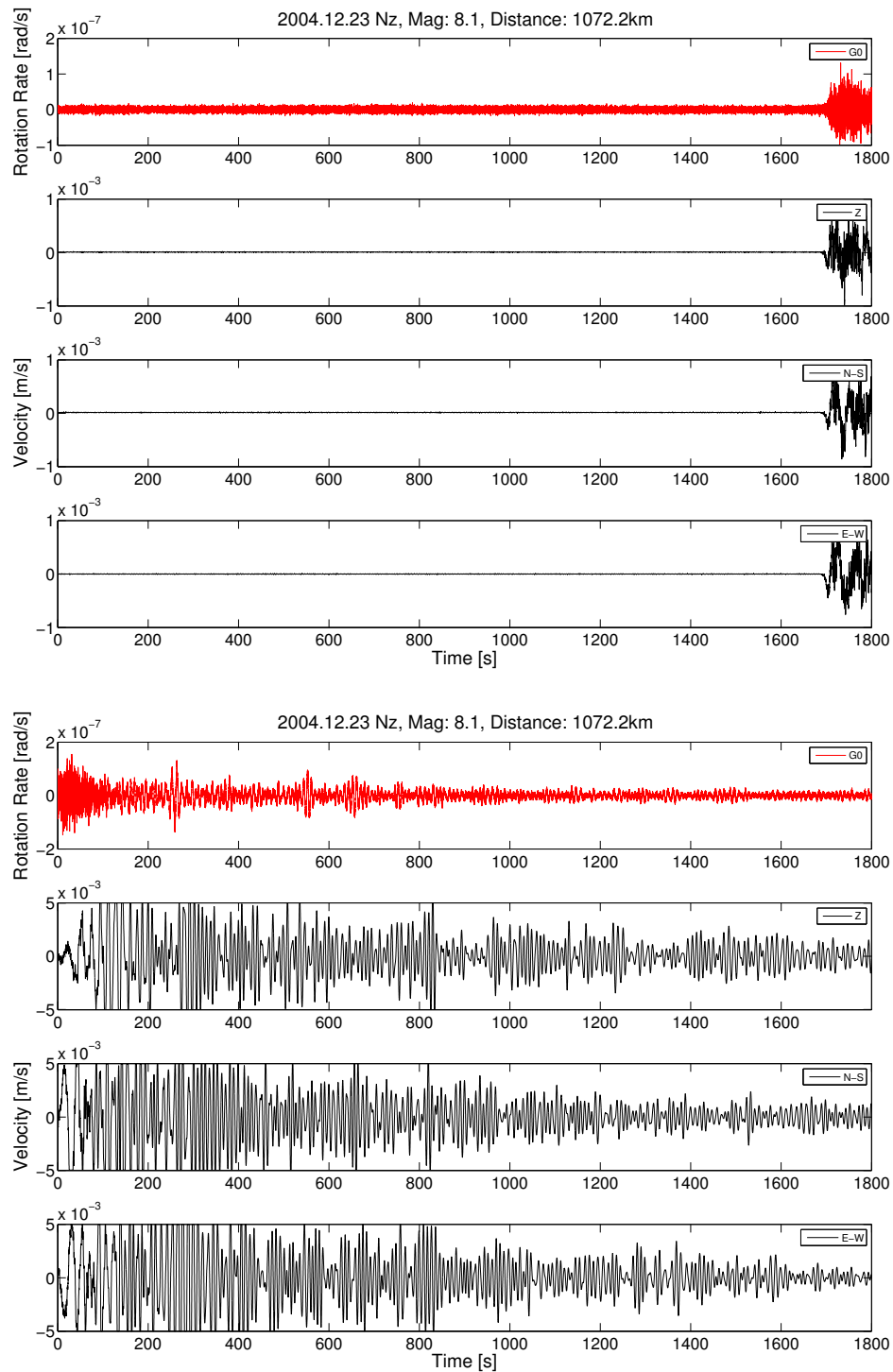
Figure 3.5: Data of the 2004.12.23 Macquaire, Nz earthquake showing one ring laser component (red) and three seismometer components (black). Note that the event was split in half due to the 30 min datalength limit. The event was so big that it clipped the seismometer traces, while the ring laser still delivered excellent data.

This leads to an unequal distribution of recorded events of the three ring lasers for 2003 and 2004:

$$
\begin{array}{lll}
\text{'C-II':} & 12 & \text{recorded events,} \\
\text{'UG-1':} & 7 & \text{recorded events and} \\
\text{'G0' :} & 20 & \text{recorded events.}
\end{array}
$$

Hence, in total there are 21 events available where final data analysis can be applied to (Table B.1). There are six events in 2003 available that were recorded by all three ring lasers along with all seismometer components. None of the earthquakes in 2004 fullfills these requirements.

3.4. Summary

The LabView based acquisition system in the Christchurch observatory records the data of three ring lasers and a broadband seismometer, transforms them from optical to digital signals and - until early 2008 - stored them locally on DVDs. As an optical instrument the ring laser only needs an unit conversion, while the seismic data additionally needs to be corrected for the seismometer response. These conversions and corrections together with a LabView pre-processing tool described in the preceding sections are applied to each event file.

Every file is stored in a 7-column ASCII format, uniformly composed and ready for further processing. Mainly technical problems led to a maximum file length of 30 min, a 8 s time gap between every consecutive file and a timing problem allowing the acquisition system to use only internal computer time for the time stamping. All these obstacles were overcome by the installation of a new data logger.

As a result, all 21 events used in this study (Table B.1) are structured similarly, showing one to three rotational components in rad/s and three translational components in nm/s. They all went through the same conversions and corrections. Figure 3.6 shows two examples of the resulting rotational and translational seismograms (in this case is the velocity given in m/s). All plots for 2003 can be found in Appendix C and for 2004 in Appendix D.
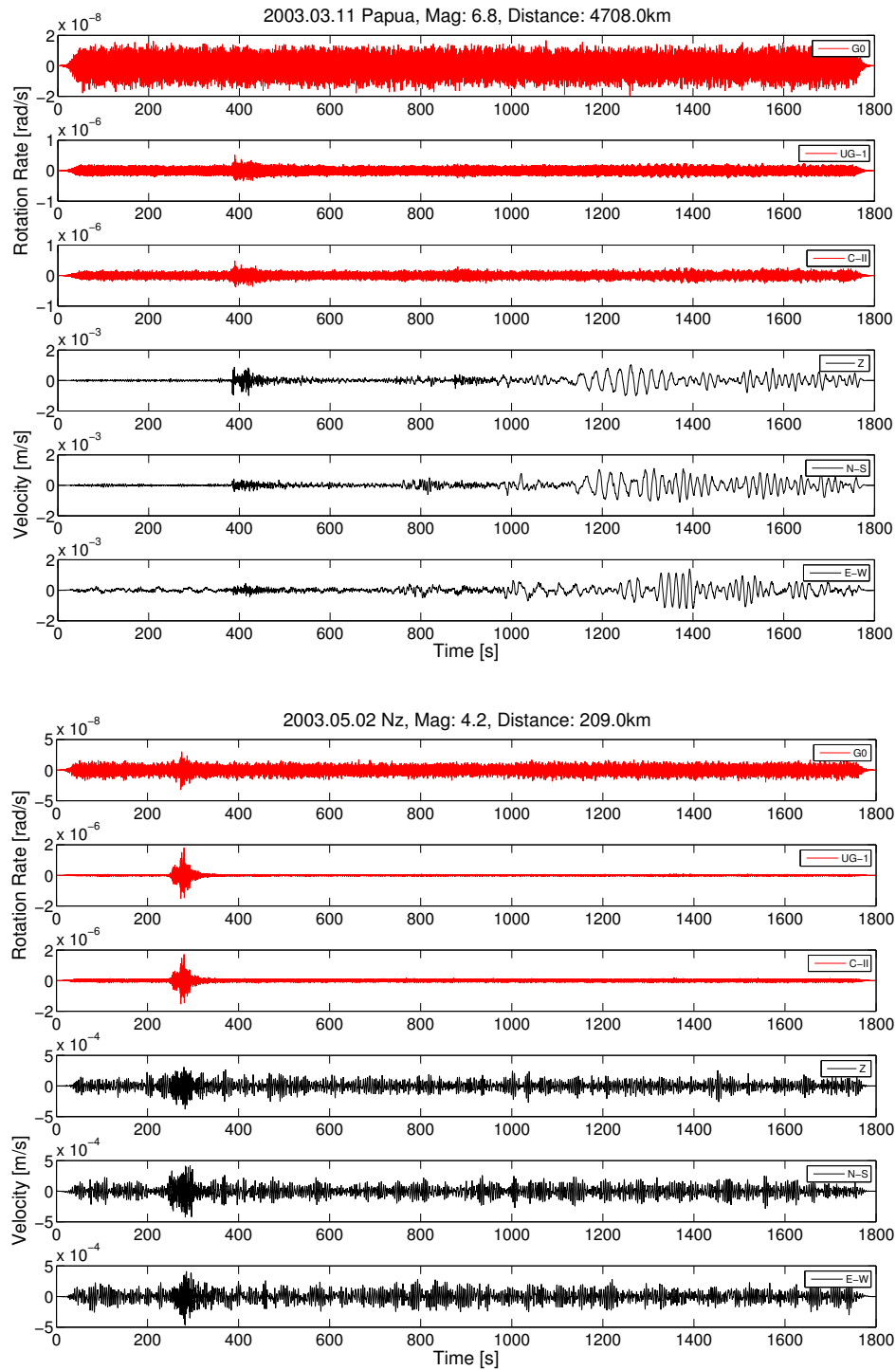
Figure 3.6: Unfiltered data of the 2003.03.11,M 6.8 Papua Region event (top) and of the 2003.05.04, M 6.7 Nz event (bottom) after correction and conversion. The rotational data of the three ring lasers ('G0', 'UG-1' and 'CII') are shown in red, while the translational components (Z, N-S and E-W) are shown in black.

Chapter 4.

Data analysis

After the theory behind rotational motions in seismology has been discussed in detail in Chapter 1 and after we learned about the recording instruments and the final data structure itself in Chapter 2 and 3, we are now able to have a closer look at the information behind those 21 event files provided (Table B.1). In this chapter we will carry out analysis of rotational data based on the theory previously discussed in Chapter 1. We start with data recorded by the ring lasers with a vertical axis of rotation ('C-II' and 'UG-1') and will refer to event data delivered by the ring laser with a horizontal axis ('G0') in the second part of this chapter. The goal is to test the observations for their compatibility with theory.

4.1. 'C-II' and 'UG-1'

As both ring lasers deliver the same component of rotational motion ω_z, the focus is laid on direct comparison of 'C-II' and 'UG-1' data at first. The next step is the investigation of the consistency of the observed data with respect to theoretical expectations according to Chapter 1. Throughout the whole chapter the following applies: whenever the term Magnitude or M is used, this can refer to Mb (Body wave magnitude), Ms (Surface wave magnitude), ML (Local magnitude) or Mw (Moment magnitude) as stated in the event Table B.1.

4.1.1. Magnitude-distance distribution

Because 'C-II' was able to record altogether 12 events and 'UG-1' only seven, 'C-II' offers a higher running stability over time. Hence, there are only five earthquakes

available recorded by both instruments simultaneously. All events obtained by the two ring lasers are shown in the following magnitude-distance distribution (Figure 4.1). In total, 14 earthquakes from 2003 and 2004 contributed to this figure. They cover a range of almost 88° (9785 km) of epicentral distance and vary from M 4.2 to M 8.3.
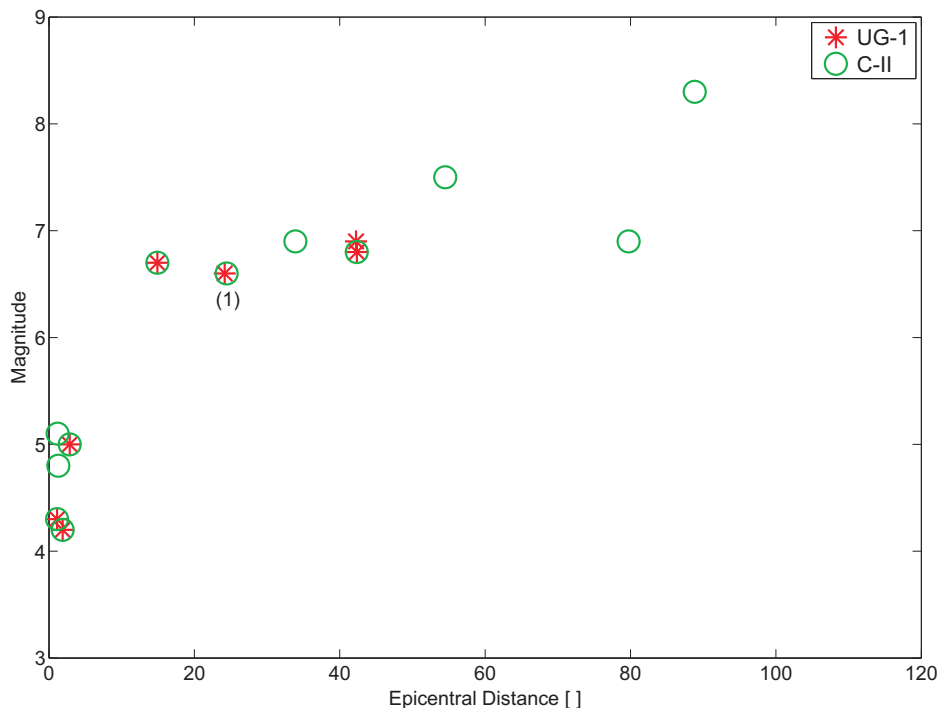
Figure 4.1: Magnitude-distance distribution for all 14 earthquakes recorded by 'C-II' (green) and/or 'UG-1' (red) in 2003 and 2004 used in this study. Note that for only five events data of both instruments is available. (1) These are two different events with the same magnitude and nearly the same distance (24.17 and 24.44 °), one recorded by 'UG-1' and one by 'C-II'.

The distribution reveals two major groups of recorded events: the first cluster lies within 3° (about 333 km) distance. These are light to moderate earthquakes, achieving magnitudes from 4.2 up to 5.1. The second group consists of events with epicentral distances ranging from 14° to over 88° (about 1556 to 9785 km). They need to achieve higher magnitudes (in our case at least M 6.6) in order to generate enough energy to be recorded by the ring laser far away from the source.

As a result, the two ring lasers make it possible to observe teleseismic as well as regional earthquakes, both with various magnitudes. Even though 'C-II' has a lower resolution

than 'UG-1', it was able to record more earthquake in the same period of time and therefore offers a broader range of distances and magnitudes.

4.1.2. Comparison of 'C-II' and 'UG-1' data

From a first look at the rotational seismograms - like in Figure 3.6 - one can estimate a good fit of onset times (top event) and additionally, of the signal envelopes (bottom event) from the 'UG-1' and 'C-II' signals. But, as they are collocated ring lasers (the smaller 'C-II' lies within the area encircled by the larger 'UG-1') both with a vertical axis of rotation, they should deliver exactly the same signal for any rotational motion. To verify this and to stress the quality of our ring laser measurements we here present
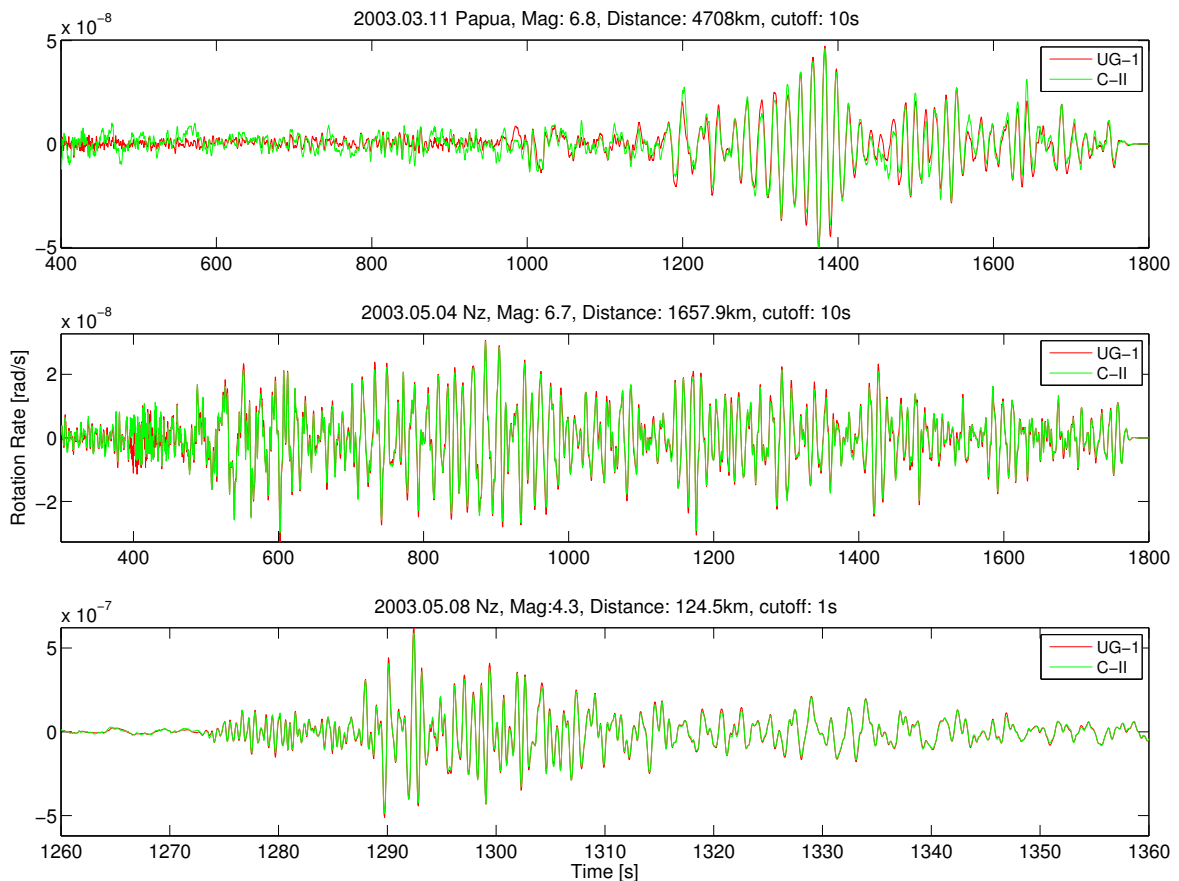
Figure 4.2: Superposition of lowpass-filtered 'UG-1' (red) and 'C-II' (green) rotation rate in rad/s for three selected events with different magnitudes and epicentral distances.

superposition plots of three selected events displaying 'UG-1' and 'C-II' rotation ratesc in rad/s directly compared to each other (Figure 4.2). We chose three events from 2003 - ranging from M 4.3 to M 6.8 with epicentral distances covering a range of 1.12° to 42.34° (124.5 to 4708km) - to display the fit for different frequency contents. More information about the corresponding earthquakes can be found in Table B.1 and B.2. After the data was lowpass-filtered with a cutoff period of 10s and 1s respectively, we can observe a very good fit in all three plots stressing the quality of the ring lasers and their measurements.

The top event with more than 42.34° (4708 km) distance represents a teleseismic earthquake. Mainly low frequencies (below 0.1 Hz) are dominant and the signal is weaker due to the distance. However, the fit of the two signals is almost perfect in the surface wave domain starting at about 1200 s. The discrepancies in the first part of the rotational seismogram are caused presumably by noise.

The middle event with its higher frequency (around 0.1 Hz) content and a distance of 14.91° (1657.9 km) shows also an excellent fit throughout the whole signal. Again, the discrepancy at about 400 s can be explained by a high noise level affecting both ring lasers at that time.

The bottom event represents a regional event with its source being only 1.12° (124.5 km) away. Here, mainly high frequencies (around 0.2 Hz and higher) are visible. Also for this earthquake the ring laser managed to record the rotations with a very good consistency.

The according maximum CC-Coefficients (Cross Correlation Coefficients) between 'UG-1' and 'C-II' calculated for the three chosen earthquakes are: 0.9833 (top event), 0.9986 (middle event) and 0.9979 (bottom event) with 1 marking perfect correlation. A comparable good fit can be seen in Figure 4.3, illustrating the direct comparison of the frequency spectra of both instruments again for the three selected events. This shows once more that the signals of the two collocated ring lasers are almost 100% identical.

Not only the excellent fit is clearly visible, but also that the 'C-II' rotation rate is in general a little noisier than the corresponding 'UG-1' signal, especially of the weaker signals (top and middle). This can be explained with a difference of about a factor 20 between the corresponding scale factors (Subsection 1.2.1).
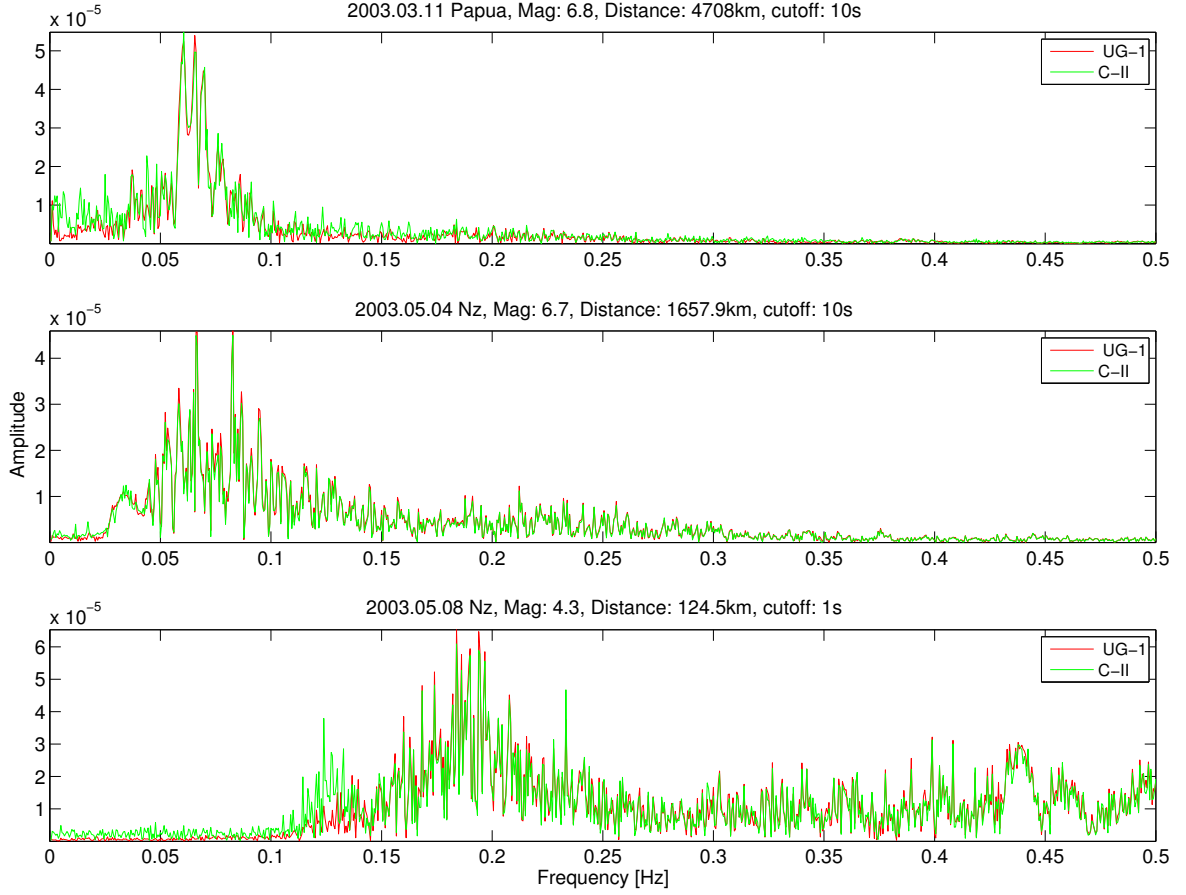
Figure 4.3: Superposition of 'UG-1' (red) and 'C-II' (green) spectra corresponding to the three events of Figure 4.2.

4.1.3. Rotation rate derived from Surface wave magnitudes

According to Equation (1.12) it is possible to derive the distance- and period-dependent rotation rate around the vertical axis from the Moment magnitude Ms. This leads to the colour-coded lines in the semi-log plot of Figure 4.4, representing the expected peak rotation rates at certain magnitudes and epicentral distances (Igel et al., 2007). The required Love wave phase velocity c_L was defined as 4200 m/s. This value is obtained from the theoretical Love wave dispersion curve for a spherically symmetric earth model based on ak135 (Kennett et al., 1995).

The peak rotation rates of all earthquakes recorded either by 'UG-1' or 'C-II' with an epicentral distance exceeding 20° (2223 km) were included into the figure. The fact that Ms is only applicable to distant earthquakes reduces the number of relevant events

to eight. They range from M 6.6 to M 8.3 with distances up to 88.83° (9877 km). All events were filtered in a narrow band with central period of 30 s to be comparable to the theoretical peak values. Now, the observed peak rotation rates (black crosses) in comparison to the expected peak rotation rates (coloured lines) can be withdrawn from Figure 4.4.

'Given the relatively large uncertainties of single station magnitude estimation' (Igel et al., 2007), the observed rotation rates meet the theoretical values quite well. Especially the 2003.09.25 Hokkaido (M 8.3) rotations show an excellent correlation with the estimations.
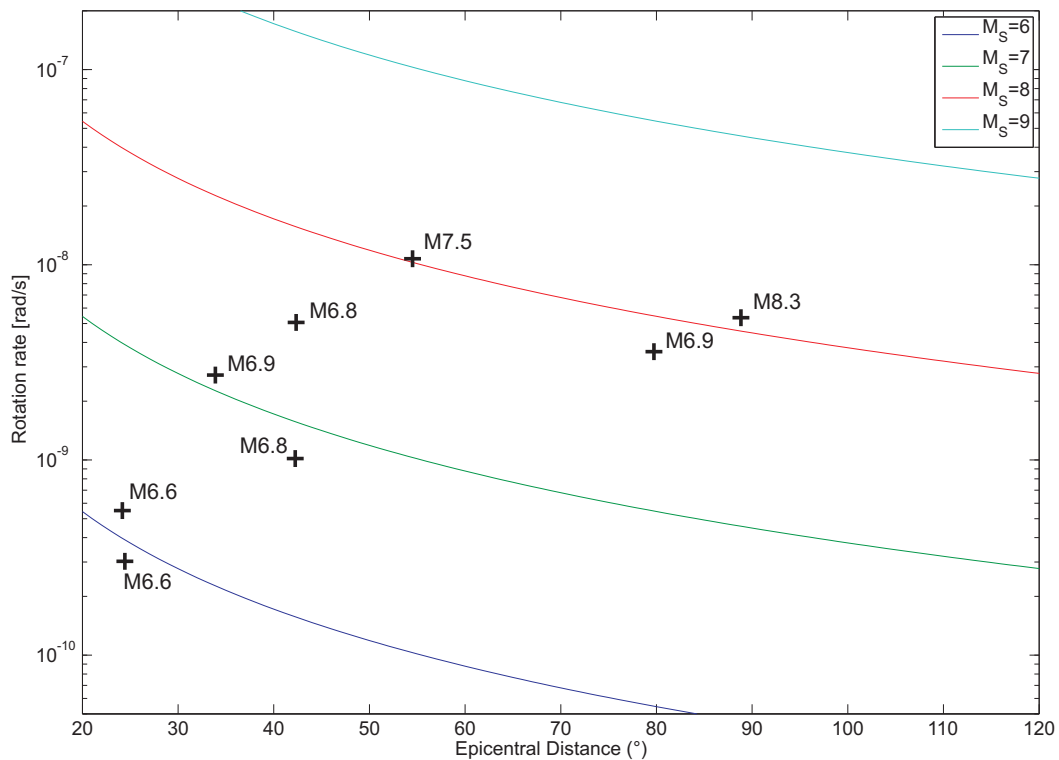
Figure 4.4: Peak rotation rates (black crosses) observed by 'UG-1' and 'C-II' over distance compared to the theoretical peak rotation rates derived from the Surface wave magnitude Ms (coloured lines). The observed data was filtered with a central frequency of 30 s.

4.1.4. Transverse acceleration and rotation rate

Theory tells us that transverse acceleration is comparable in phase and amplitude to rotation rate around a vertical axis (Subsection 1.1.1). In this part of the thesis we will investigate if this is also true for our observed data, as it was shown by Igel et al. (2007) for the data of the ring laser 'G0' at the Wettzell station. Thus, superposition plots displaying the fit between rotation rate in rad/s of either 'C-II' or 'UG-1' and the corresponding transverse acceleration component in m/s^2 are generated here for direct comparison.

In Figure 4.5 the signals from the 2003.03.11 Papua New Guinea Region (M 6.8) earthquake are shown. The two top plots represent the superposition of transverse acceleration (black) and 'UG-1' rotation rate (red) plus its related plot of maximum CC-Coefficients generated in a sliding 20 s time window, quantifying the correlation between the two components. The latter gives a good impression of the fit with 1 being maximal and 0 the minimal correlation between the two signals. The bottom two plots are the corresponding analysis for the 'C-II' rotation rate (green). All signals were processed by a lowpass filter with a cutoff period of 10 s. The backazimuth angle required for the calculation of the transverse component from the two horizontal translational components accounts to 330.6° for this event.

Firstly, in both superpositions we can see an excellent fit in phase mainly in the surface wave sector starting at about 1200 s. This is stressed once more by the maximal CC-Coefficient values of about 0.9852 ('UG-1') and 0.9849 ('C-II'). And secondly, as we stated in Subsection 4.1.2, 'C-II' and 'UG-1' deliver almost the same signal. While the two rotation signals look almost identical at first, the comparison with the transverse acceleration reveals the differences more clearly. The higher maximal CC-Coefficients for the 'UG-1' rotation rate and the transverse acceleration supports the conclusion that its signal is more accurate than 'C-II's.

We now carry out the same investigations for all other 14 events, relying on 'UG-1' and/or 'C-II' recordings depending on which ring laser was operating at the time of the relevant earthquake. The resulting plots are comparable to Figure 4.5 and can be found in Appendix E for 2003 and 2004 events. For detailed analysis we chose the same three earthquakes as in the preceding sections. The required backazimuth values can
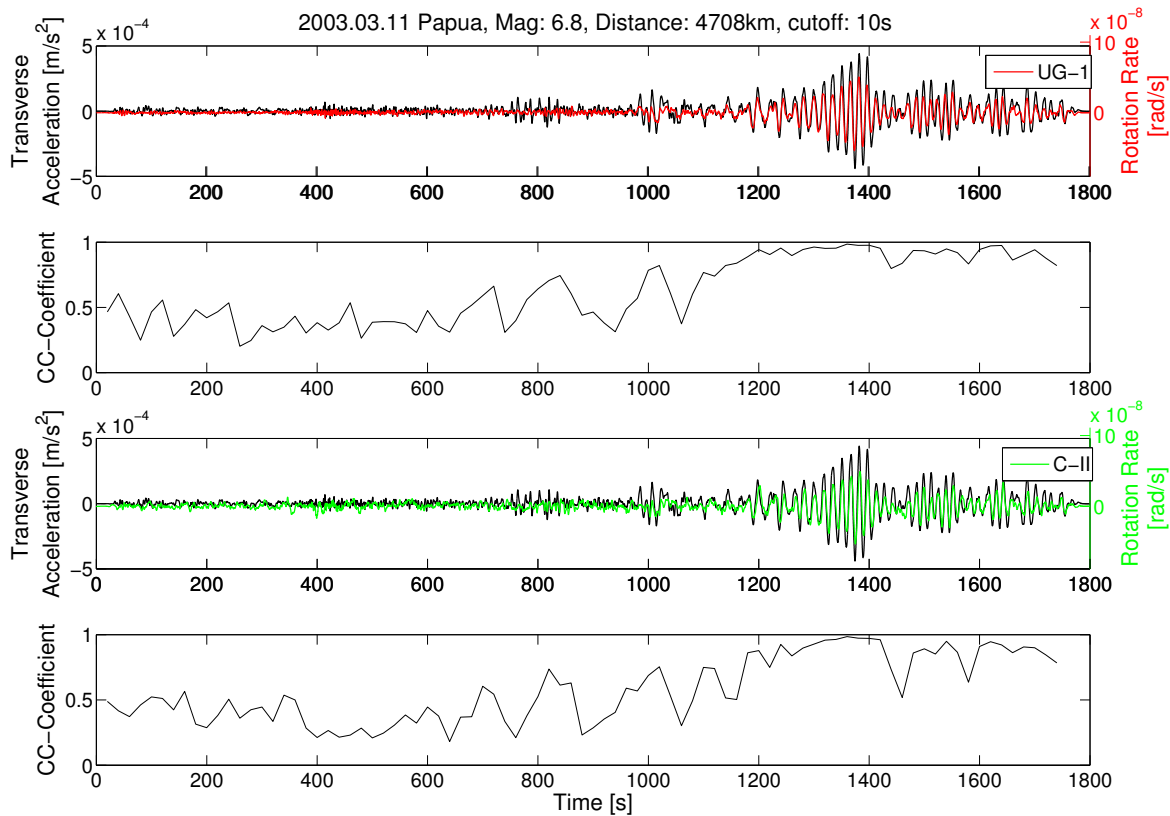
Figure 4.5: Top: Superposition of transverse acceleration (black, left axes) and rotation rate of the ring laser 'UG-1' (red, right axes) plus the corresponding maximal CC-Coefficients over time. Bottom: the two comparable plots for 'C-II' data (green).

be obtained from Table B.1. The signals were again lowpass-filtered with 10 s and 1 s, respectively. The comparison between vertical component of rotation ('UG-1') and transverse acceleration for the three events achieved results displayed in Figure 4.6.

The top event confirms the theory and shows an excellent fit in phase throughout the signal, but mainly in the surface wave section starting at about 1200 s.

The middle event reveals for indefinable reasons a very bad correlation. An explanation could be the high noise level of the translational data clearly visible in Figure C.4.

The bottom event shows a convincing fit in phase as well as in amplitude only in the first part of the signal. However, for earthquakes with low epicentral distances the planar wave assumption is not valid anymore.
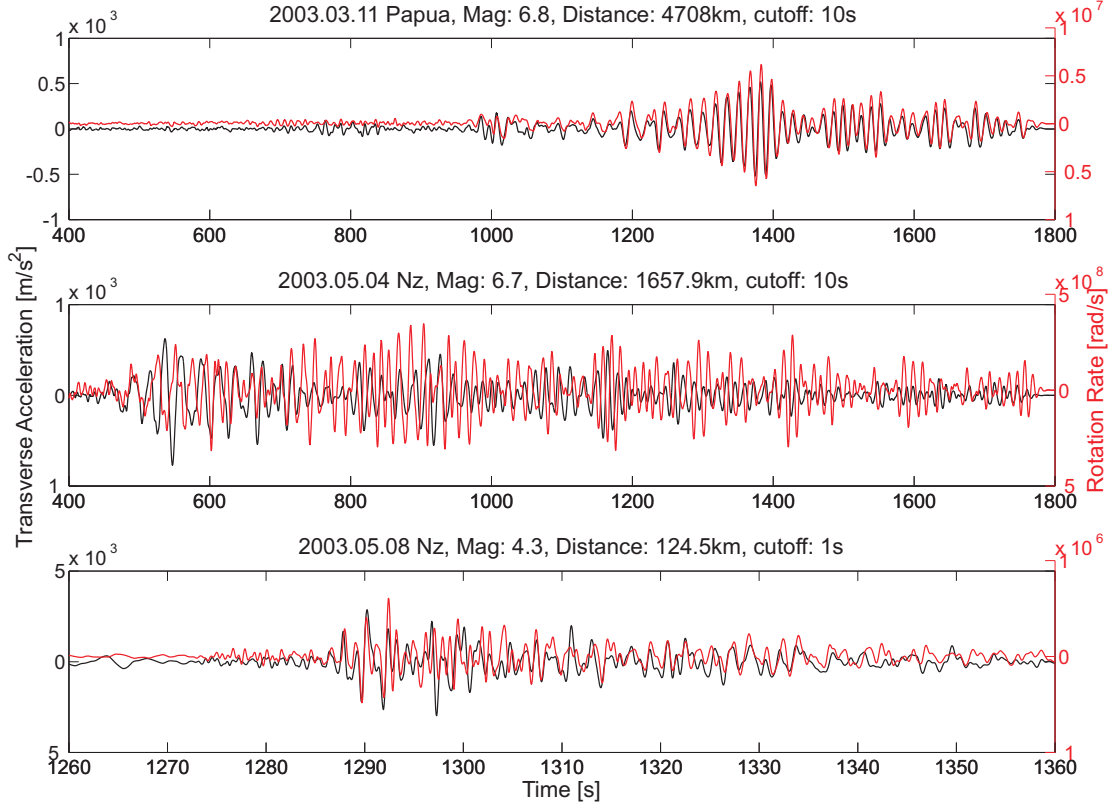
Figure 4.6: Superposition of transverse acceleration (black, left axes) and 'UG-1' rotation rate (red, right axes) for three selected events with different magnitudes and epicentral distances. The data was lowpass-filtered with a cutoff period of 10 s and 1 s, respectively.

The effect of Instrument Correction and its importance for translational data has already been discussed in Subsection 3.2.2. It was stated that all seismometer data need a correction for the instrument response. In combination with the latter section we can now clearly demonstrate the positive effect of the associated correction.

Therefore, we show in Figure 4.7 the superposition of the CC-Coefficient values over time between the filtered rotation rate recorded by 'UG-1' and transverse acceleration before (blue) and after (black) the elimination of the instrument response. For both CC-Coefficient the 2003.03.11 Papua New Guinea (M 6.8) earthquake served as source. The fit is better for corrected data (higher CC-Coefficient values) especially in the surface wave section. This implies that the correction actually improves the data.
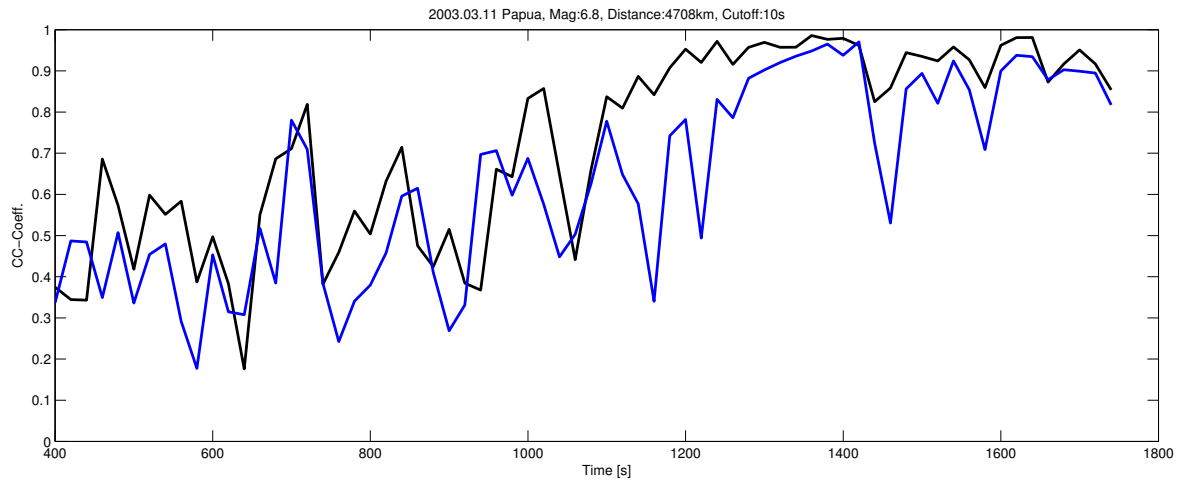
Figure 4.7: Effect of the instrument response shown by means of the max. CC-Coefficients over time between filtered transverse acceleration and rotation rate before (blue) and after (black) the correction of the 2003.03.11 Papua New Guinea event. Note the increase of correlation especially in the surface wave part starting at about 1200 s.

Backazimuth angles are required for the calculation of transverse acceleration for each event. They represent the angle that expresses the location of the earthquake origin relative to the station with 0/360° equal to north. Therefore, the backazimuth describes the direction the earthquake waves are propagating from.

To evaluate the quality of the fit between rotation rate and transverse acceleration, we now present polar plots for which we calculated the transverse acceleration of one event for each angle of possible backazimuth(0° - 360°) in 1° steps, compared the resulting signals to the observed rotation rate and calculated the maximum CC-Coefficient for the whole 30 min file length for each angle. We expect the CC-Coefficients (black) reaching maximum values at the actual backazimuth angle (red) (Figure 4.8 and Figure 4.9).

Again, we chose our three selected events from 2003 (2003.03.11 Papua New Guinea, 2003.05.04 New Zealand and 2003.05.08 New Zealand) to show the backazimuth dependence of the correlation between rotation rate and transverse acceleration.

The top event of Figure 4.6 leads to the polar plot of Figure 4.8. It confirms with its good correlation between max. CC-Coefficients and the actual backazimuth angle that the good results of the superposition plots are not coincidental.

The middle event of Figure 4.6 shows - as expected - a bad fit in the polar plot of
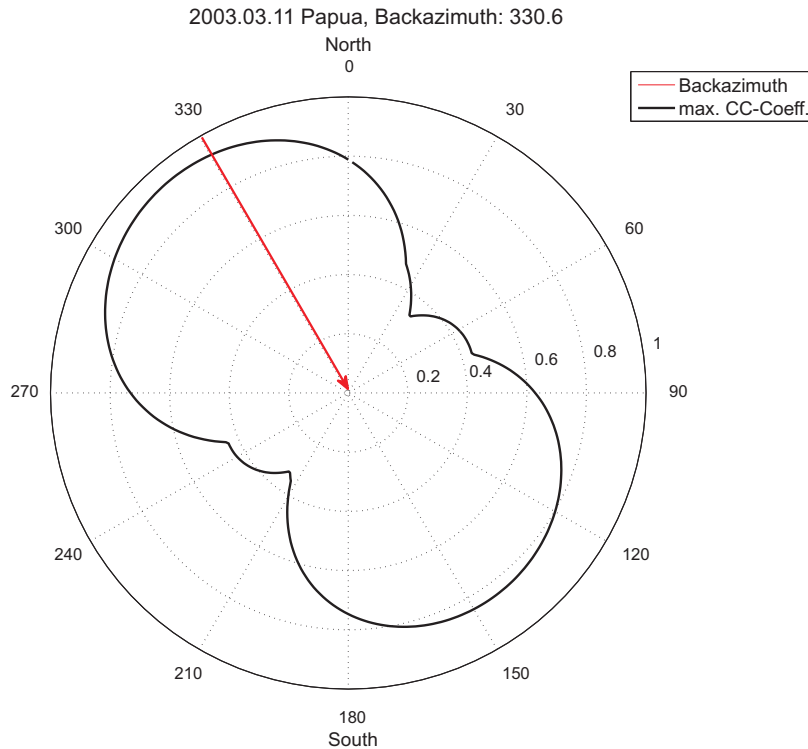
Figure 4.8: Polar plot of the peak CC-Coefficients (0 being no correlation, 1 maximal) between transverse acceleration (calculated for 0° to 360°) and observed rotation rate. The red arrow marks the actual backazimuth angle.

Figure 4.9 (top) as well, confirming the results of the previous section. Though, the peak around 120° remains to be understood.

The bottom event of Figure 4.6 reveals in its polar plot (Figure 4.9 (bottom)) a less good correlation than expected from the superposition plots. Hence, we zoom into two promising sections of the event: between 1270 s and 1295 s and between 1310 s and 1340 s. The corresponding polar plots can be found in Figure 4.10 and reveal a much better fit for both timewindows. The change of the max. CC-Coefficients can be explained by a disadvantageous distribution of the 20 s time windows before the zoom was applied.

2003.05.04 Nz, Backazimuth: 32.2

2003.05.08 Nz, Backazimuth: 334.2

Figure 4.9: See Figure 4.8.

2003.05.08 Nz, Backazimuth: 334.2

2003.05.08 Nz, Backazimuth: 334.2
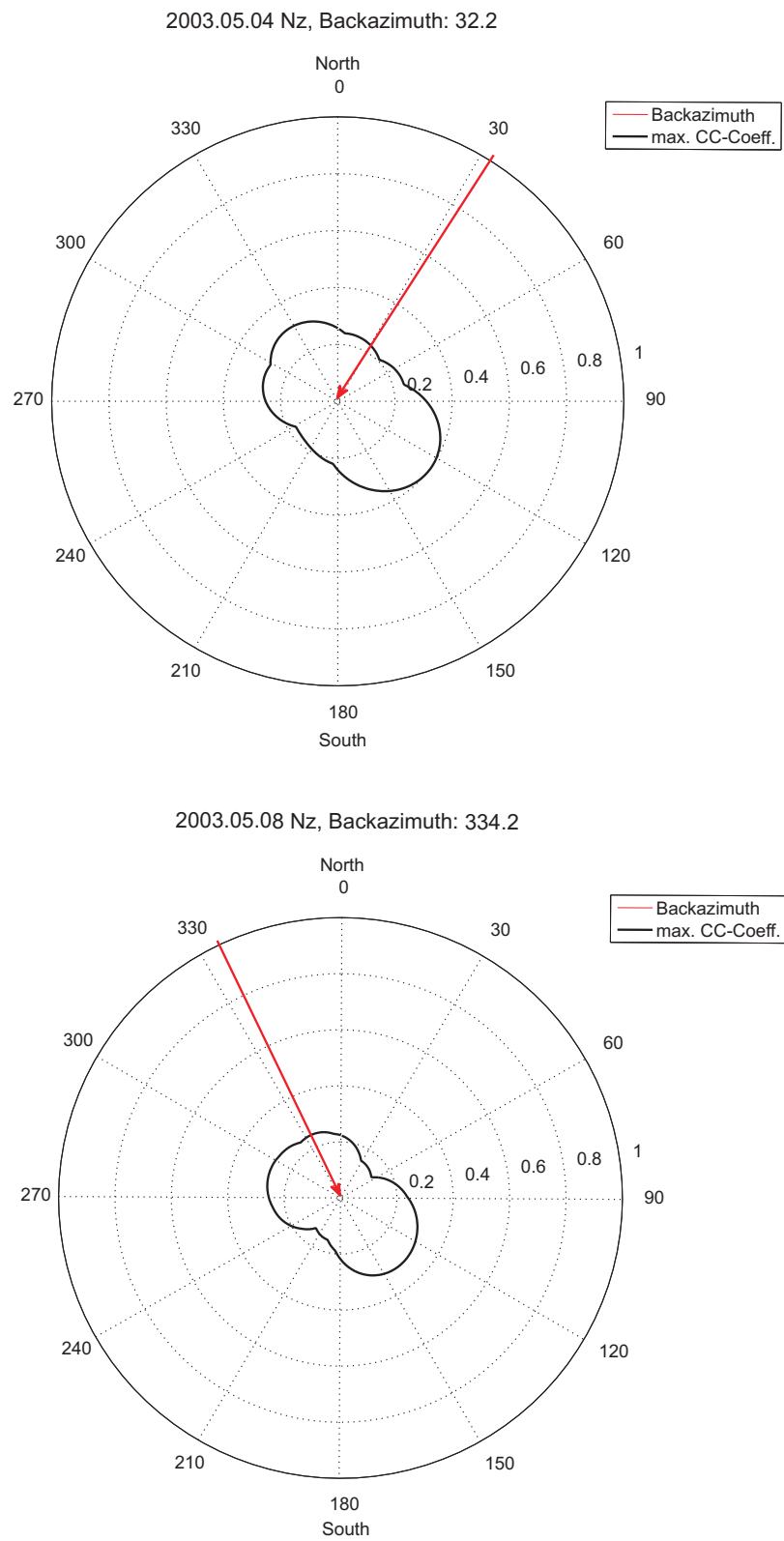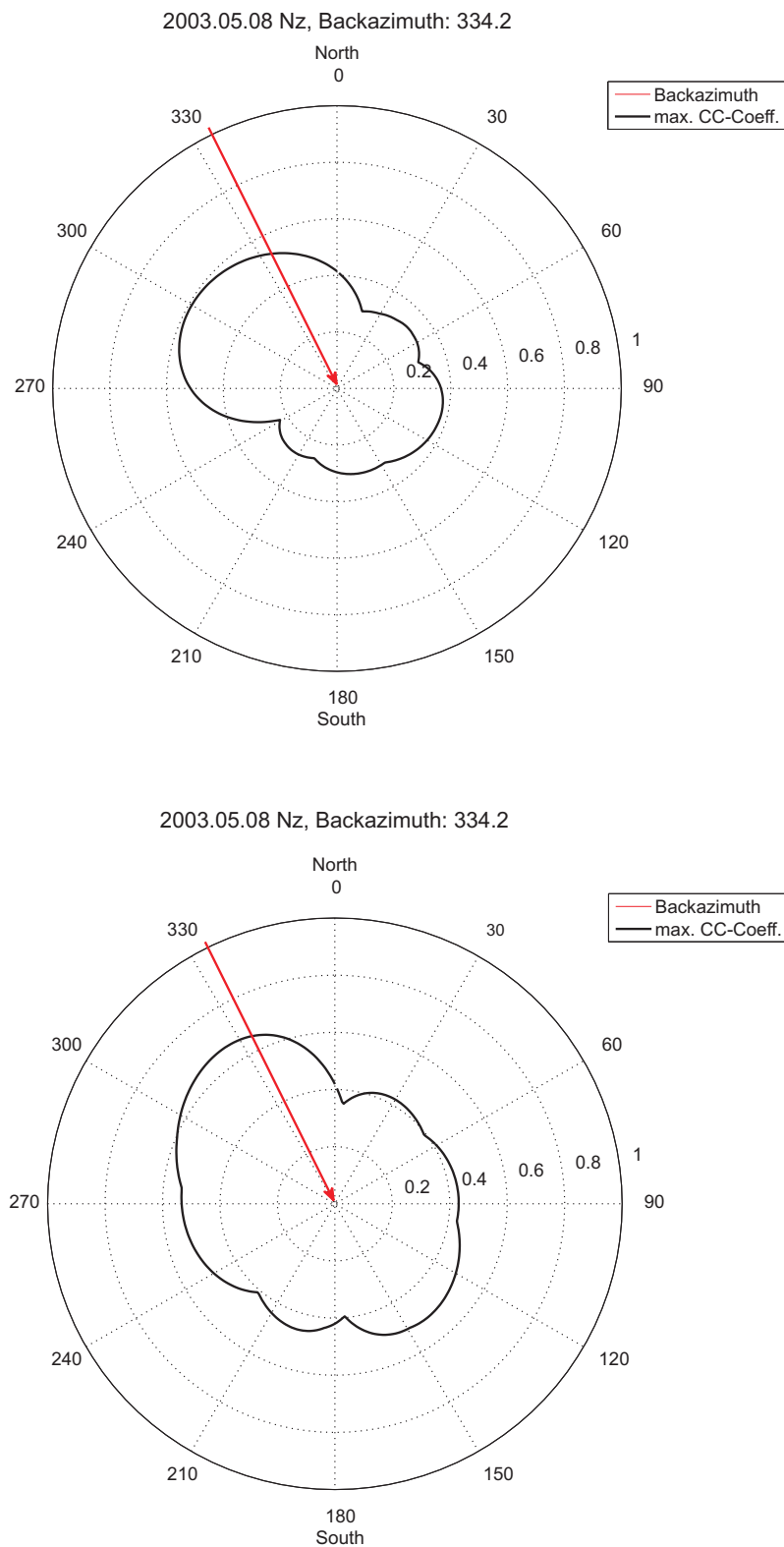
Figure 4.10: See Figure 4.8, data of the 2003.05.08 event after zooming into two sections of the acceleration and rotation signals. Note the increase of fit between peak CC-Coefficients and backazimuth (red) compared to the fit in Figure 4.9 (bottom).

4.1.5. Phase velocity derived from rotations

As described earlier in Subsection 1.1.1 it is possible to calculate the phase velocity from the relation between transverse acceleration and rotation rate. Equation (1.9) states that the acceleration needs to be divided by double the rotation rate to get the phase velocity under the measurement point. Only if the maximal CC-Coefficient of transverse acceleration and rotation rate in the corresponding time window of an event reaches over 0.8, the correlation is sufficiently high to derive the phase velocity.

Figure 4.11 shows the calculated phase velocity values (black crosses) for our observed data from the 2003.03.11 Papua New Guinea (M 6.8) event in addition to the super-position plots of transverse acceleration and rotation rate for 'UG-1' (red) and 'C-II' (green). Before the velocity was determined over a shifting 20 s time window, the signals were lowpass-filtered with a cutoff period of 10 s. In the first plot the increase in phase velocity due to dispersion is not visible through the very slightly downward tilted, dotted line representing the average phase velocity. The phase velocity for the peak values of transverse acceleration and of rotation rate in this case reaches 4.3541 km/s. The results of the 'C-II' data are - as expected - almost identical with the 'UG-1' data. However, latter shows even more clearly the effect of dispersion.

For other events with CC-Coefficient of at least 0.8, this analysis does not deliver convincing results as shown for the Papua New Guinea event. A main problem was that for two earthquakes (the 2003.06.07, Papua New Guinea event with a maximal CC-Coefficient of 0.98 and the 2003.09.25 Hokkaido event with a maximal CC-Coefficient of 0.92) only parts of the events are available in our dataset.

Despite the good results for some events, for most of our earthquakes the correlation between transverse acceleration and rotation rate is not distinctive enough. Quantitatively and qualitatively these investigations are not comparable to the corresponding analysis based on data from the 'G' ring laser in Wettzell, Germany by (Igel et al., 2007). One possible cause of the occuring difficulties could be due to incorrect translational data e.g. by wrong orientation of the seismometer. As already mentioned, there is a lack of instrument documentation. Therefore, associated problems can not be totally excluded.
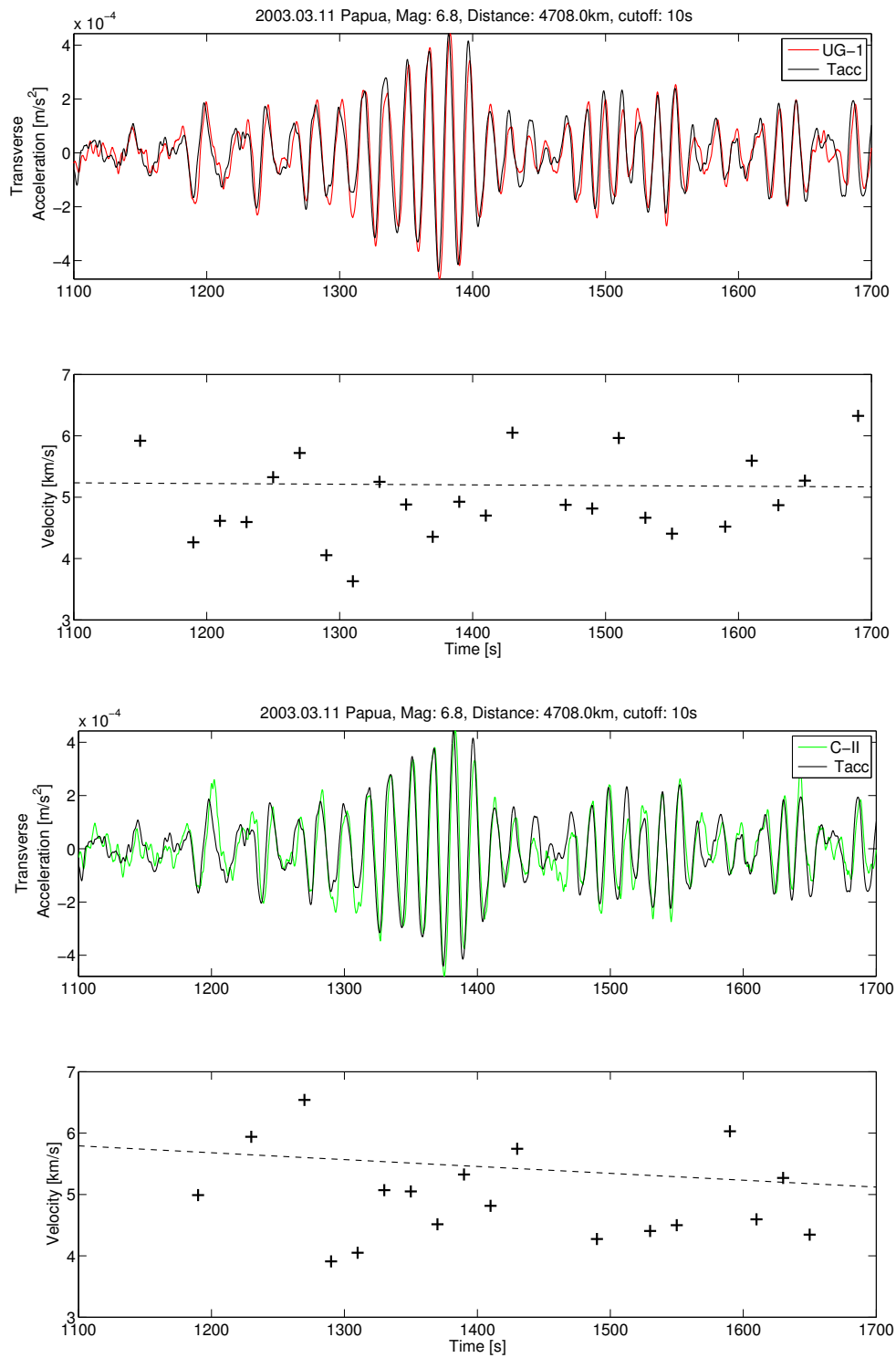
Figure 4.11: Superposition of transverse acceleration and rotation rate (above) and the phase velocity values over a 20s time window (below) of 'UG-1' and 'C-II' data, respectively. The dotted line represents the average phase velocity.

4.2. G0

After the evaluation of data provided by ring lasers with a vertical axis, we will now concentrate on 'G0' and its recorded rotational seismograms. Because 'G0' is the only ring laser with a horizontal axis we can not conduct the same analysis as done with 'C-II' and 'UG-1' recordings in Section 4.1. Therefore, the discussion starts with basic analysis concerning epicentral distances and magnitude distributions, revealing the general quality. Then the focus is laid on rotation rate compared to theoretically derived tilt data.

One of the most promising quality checks would have been to compare 'G0' rotation rate directly with tilt rate measured by a tiltmeter, because at the Earths surface rotation around a horizontal axis is equal to tilt (Subsection 1.1.1). By the time writing this thesis there was no collocated tiltmeter available in the Cashmere Cavern. Consequently, this analysis is not feasible at the moment. More recent stations like Piñon Flat Observatory in California are automatically equipped with the latter instrument (Velikoseltsev and Schreiber, 2005).

4.2.1. Running stability

From the 21 earthquakes of the dataset for this study, 'G0' was able to record 20. Hence, it offers the highest running stability over time amongst all Christchurch ring lasers. One of the main goals of future projects will be to stabilise 'C-II' and 'UG-1' allowing more continuous data like already provided by 'G0'.

Furthermore, only 'G0' was able to record both most significant earthquakes in New Zealand in 2003 and 2004:

2003.05.04	Kermadec Islands	M 6.7
2004.11.22	Off West Coast of	M 7.1
	the South Island Nz	

The according plots for these two events can be found in Appendix C and D on page 87 and page 96.

4.2.2. Magnitude distance distribution

The high running stability of 'G0' mentioned before, leads to a higher number of recorded events presented in the magnitude-distance distribution (Figure 4.12), resulting in a more balanced spreading than for the ring laser 'C-II' and 'UG-1' (Figure 4.1). With more events contributing, this plot is even more representative.

Analogue to the magnitude-distance distribution of the other two ring lasers' data, the events recorded by 'G0' cover a range of almost 88° (9785 km) of epicentral distance and vary from M 4.2 to M 8.3. We can again see a rough division into two clusters, one representing the regional and the other one the teleseismic events. In contrast to the latter instruments, 'G0' offers more data in the teleseismic range, with two earthquakes even larger than M8. Unfortunately one of them, the 2004.12.23 Nz (M 8.1) event is not suitable for further analysis, because the seismometer traces are clipped.
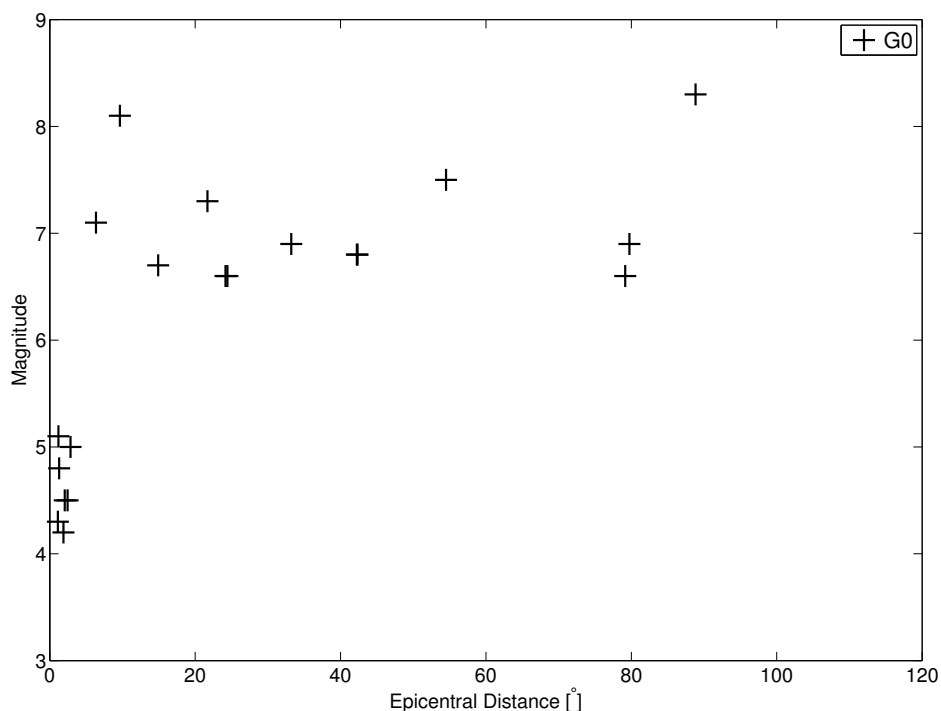
Figure 4.12: Magnitude-distance distribution of all 20 events recorded by 'G0' in 2003 and 2004.

4.2.3. Surface wave magnitudes

The derivation of rotations   from the Surface wave magnitude Ms definition was carried out here in analogy to the analysis in Section 4.1.3. For 'G0' the number of relevant earthquakes accounts to ten, because the Surface wave magnitude is only applicable above an epicentral distance of 20°. The required Rayleigh wave phase velocity c_R was defined as 3800 m/s according to the Gutenberg Earth model (Aki and Richards, 2002).

Figure 4.13, represents the observed peak rotation rates in rad/s (black crosses) in comparison to the expected values (coloured lines) at certain magnitudes and epicentral distances (Igel et al., 2007). All data was bandpass-filtered and hence presented here in a narrow frequency band of about 30 s. Unlike in Section 4.1.3, here the larger events (M 7.1, M 7.5 and M 8.3) show the maximal deviation, while the smaller earthquakes
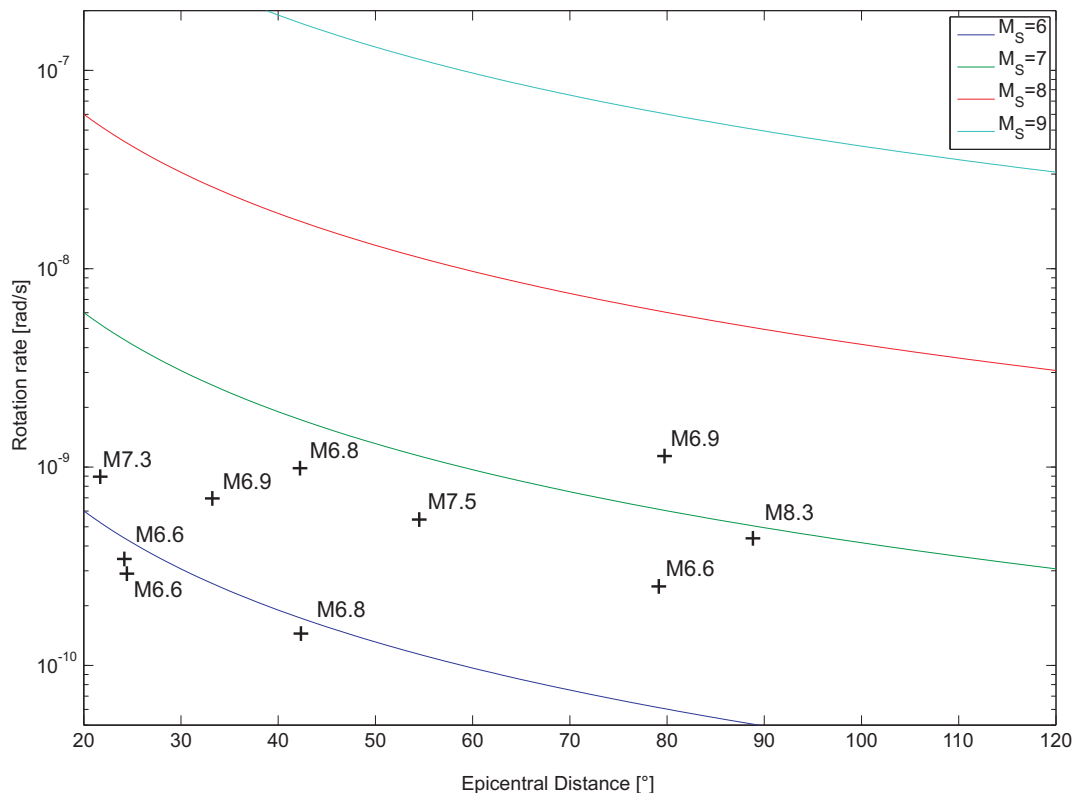
Figure 4.13: 'G0' peak rotation rates (black crosses) over distance compared to the theoretical peak rotation rates derived from the Surface wave magnitude Ms (coloured lines). The observed data was filtered with a central frequency of 30 s.

fit the expectations quite well. Especially, the 2003.09.25 Hokkaido (M 8.3) event shows a relatively bad fit between observed and theoretical data.

The derivation of velocity according to the Surface wave magnitude Ms in Equation (1.10) is carried using the calculation of amplitudes first:

$$A = T \cdot 10^{Mag - 1.66 \cdot log_{10} d - 3.3}. \tag{4.1}$$

The differentiation of Equation (4.1) leads to the expected velocity over time. We chose again T=30 s. Figure 4.14 shows the theoretical peak velocity in m/s (coloured lines) over distance compared to the observed peak Z-component values of translation (black crosses). The large scatter is comparable to the one observed in Figure 4.13.
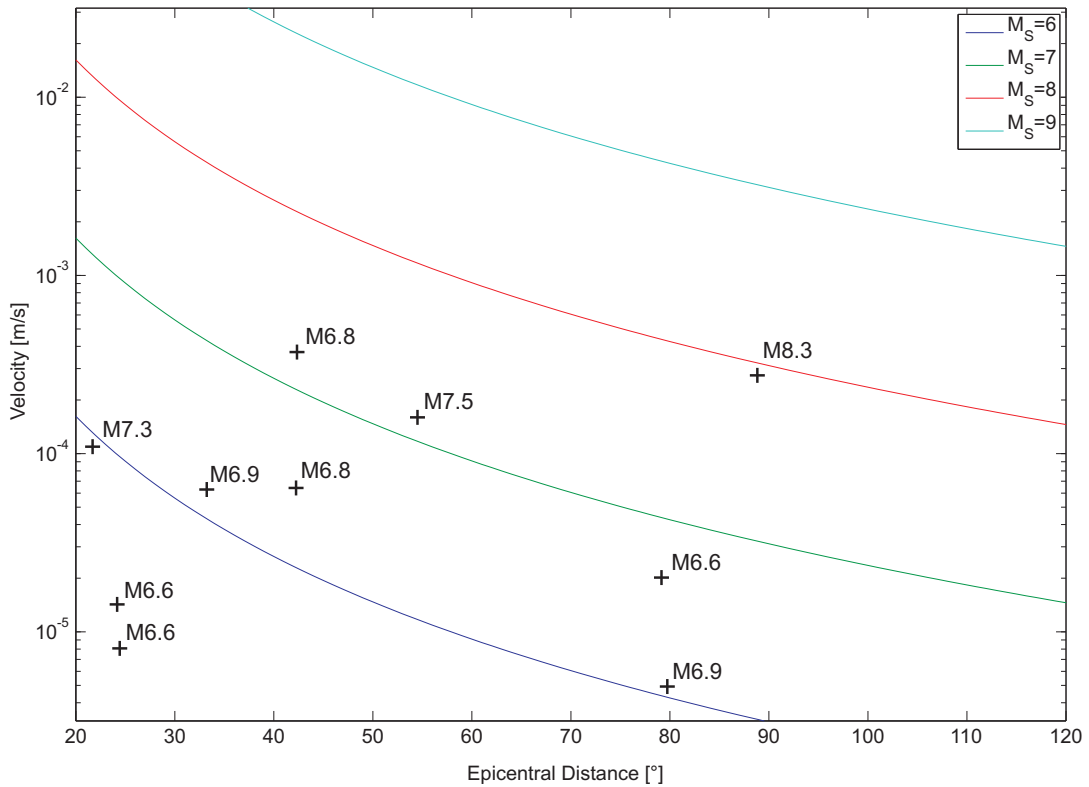
Figure 4.14: Z-component peak velocities (black crosses) over distance compared to the theoretical peak velocities derived from the Surface wave magnitude Ms (coloured lines). The observed data was filtered with a central frequency of 30 s.

4.2.4. Rotations and Li-Tilt

According to Equation (1.16) and (1.17), rotation around a horizontal axis is identical with tilt at the free surface. Hence, the rotational data offered by 'G0' is comparable to tilt data. Though, as there is no tiltmeter data available for the observatory, we chose derived tilt for direct comparison. Besides theoretical tilt and tilt derived from array measurements, there is also the possibility to obtain tilt derived from translations with the Li-method (Li et al., 2001, 2002).

Pham et al. (unpublished) obtained excellent correlation between theoretical tilt for the Wettzell observatory and tilt derived with Li's approach (Figure 4.15), proving that this method can be used to generate a reliable tilt signal for suitable cases.

The approach allows us to derive tilt from P or Rayleigh waves, because mainly they cause the ground tilting. In our case we rely on the Rayleigh wave part, therefore the tilt component in y-direction - according to elastic theory - can be calculated (Li et al., 2002) by:

$$\Omega_y \quad = \quad \frac{\delta D_Z}{\delta x} = ia D_Z \tag{4.2}$$

$$= \quad i\frac{\omega}{c_R} D_Z \tag{4.3}$$

where the translational component D_Z is the vertical displacement, ω the angular frequency of the Rayleigh wave and c_R the Rayleigh wave phase velocity in x direction. For all events we chose a constant Rayleigh wave phase velocity of 3800 m/s according to the Gutenberg Earth model (Aki and Richards, 2002).

The resulting transverse Li tilt is comparable to the transverse component of rotation. However, the Christchurch observatory is equipped with only one ring laser recording a horizontal component. So we are not able to use the transverse tilt and transverse rotation, because the calculation of the transverse rotation needs both horizontal components. We therefore use the backazimuth angle and calculate the tilt comparable to our observations. The corresponding Figure 4.16 illustrates the superposition of the unfiltered Li tilt rate (black) and observed unfiltered rotation rate (red) around the y-axis (top) and the same superposition for the data lowpass-filtered with a cutoff
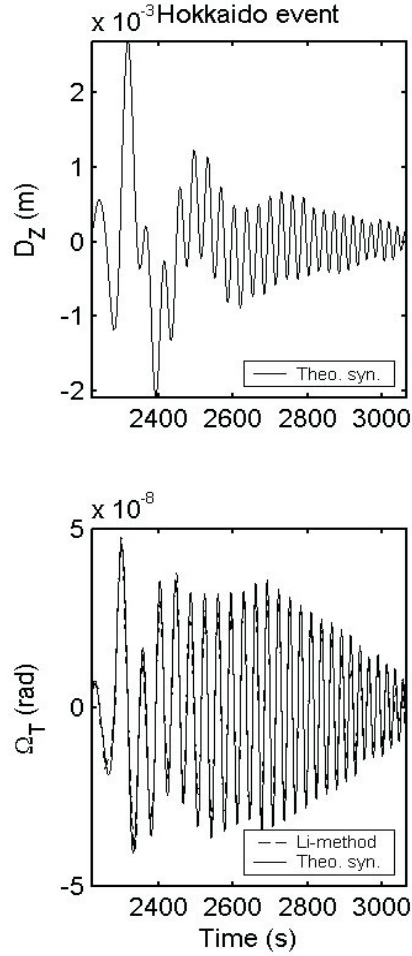
Figure 4.15: Top: Theoretical seismic signals in the Rayleigh wave section of the 2003.09.25 Hokkaido (M 8.3) event received at Wettzell observatory. DZ is the vertical component of theoretical displacements. Bottom: Superposition of the theoretical tilt and Li-tilt (Pham et al., unpublished).

frequency of 10 s (middle) for the 2003.09.25 Hokkaido (M 8.3) earthquake. Note that the Li tilt is calculated here for the total file length, while being only applicable for the Rayleigh wave section.

The two upper plots reveal that the observed data is comparable in phase but not in amplitude to the derived Li tilt rate throughout the Rayleigh wave part (starting at 116 s). We observe a good fit in phase for the filtered data but it remains to be understood why there is a correction factor needed to achieve a fit in amplitude. A possible reason could be the uncertainties relying to the phase velocity c_R values. In the
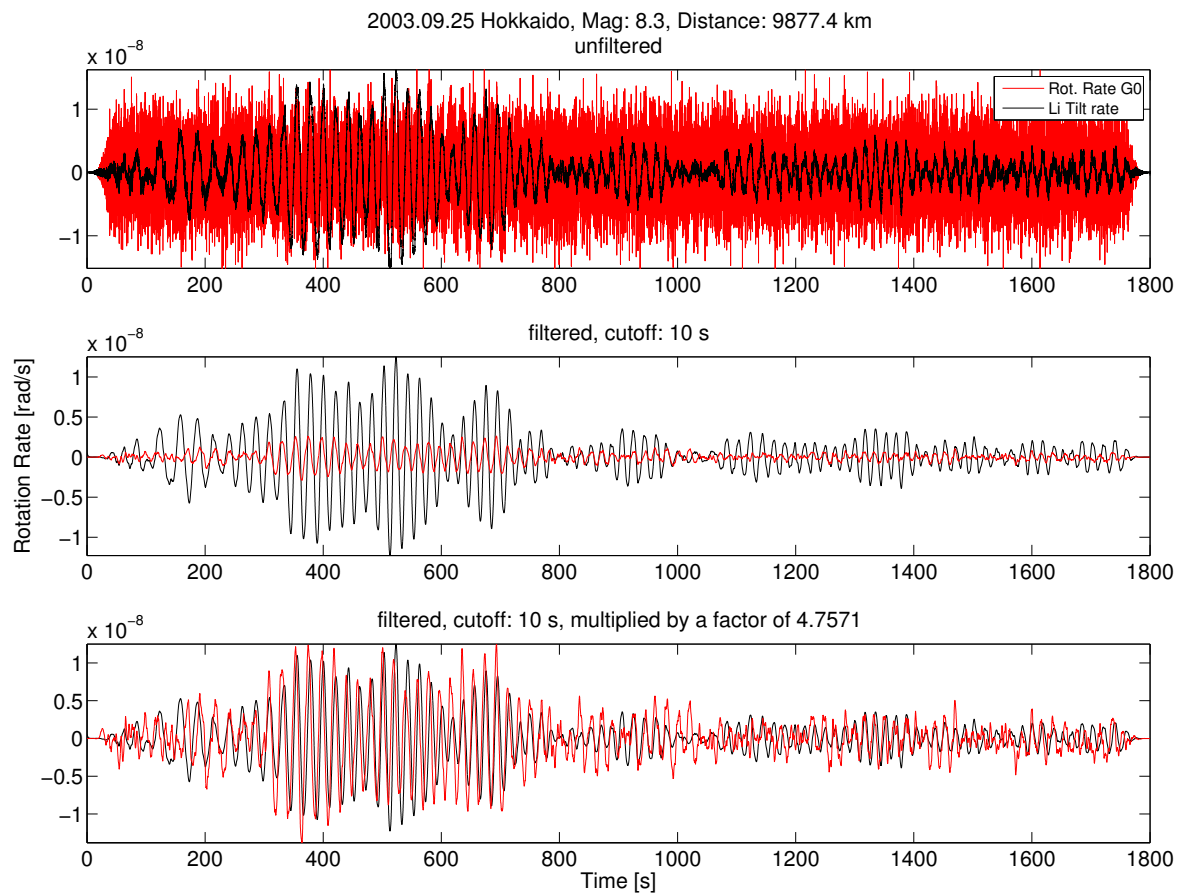
Figure 4.16: Superposition plots of Li tilt rate (black) and rotation rate (red) around a horizontal axis. Top unfiltered data, middle filtered with a cutoff frequency of 10s, and bottom filtered and rotation rate multiplied with a correction factor to fit the Li data.

bottom plot the Li tilt rate and the rotation rate are superimposed after the observed data was multiplied with a correction factor, stressing the good phase correlation. For the selected event this correction factor accounts to 4.7571. The distribution of the correction factors for all relevant earthquakes is plotted over distance (top) and over magnitude (bottom) in Figure 4.17. Both plots reveal a similar distribution. The correction factor varies between 0.13 and 28.91 (Table B.2). The minimal deviation from the expected tilt indicated by the value 1 was almost achieved by only two teleseismic events with correction factors of 0.13, 0.56.

This method is only reasonable for teleseismic events with a dominant Rayleigh wave section. The corresponding plots for the relevant ten events (with an epicentral distance

larger than 20 °) recorded by 'G0' can be found in Appendix F. Why only half of the events show a good fit in phase will be a topic of future investigations.
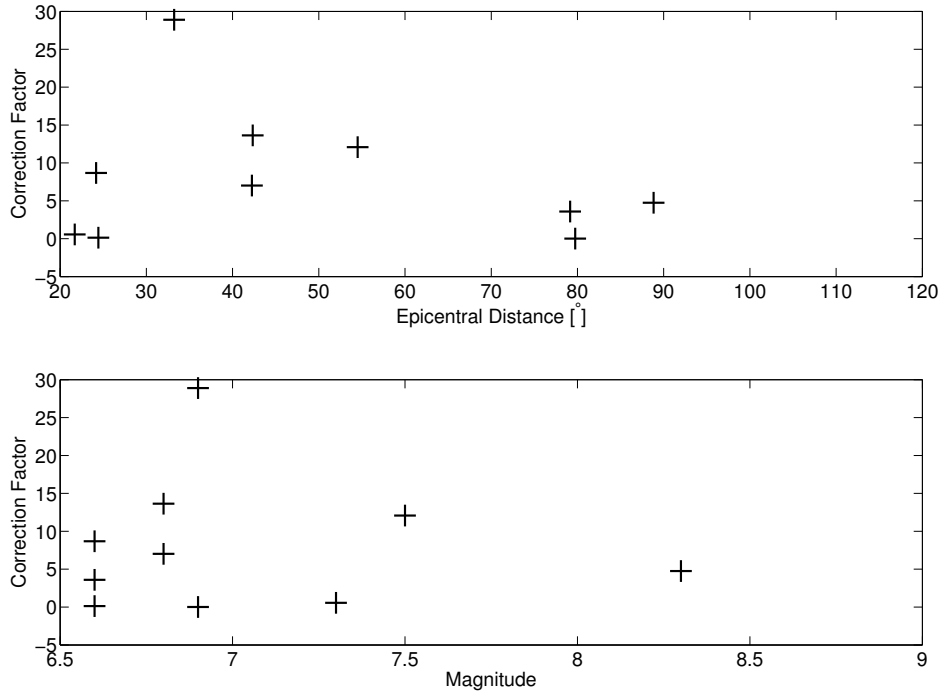
Figure 4.17: Correction factors for the observed data to fit the Li tilt data over distance (top) and over magnitude (bottom).

4.3. Summary

In the last chapter we analysed the observed rotational data based on different theoretical approaches, revealing excellent correlation between 'UG-1' and 'C-II' data but also unidentified problems for some transverse acceleration compared to rotation rate plots and superposition plots of li tilt and observed tilt. Throughout the evaluation we can assess that the low frequency contents of teleseismic events show a better fit than the high frequency parts of the local or regional quakes. Furthermore, we can state that 'G0' is the most reliable ring laser in Christchurch in terms of running stability, with in total 20 events recorded in 2003 and 2004, even though it was not designed for geoscientific purposes.

Chapter 5.

Conclusion/Discussion

In this thesis, we analysed 21 earthquakes - covering a wide range of magnitudes and epicentral distances - recorded by three ring lasers in Christchurch, New Zealand in 2003 and 2004 regarding the data's compatibility with theory according to Cochard et al. (2006) and Igel et al. (2007).

The rotational data - supplemented by three components of translation of a collocated broadband seismometer - is provided in ASCII format and can be divided into two major groups: rotation rate around a vertical axis ω_z and rotation rate around a horizontal axis ω_y, both in rad/s.

For ω_z, the focus was laid on its correlation with transverse acceleration derived from the horizontal translational components. This analysis is applicable to 14 events of our database. The observed fit in phase, as predicted by theory, is expressed by means of maximal Cross Correlation Coefficients. Latter reach excellent values between 0.92 and 0.99 for three teleseismic events with epicentral distances of at least 42° and a minimum magnitude of 6.8., making these observations consistent with previous investigations based on data of the more sophisticated ring laser 'G' of the Wettzell observatory (Igel et al., 2007). Five out of 14 events, all of them teleseismic, deliver a Cross Correlation Coefficient higher than 0.8, indicating a noteworthy correlation. The signals of weaker, regional events reveal a bad fit between transverse acceleration and rotation rate of maximal 56%. Despite the observed excellent correlations (up to 99%) between collocated 'UG-1' and 'C-II' data for different frequency contents, the further analysis affecting transverse acceleration altogether surprises with less correlation than expected. Hence, the derivation of phase velocity (point measurement) from

the relation just mentioned, was only possible for the six events with Cross Correlation Coefficient of 0.8 and higher. But due to several problems we achieved reliable results for only one earthquake (2003.03.11 Papua New Guinea (M 6.8) event). The phase velocity derived from peak rotation rate and peak transverse acceleration values accounts in this case to 4.3541 km/s. This observation is comparable to the theoretical value of Love wave phase velocity of about 4.1 km/s in the frequency band of 30 s according to the Gutenberg Earth model (Aki and Richards, 2002).

The results concerning evaluation of ω_y (this component is equal to tilt at the free surface) are mainly based on comparison with derived tilt data according to the Li method (Li et al., 2001, 2002). For five of the ten relevant teleseismic earthquakes of our database we observe a good fit in phase during the Rayleigh wave section, while significant differences in amplitude for all events needed factors of correction between 0.1297 and 28.9090. Difficulties according to the estimations of the required Rayleigh wave phase velocities could be imposed. However, the lack of correlation remains to be understood and will be subject to future projects based on e.g. additional tiltmeter data. Hence, the measurements of horizontal rotation rates still promise good appliance for seismometer tilt corrections.

Further detailed analysis of the data is required to fully exploit the potential of ring laser and their applicability for seismology. Comparison with synthetics and tiltmeter data is expected to emphasis the high quality of the recorded data and will further increase the importance of ring laser technology for seismology.

Abbreviations and symbols

Abbreviation	Meaning
ADC	Analogue to Digital Converter
CC-Coeff.	Cross-Correlation Coefficients
C-I	Canterbury Ring I
C-II	Canterbury Ring II
FESG	Forschungseinrichtung für Satellitengeodäsie, Germany
FOG	Fibre-Optic Gyro
G	Grossring
G0	Grossring 0
GNS	Institute of Geological and Nuclear Sciences, New Zealand
LabView	Laboratory Virtual Instrumentation Engineering Workbench by National Instruments
LLR	Lunar Laser Ranging
LSBvalue	Least Significant Bit value
Mb	Body wave magnitude
ML	Local magnitude

Abbreviation	Meaning
Ms	Surface wave magnitude
Mw	Moment magnitude
NEIC	National Earthquake Information Center, USA
PD	Photo Diode
PMT	Photo Multiplier Tube
SH	Horizontally polarised S waves
SLR	Satellite Laser Ranging
SV	Vertically polarised S waves
UG-1	Ultra Grossring 1
UG-2	Ultra Grossring 2
USGS	United States Geological Survey, USA
UTC	Coordinated Universal Time
Vi	Virtual instrument
VLBI	Very Long Baseline Interferometry

Symbol	Meaning	Unit
a	Acceleration	m/s^2
A	Amplitude	m
A_R	Effective area of the ring laser	m^2
c_L	Love wave phase velocity	m/s
c_p	Phase velocity of a point measurement	m/s
c_R	Rayleigh wave phase velocity	m/s
d	Epicentral distance	degree
D	Displacement	m
δf	Beat frequency	Hz
ϵ	Strain tensor	
f	Optical frequency	Hz
G	Deformation gradient	
h	Damping constant	
k	Wave number	1/m
λ	Optical wavelength	nm
p	Pressure	Pa
Ω	Rotation rate	rad/s
P	Perimeter	m
T	Period	s
ω_0	Natural frequency	1/s
ω	Frequency	1/s

List of Figures

List of Tables

Appendix A.

Ring laser specifications

Here we present additional information about the three ring lasers whose data this study is based on: 'C-II', 'UG-1' and 'G0'.

Table A.1: List of parameters of the ring laser 'C-II'.

C-II		
Axis of rotation		vertical
Area	A_R	$1m^2$
Perimeter	P	4 m
Wavelength	λ	632.9914 nm
Sagnac frequency	Δf	79.4 Hz
Pressure	p	266.64 Pa
Latitude		$-43.57475°$
Longitude		$172.62328°$
Gas mixture		He:Ne (40:1)
Isotope mixture		Ne20:Ne22 (50:50)
Zerodur$^®$		yes
Year of Construction		1995-1996

Table A.2: List of parameters of the ring laser 'UG-1'.

UG-1		
Axis of rotation		vertical
Area	A_R	$366.8633 m^2$
Perimeter	P	76.9340 m
Wavelength	λ	632.9914 nm
Sagnac frequency	Δf	1512.85 Hz
Pressure	p	799.92 Pa
Latitude		$-43.57475°$
Longitude		$172.62328°$
Gas mixture		He:Ne (40:1)
Isotope mixture		Ne20:Ne22 (50:50)
Zerodur$^{®}$		no
Year of Construction		2001

Table A.3: List of parameters of the ring laser 'G0'.

G0		
Axis of rotation		horizontal
		10° west of north
Area	A_R	$12.25 m^2$
Perimeter	P	14 m
Wavelength	λ	632.9914 nm
Sagnac frequency	Δf	288 Hz
Pressure	p	346.632 Pa
Latitude		$-43.57475°$
Longitude		$172.62328°$
Gas mixture		He:Ne (40:1)
Isotope mixture		Ne20:Ne22 (50:50)
Zerodur$^®$		no
Year of Construction		2000

Appendix B.

Earthquake Lists

A list of parameters and additional information about all earthquakes used in this study can be found in Table B.1 and Table B.2. The given information is partially based on the USGS/NEIC global seismic database on earthquake parameters (NEIC, 2007).

Additional assistance for the use of Table B.1:

It includes date, origin, magnitude, depth, distance (in km and degree), and backazimuth of the earthquakes.

■ marks an instrument that was able to record the event.

☐ marks an instrument that was not able to record the event.

For each event a basic plot can be found either in Appendix C or Appendix D according to the page number given in the table.

Additional assistance for the use of Table B.2:

The given information includes date, origin, magnitude, distance form Table B.1 and maximum rotation rate of the three ring laser, the maximum CC-Coefficients of the comparison between filtered rotation rate and transverse acceleration and the li tilt correction factor.

The maximum rotation rate is extracted from unfiltered data.

The Li tilt correction factor is given for events with at least 20° distance.

Table B.1: List of all earthquakes discussed in this thesis.

Date	Time [UTC]	Region	Lon. [°]	Lat. [°]	Mag.	Depth [km]	Dist. [km]	Dist. [°]	Backaz. [°]	C-II	UG-1	G0	plot page
2003.01.15	23:53:56	NZ	-40.96	174.14	5.0 Mb	72	316.9	2.85	23.8	■	□	■	86
2003.03.11	07:27:32	Papua	-4.69	153.24	6.8 Ms	40	4708.0	42.34	330.6	■	□	■	86
2003.05.02	19:05:38	NZ	-41.74	172.04	4.2 ML	12	209.0	1.88	346.6	■	□	■	87
2003.05.04	13:15:18	Kermadec Islands	-30.53	-178.23	6.7 Mw	62	1657.9	14.91	32.2	■	□	■	87
2003.05.08	21:08:09	NZ	-42.56	171.96	4.3 ML	12	124.5	1.12	334.2	■	□	■	88
2003.06.07	00:32:45	Papua	-5.09	152.50	6.8 Ms	33	4696.9	42.24	329.4	■	■	■	88
2003.07.27	02:04:11	Fiji	-21.08	-176.59	6.6 Mw	212	2687.6	24.17	25.3	□	■	■	89
2003.09.25	19:50:06	Hokkaido	41.81	143.91	8.3 Mw	27	9877.4	88.83	338.9	■	■	■	89
2003.11.06	10:38:04	Vanuatu	-19.26	168.89	6.6 Mw	113	2717.6	24.44	351.5	■	■	■	90
2003.12.27	16:00:59	Loyalty Islands	-22.01	169.77	7.3 Mw	10	2412.4	21.70	352.8	□	□	■	90
2004.02.11	00:31:39	NZ	-45.24	170.12	4.5 ML	12	272.4	2.45	226.3	□	□	■	92
2004.02.11	21:40:33	NZ	-42.23	174.75	4.5 ML	52	229.1	2.06	50.0	□	□	■	92
2004.05.03	04:36:50	Chile	-37.69	-73.41	6.6 Mw	21	8801.6	79.16	132.5	□	□	■	93
2004.06.23	04:28:30	NZ	-42.83	171.36	5.1 ML	14	132.3	1.19	308.4	■	□	■	93
2004.08.19	16:03:39	NZ	-43.80	170.87	4.8 ML	4	143.4	1.29	259.4	■	□	□	94
2004.09.06	12:42:59	Sandwich Islands	-55.37	-28.98	6.9 Mw	10	8866.7	79.74	167.7	■	□	■	94
2004.10.08	08:27:53	Solomon Islands	-10.95	162.16	6.9 Mw	36	3769.0	33.90	345.0	■	□	■	95
2004.11.09	23:58:23	Solomon Islands	-11.15	163.71	6.9 Mw	13	3693.9	33.22	343.9	□	□	■	95
2004.11.11	21:26:41	Indonesia	-8.15	124.87	7.5 Mw	10	6061.2	54.51	295.8	■	□	■	96
2004.11.22	20:26:23	NZ	-46.69	164.77	7.1 Ms	10	706.5	6.35	238.0	□	□	■	96
2004.12.23	14:59:04	NZ	-49.31	161.35	8.1 Mw	10	1074.1	9.66	229.7	□	□	■	97

Table B.2: List of all earthquakes discussed in this thesis (continued).

Date	Time(UTC) [UTC]	Region	Mag.	Dist. [°]	max. rotrate $\times 10^{-8}$rad/s		G0	max. CC-Coeff.	li correction factor
					C-II	UG-1			
2003.01.15	23:53:56	NZ	5.0Mb	2.85	316.49	355.62	5.28	0.29/0.31	-
2003.03.11	07:27:32	Papua	6.8Ms	42.34	48.22	51.2	1.66	0.99/0.98	13.64
2003.05.02	19:05:38	NZ	4.2ML	1.88	170.89	179.46	2.99	0.54/0.56	-
2003.05.04	13:15:18	Kermadec Islands	6.7Mw	14.91	192.95	206.03	3.51	0.48/0.46	-
2003.05.08	21:08:09	NZ	4.3ML	1.12	216.46	221.74	3.25	0.80/0.80	-
2003.06.07	00:32:45	Papua	6.8Ms	42.24	-	19.49	2.63	0.98	7.02
2003.07.27	02:04:11	Fiji	6.6Mw	24.17	-	51.91	8.20	0.64	8.68
2003.09.25	19:50:06	Hokkaido	8.3Mw	88.83	60.20	-	1.97	0.92	4.76
2003.11.06	10:38:04	Vanuatu	6.6Mw	24.44	4.08	-	3.74	0.61	0.13
2003.12.27	16:00:59	Loyalty Islands	7.3Mw	21.70	-	-	2.72	-	0.56
2004.02.11	00:31:39	NZ	4.5 ML	2.45	-	-	4.21	-	-
2004.02.11	21:40:33	NZ	4.5 ML	2.06	-	-	11.47	-	-
2004.05.03	04:36:50	Chile	6.6Mw	79.16	-	-	1.95	-	3.59
2004.06.23	04:28:30	NZ	5.1ML	1.19	28.8	-	22.1	0.37	-
2004.08.19	16:03:39	NZ	4.8ML	1.29	2.08	-	19.96	0.37	-
2004.09.06	12:42:59	Sandwich Islands	6.9Mw	79.74	58.75	-	16.82	0.67	0.009
2004.10.08	08:27:53	Solomon Islands	6.9Mw	33.90	61.92	-	-	0.82	-
2004.11.09	23:58:23	Solomon Islands	6.9 Mw	33.22	-	-	2.89	-	28.91
2004.11.11	21:26:41	Indonesia	7.5Mw	54.51	5.21	-	2.76	0.89	12.08
2004.11.22	20:26:23	NZ	7.1Ms	6.35	-	-	83.11	-	-
2004.12.23	14:59:04	NZ	8.1Mw	9.66	-	-	13.12	-	-

Appendix C.

Earthquake Catalogue 2003

The follwing pages offer figures including all recorded components (rotations and translations) for the relevant earthquakes recorded in 2003 (mentioned in Table B.1) in chronological order.

Additional assistance for the use of the provided figures:

Each file is 1800 s (30 min) long.

The data is unfiltered and presented after conversion and instrument correction (Section 3.2).

The figures show the rotational data of the ring laser traces (red) in rad/s and the three translational components of the seismometer (black) in m/s for each event.

Due to technical problems it was not possible for the ring lasers to operate year round. Thus, depending on the date there are three, two or only one ring laser trace available for each earthquake.
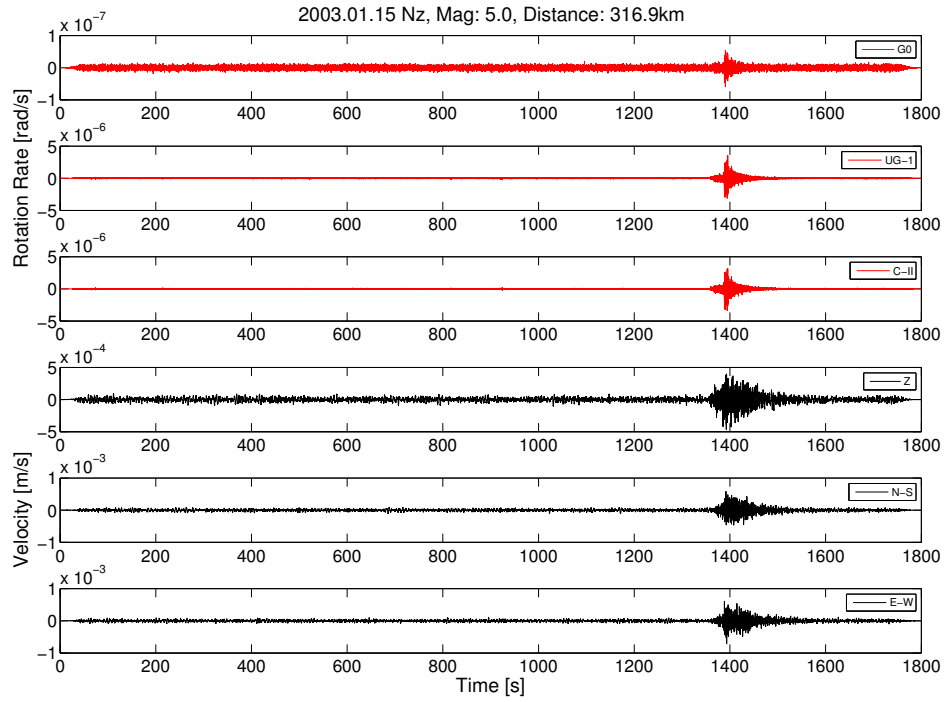
Figure C.1: Unfiltered data of the 2003.01.15 New Zealand event.
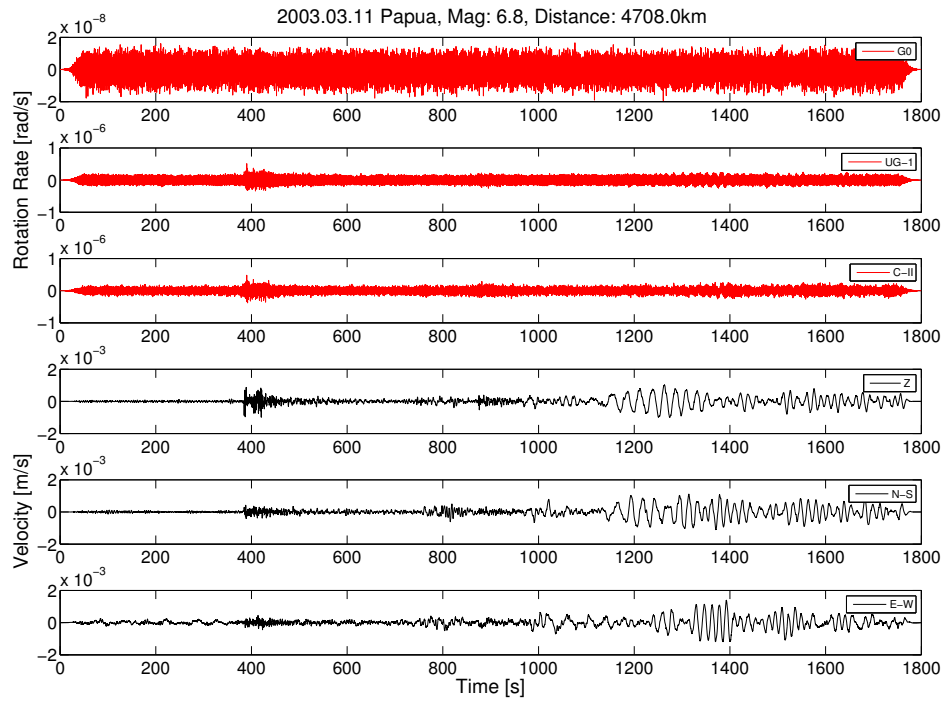
Figure C.2: Unfiltered data of the 2003.03.11 Papua Region event.
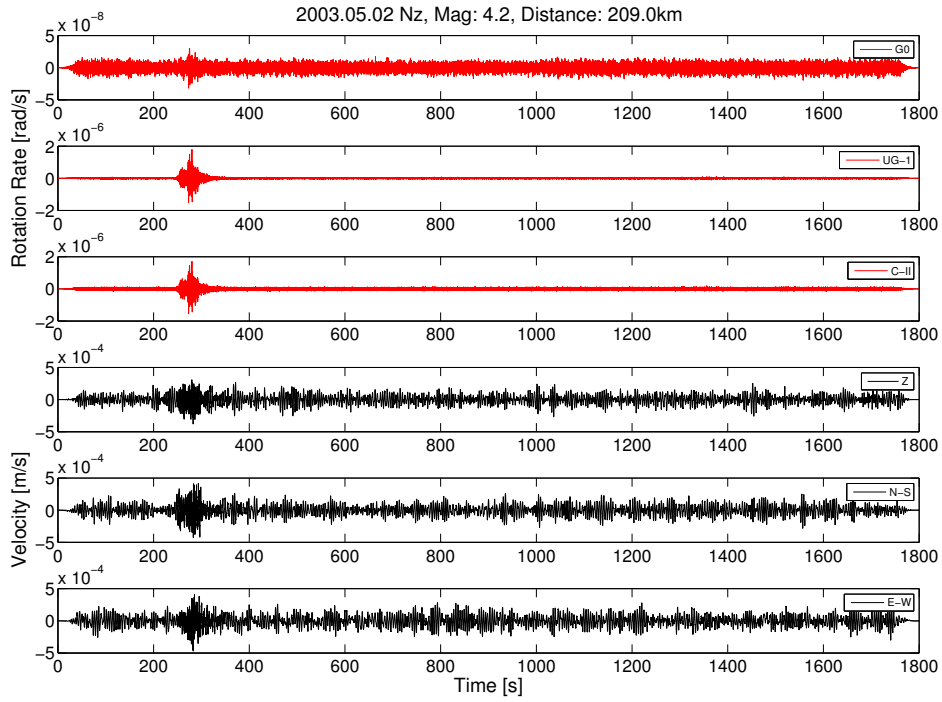
Figure C.3: Unfiltered data of the 2003.05.02 New Zealand event.
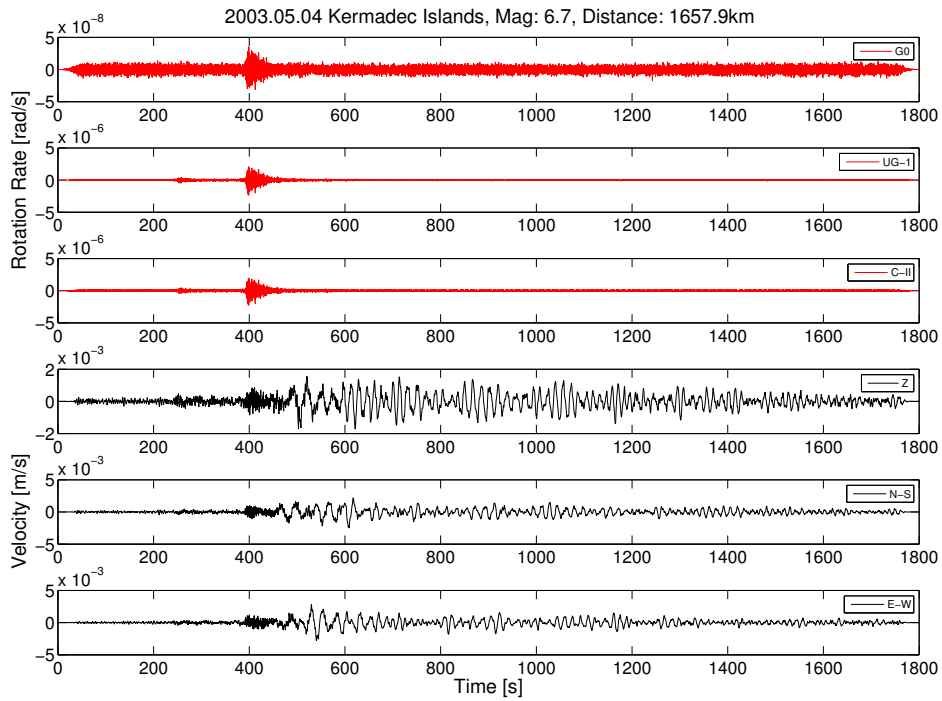
Figure C.4: Unfiltered data of the 2003.05.04 Kermadec Islands event.
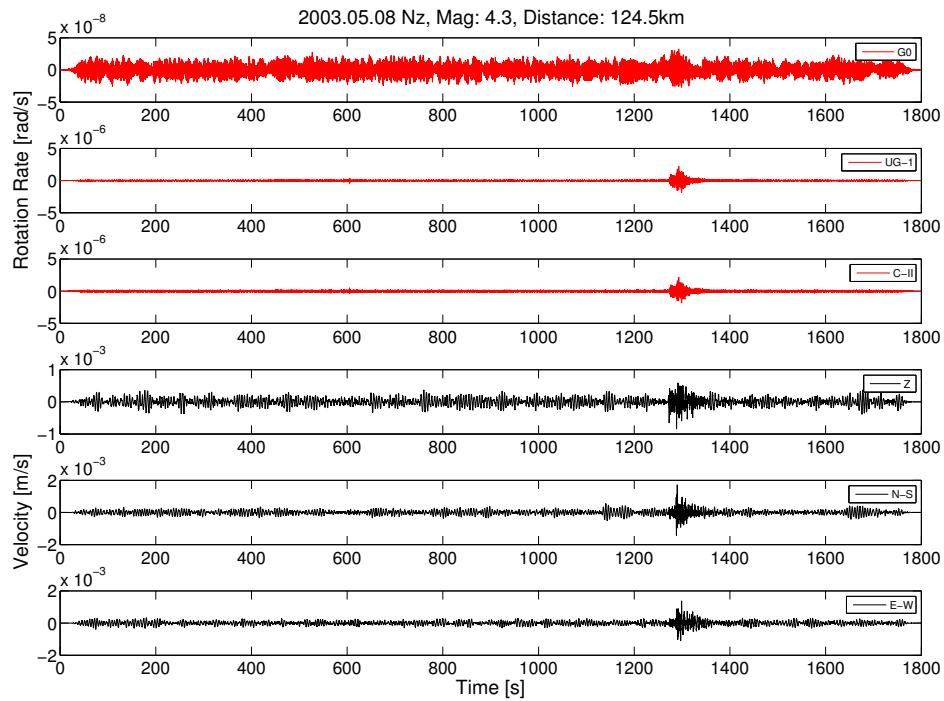
Figure C.5: Unfiltered data of the 2003.05.08 New Zealand event.
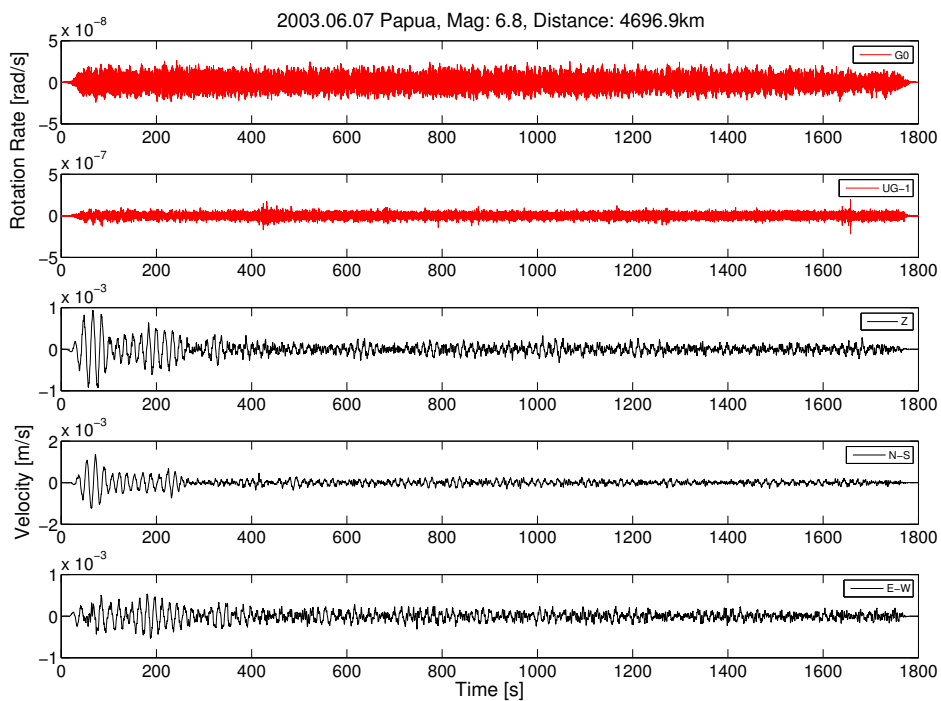
Figure C.6: Unfiltered data of the 2003.06.07 Papua Region event.
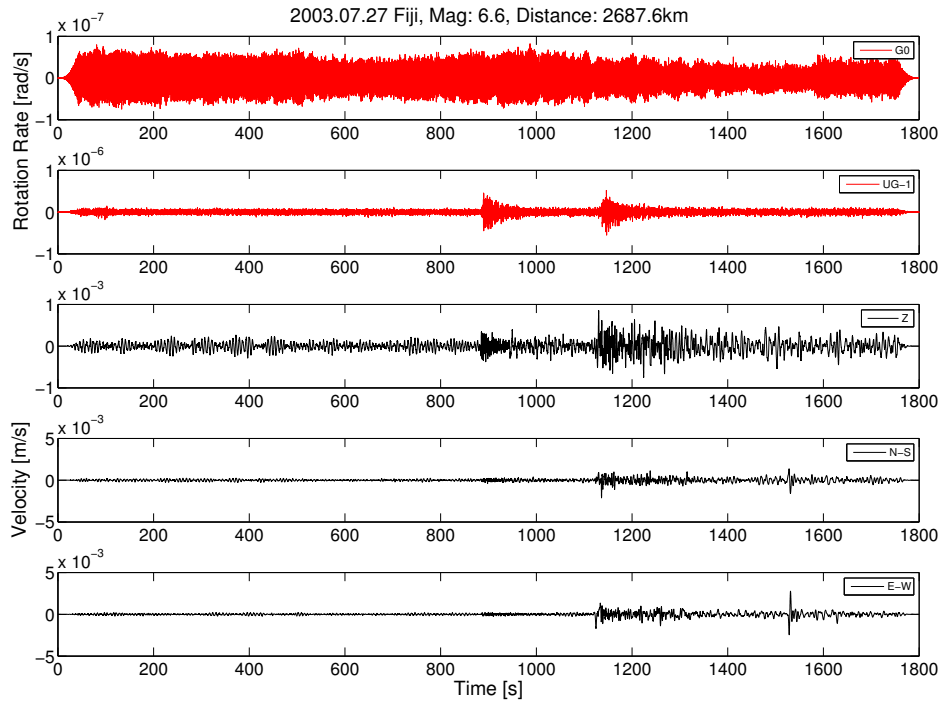
Figure C.7: Unfiltered data of the 2003.07.27 Fiji event.
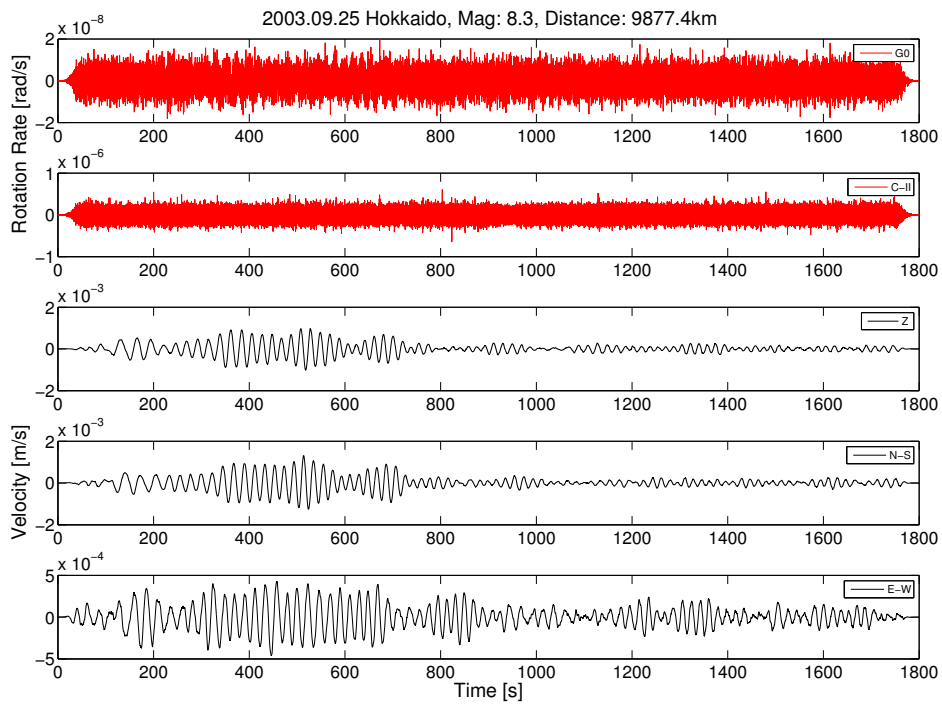
Figure C.8: Unfiltered data of the 2003.09.25 Hokkaido event.
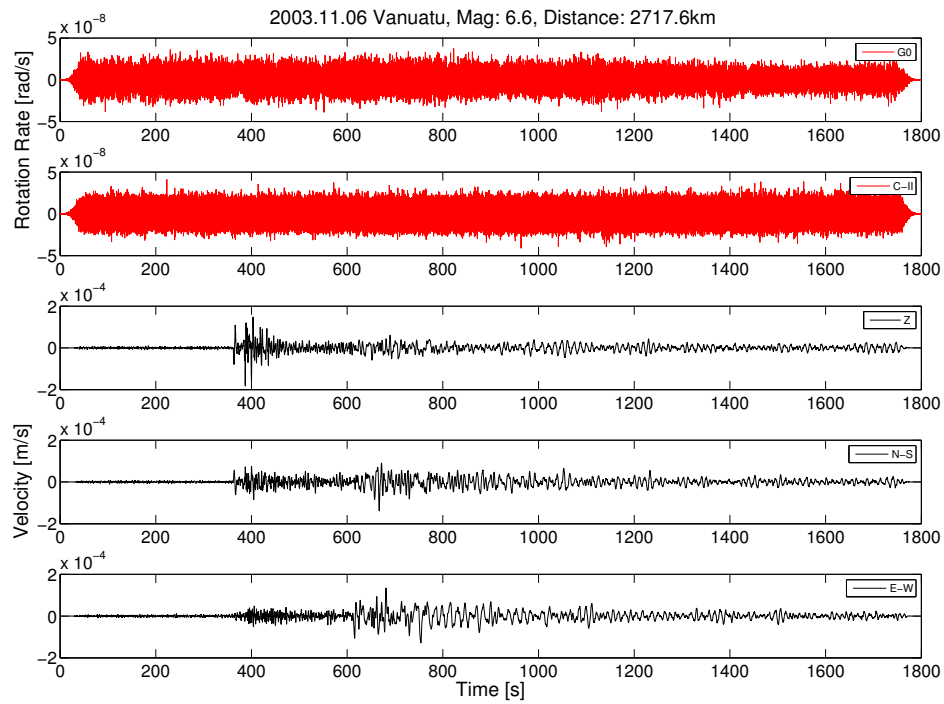
Figure C.9: Unfiltered data of the 2003.11.06 Vanuatu event.
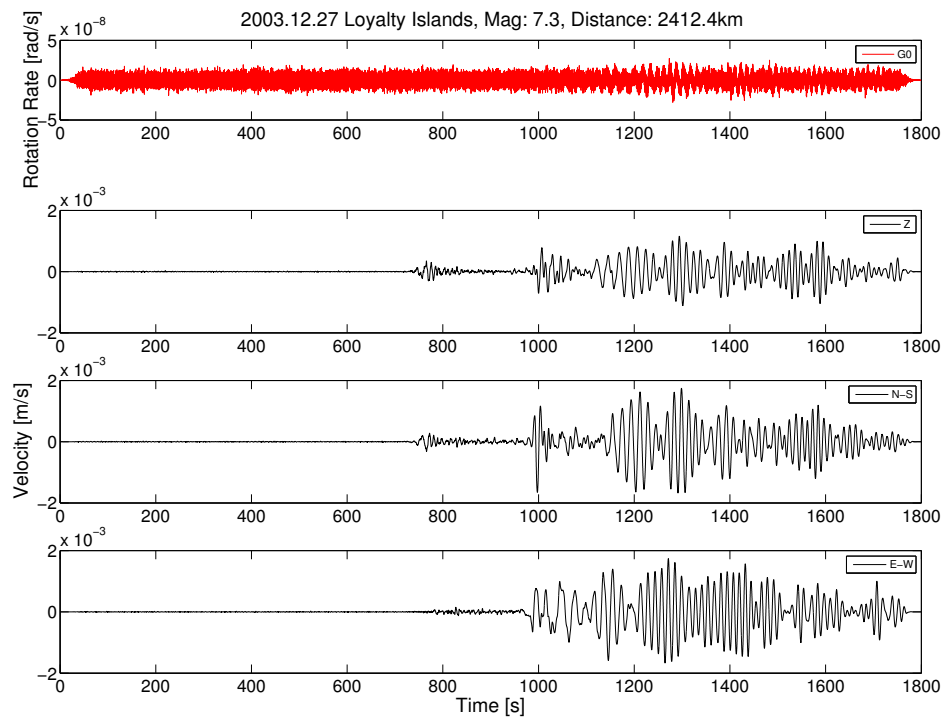
Figure C.10: Unfiltered data of the 2003.12.27 Loyalty Islands event.

Appendix D.

Earthquake Catalogue 2004

The follwing pages offer figures including all recorded components (rotations and translations) for the relevant earthquakes recorded in 2004 (mentioned in Table B.1) in chronological order.

Additional assistance for the use of the provided figures:

Each file is 1800 s (30 min) long.

The data is unfiltered and presented after conversion and instrument correction (Section 3.2).

The figures show the rotational data of the ring laser traces (red) in rad/s and the three translational components of the seismometer (black) in m/s for each event.

Due to technical problems it was not possible for the ring lasers to operate year round. Thus, depending on the date there are three, two or only one ring laser trace available for each earthquake.

The 2004.12.23 Nz (M 8.1) event on page 97 stretches over two consecutive plots.
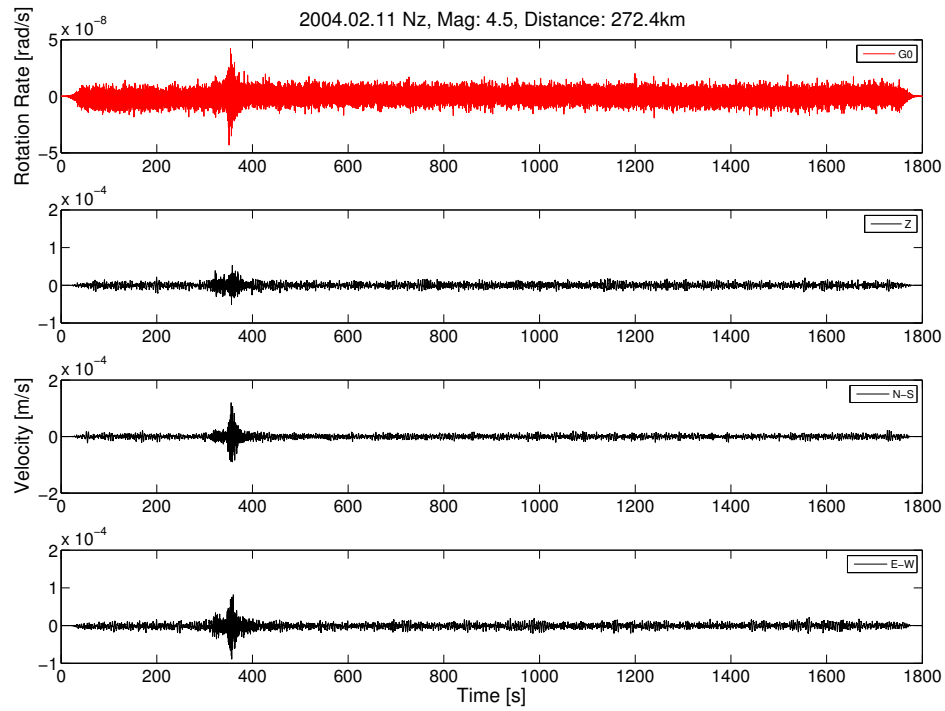
Figure D.1: Unfiltered data of the first 2004.02.11 New Zealand event.
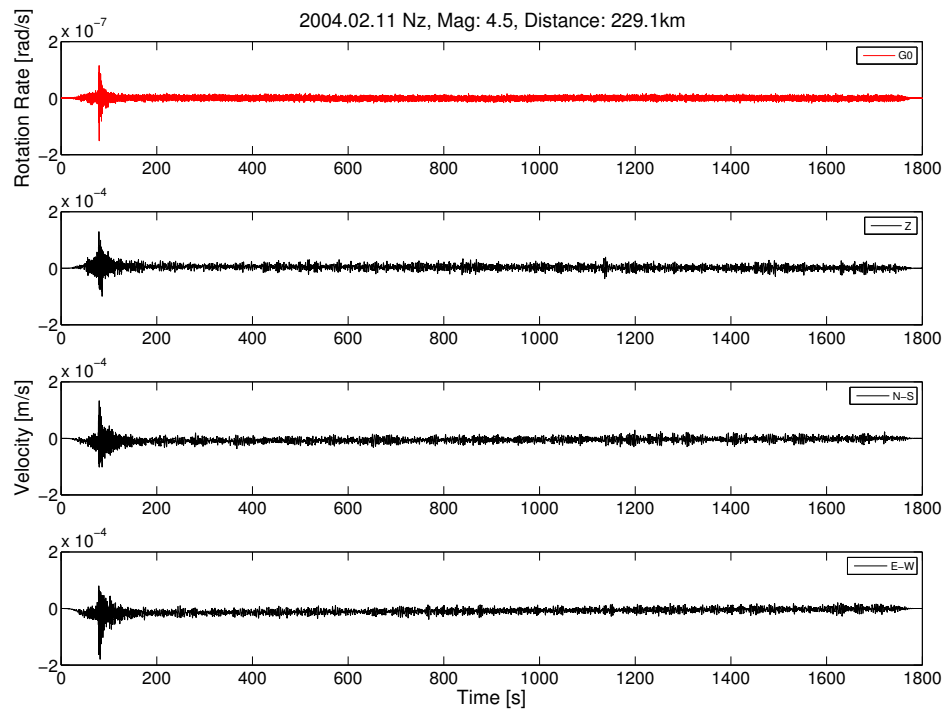
Figure D.2: Unfiltered data of the second 2004.02.11 New Zealand event.
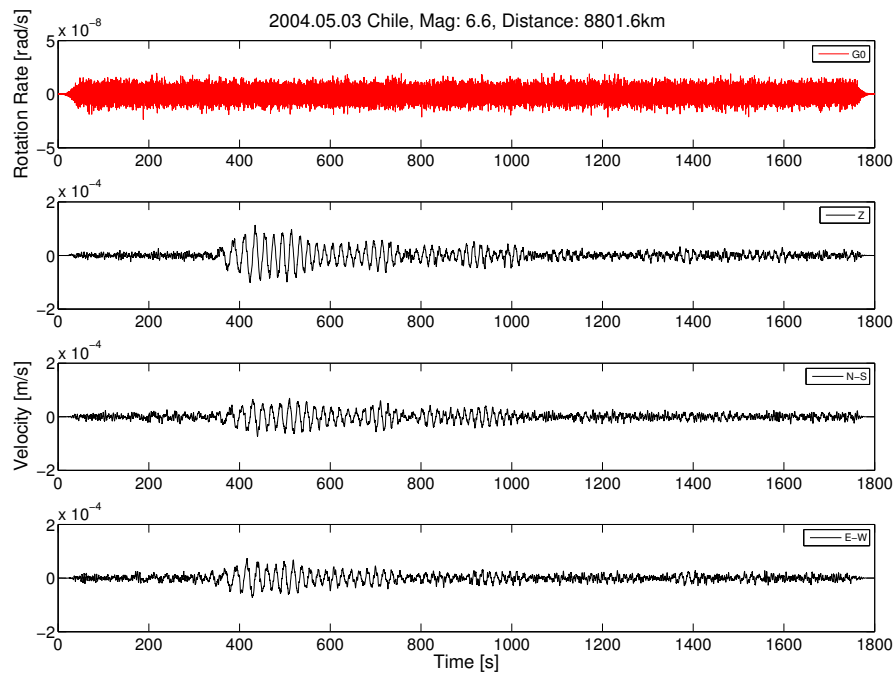
Figure D.3: Unfiltered data of the 2004.05.03 Chile event.
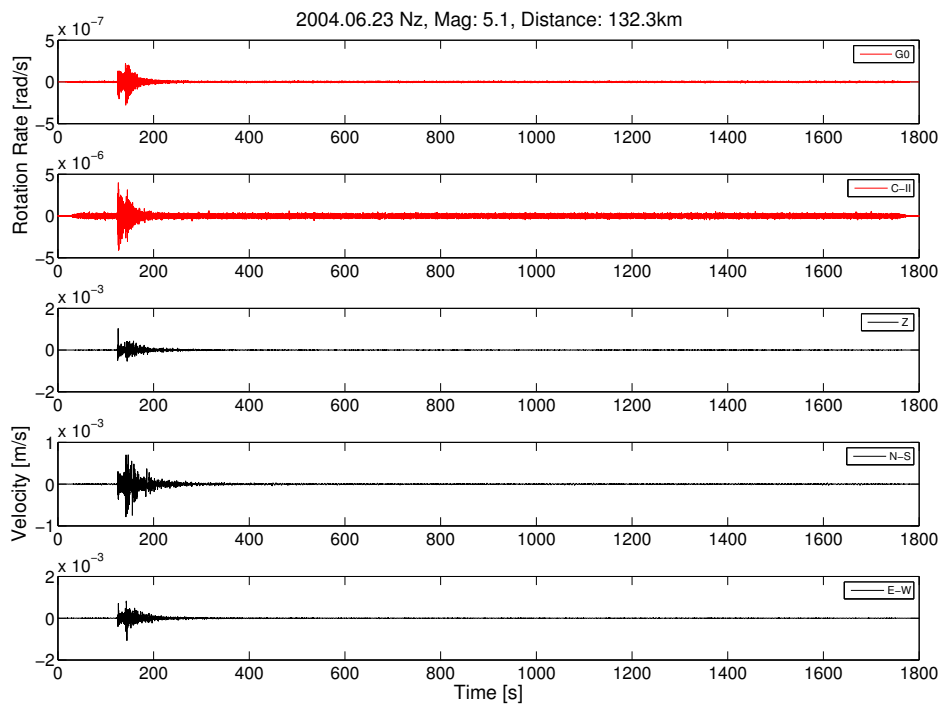
Figure D.4: Unfiltered data of the 2004.06.23 New Zealand event.
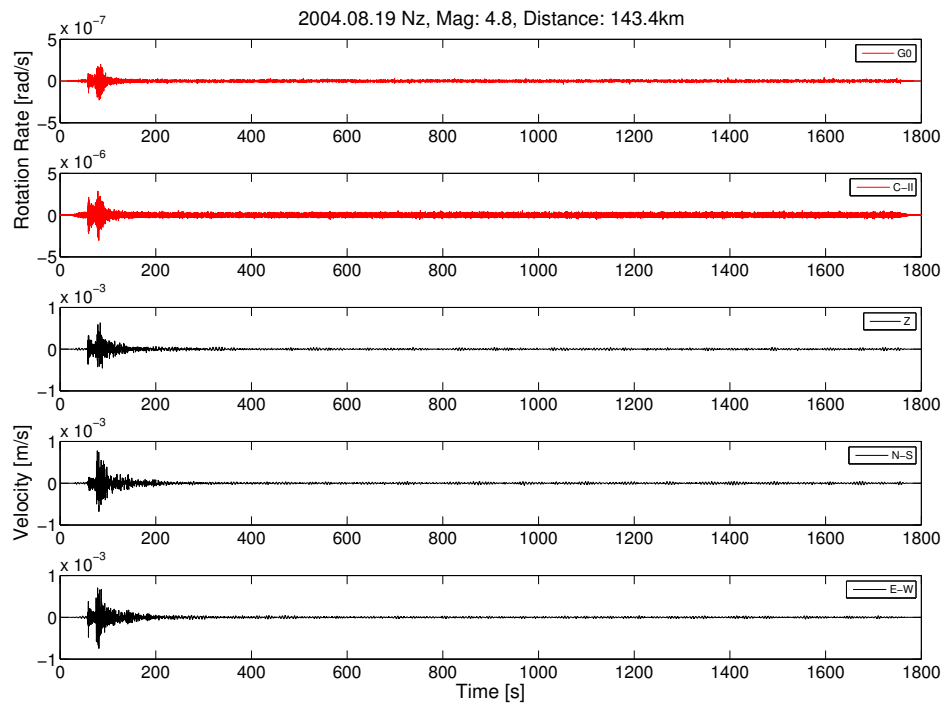
Figure D.5: Unfiltered data of the 2004.08.19 New Zealand event.
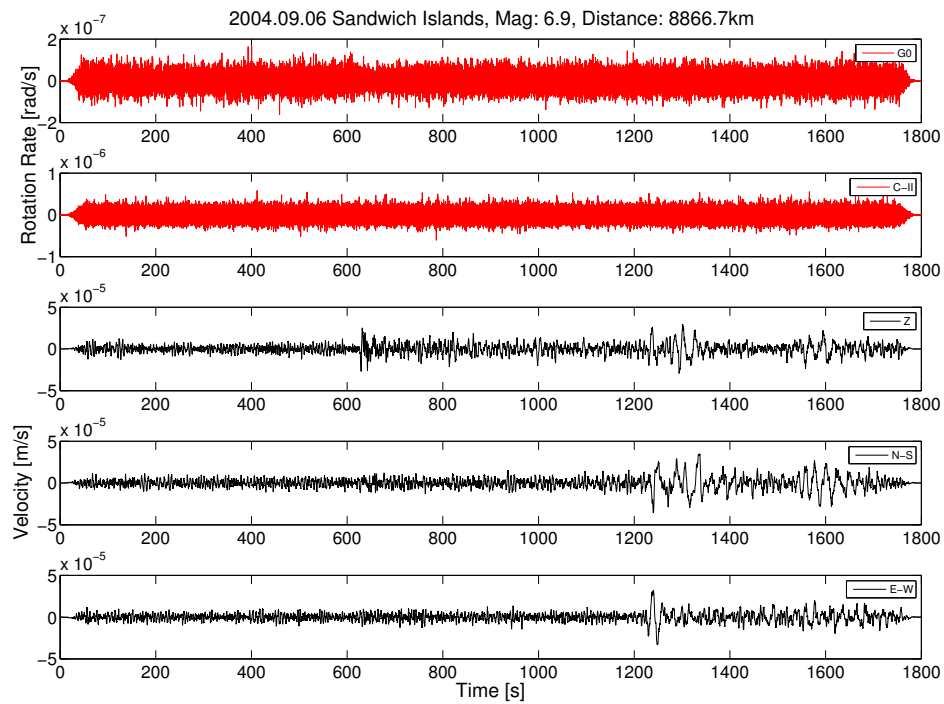
Figure D.6: Unfiltered data of the 2004.09.06 Sandwich Islands event.
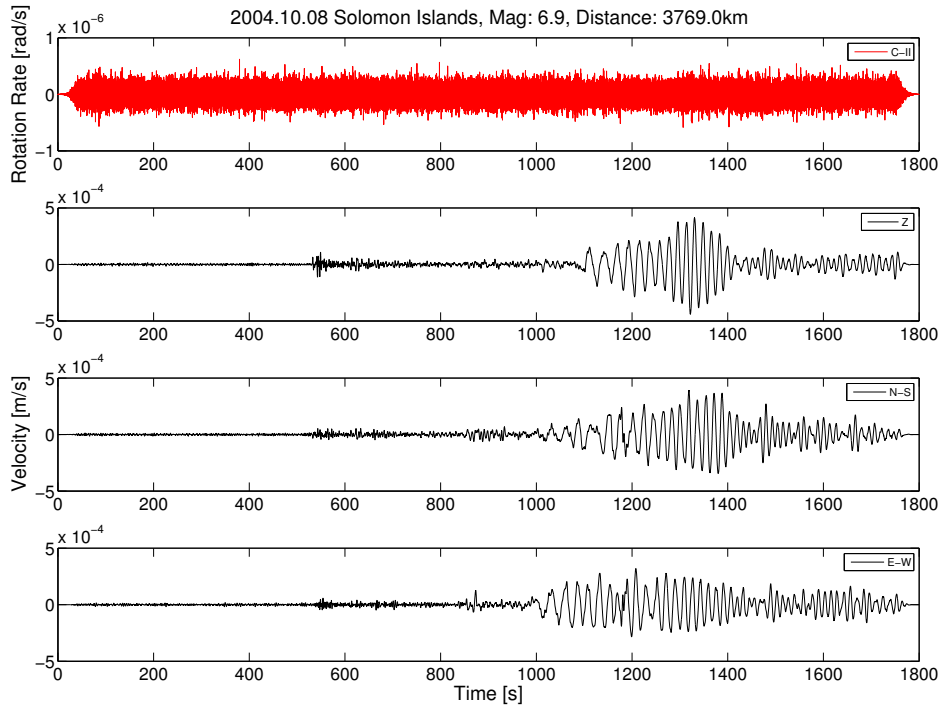
Figure D.7: Unfiltered data of the 2004.10.08 Solomon Islands event.
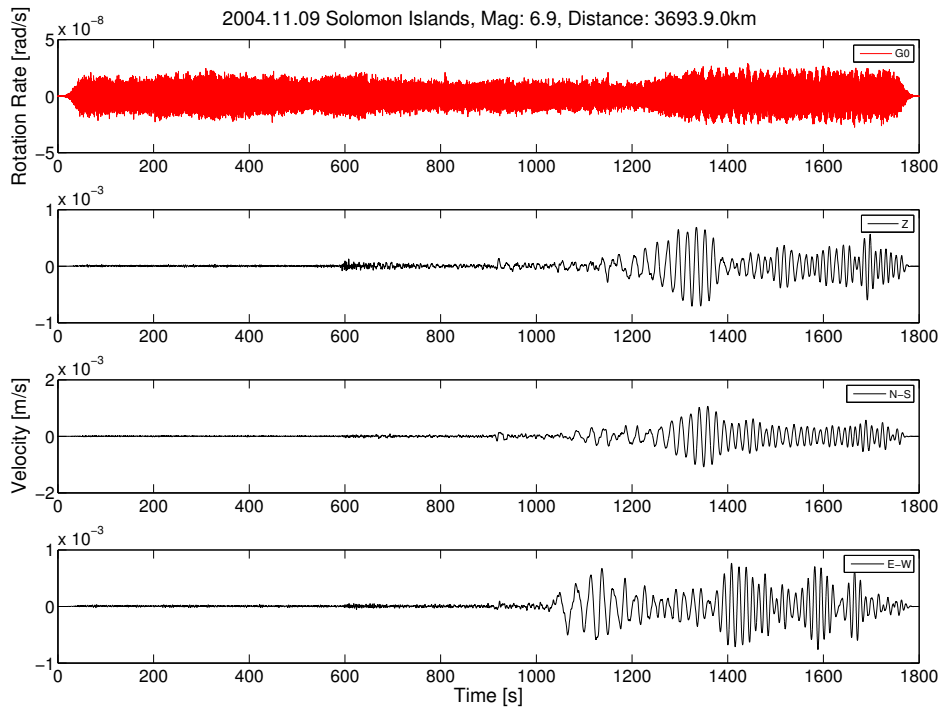
Figure D.8: Unfiltered data of the 2004.11.09 Solomon Islands event.
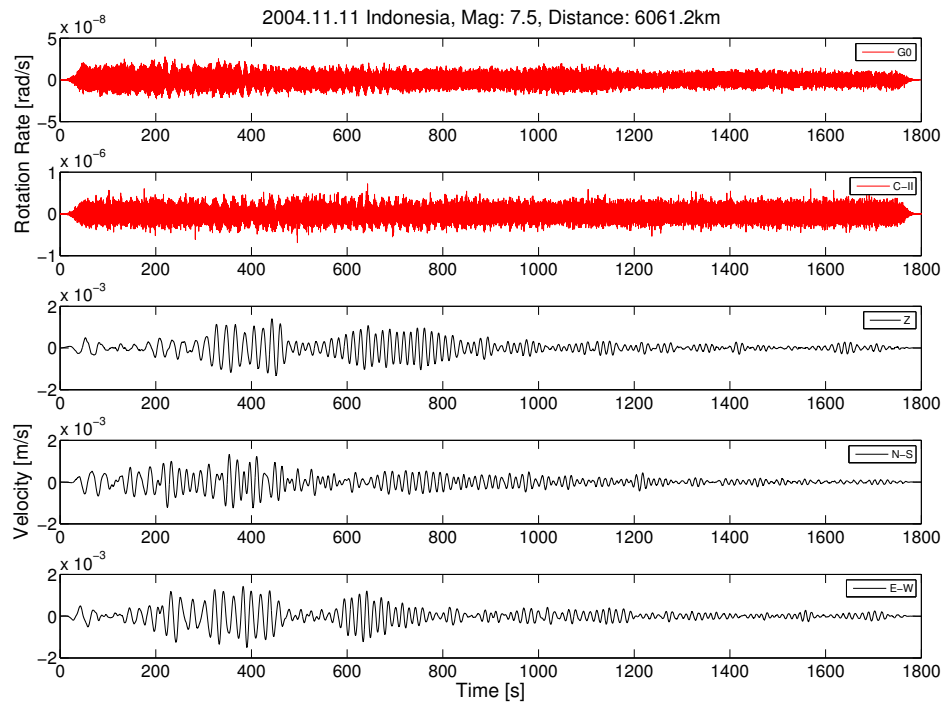
Figure D.9: Unfiltered data of the 2004.11.11 Indonesia event.
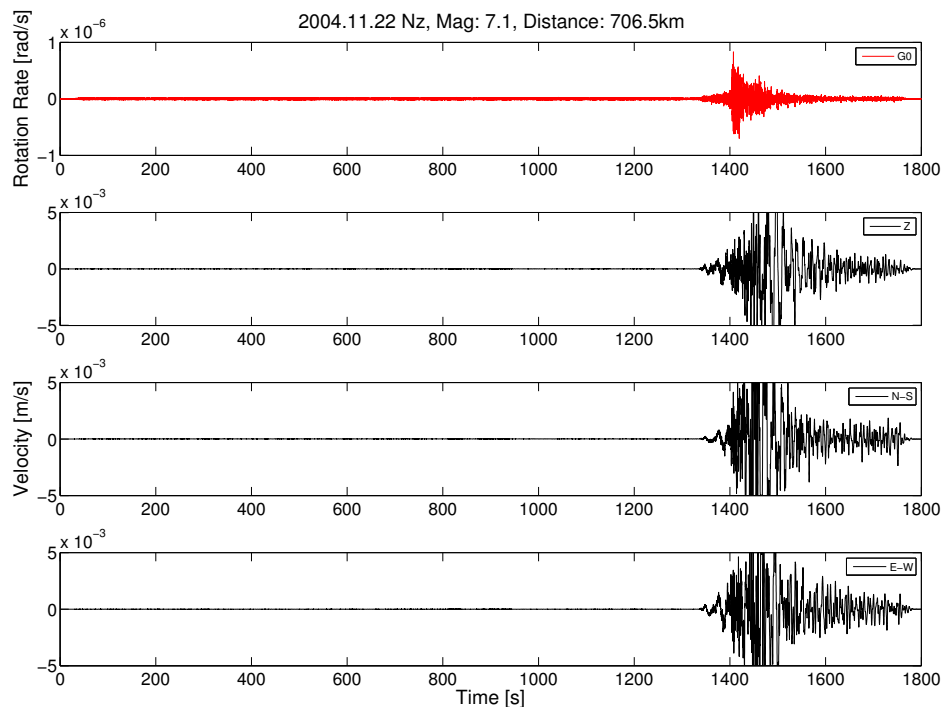
Figure D.10: Unfiltered data of the 2004.11.22 New Zealand event. Note that the seismometer traces are clipped.
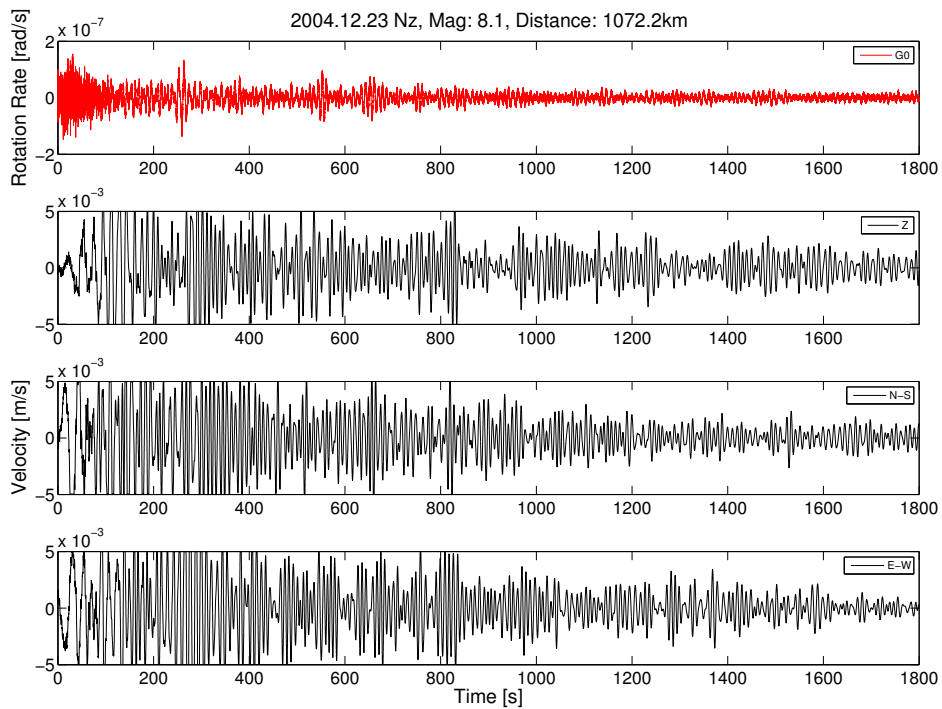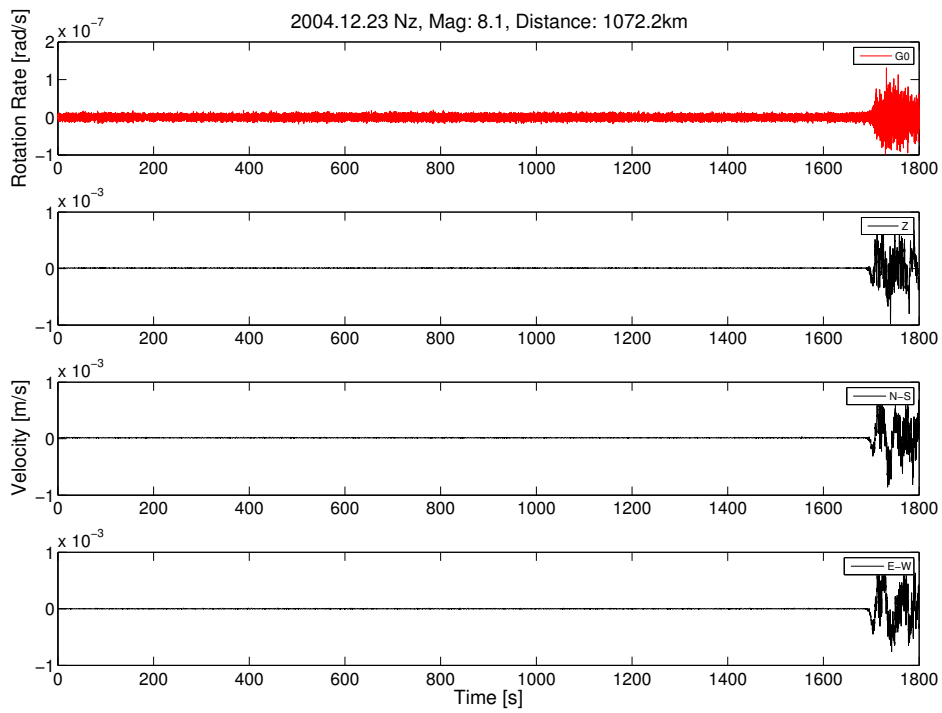
Figure D.11: Unfilterd data of the 2004.12.23 New Zealand event. Note that the seismometer traces are clipped.

Appendix E.

Superposition of rotation rate and transverse acceleration

The follwing pages offer the superposition plots of the transverse acceleration and vertical rotation rate for each relevant earthquake recorded in 2003 and 2004 (mentioned in Table B.1) in chronological order.

Additional assistance for the use of the provided figures:

Transverse acceleration (black) is given in [m/s^2] and vertical rotation rate in [rad/s].

Depending on the ring laser the rotation rate is shown in red ('UG-1') and/or green ('C-II').

Due to technical problems it was not possible for the ring lasers to operate year round. Thus, depending on the date there are two or only one rotation rate trace available for each earthquake.

Plots of the corresponding maximum CC-Coefficients over time are shown directly below the superpositions.

The maximum CC-Coefficient value for each event is given in the caption.

Figure E.1: 2003.01.15 Nz event with maximum CC-Coefficients of 0.2897 and 0.3124.
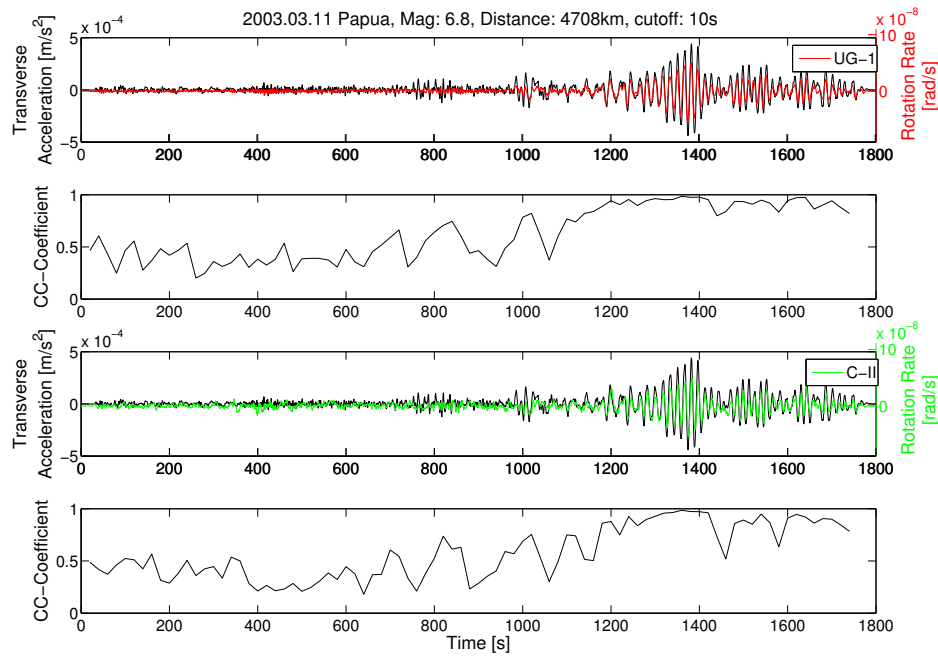
Figure E.2: 2003.03.11 Papua event with maximum CC-Coefficients of 0.9852 and 0.9849.
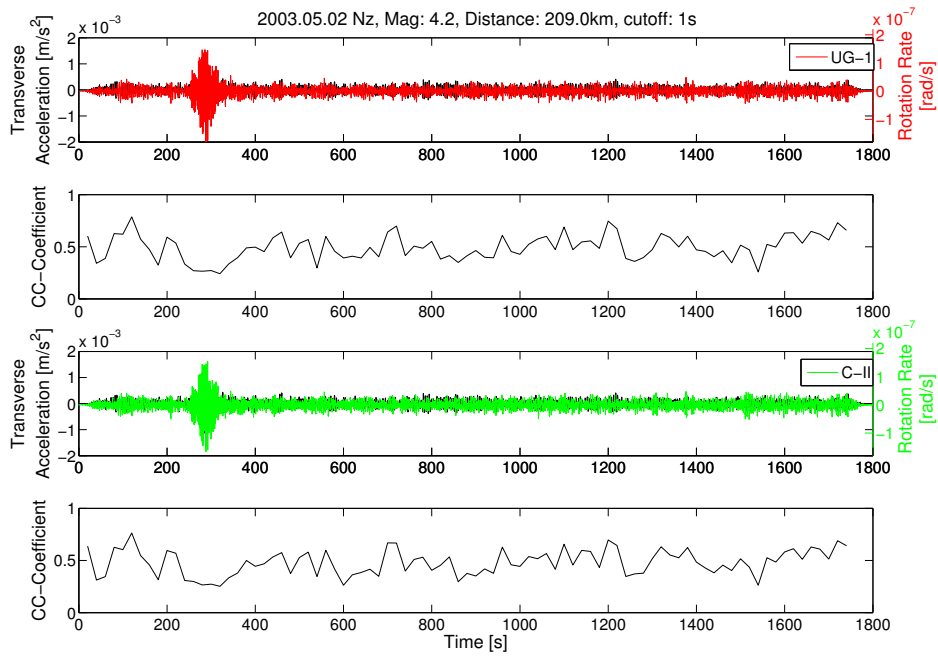
Figure E.3: 2003.05.02 Nz event with maximum CC-Coefficients of 0.5360 and 0.5632.
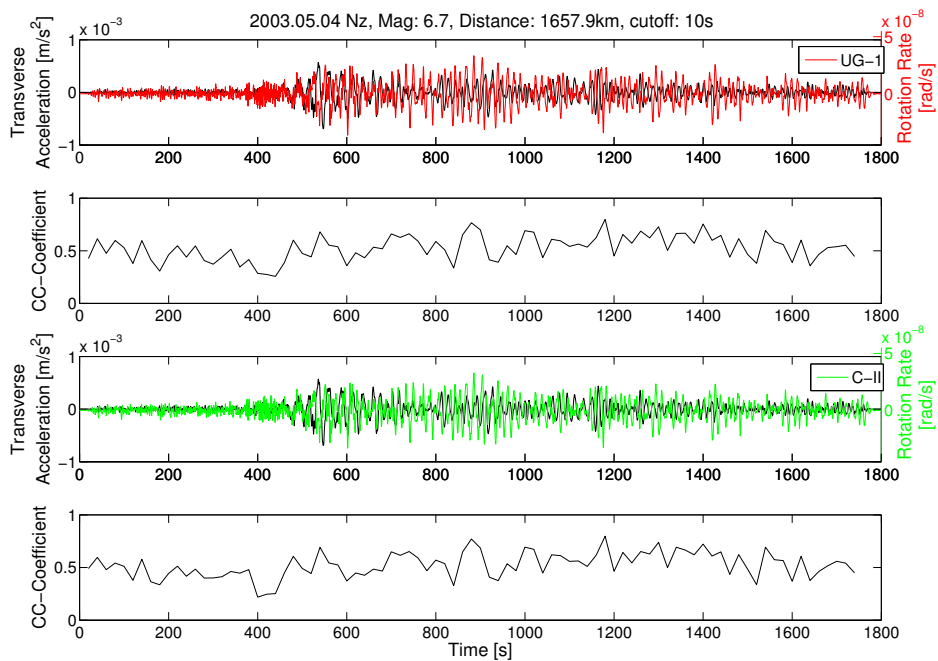
Figure E.4: 2003.05.04 Nz event with maximum CC-Coefficients of 0.4798 and 0.4620.

Figure E.5: 2003.05.08 Nz event with maximum CC-Coefficients of 0.7979 and 0.7971.
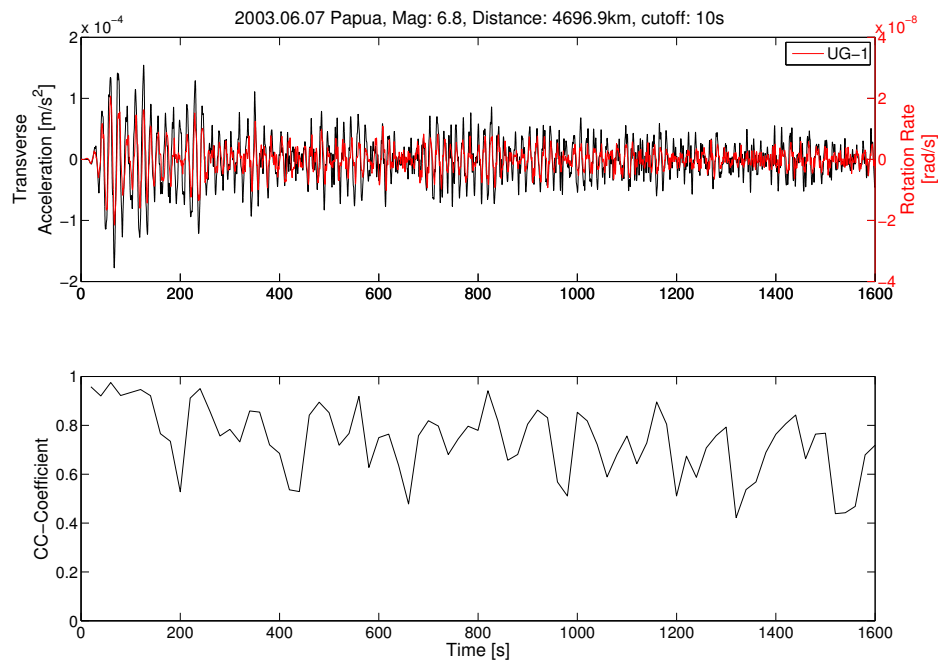
Figure E.6: 2003.06.07 Papua event with a maximum CC-Coefficient of 0.9752.
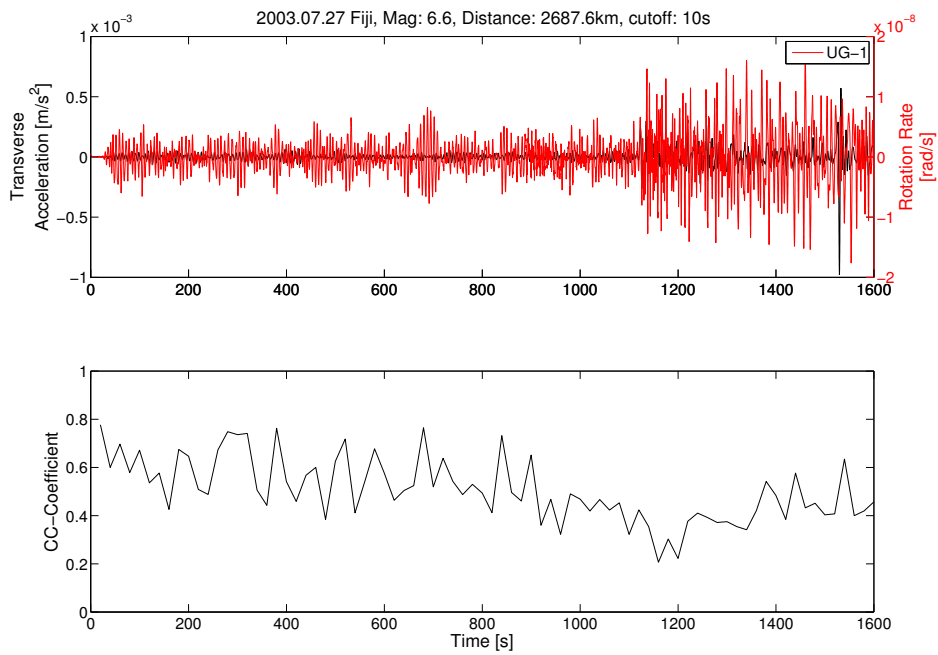
Figure E.7: 2003.07.27 Fiji event with a maximum CC-Coefficient of 0.6403.
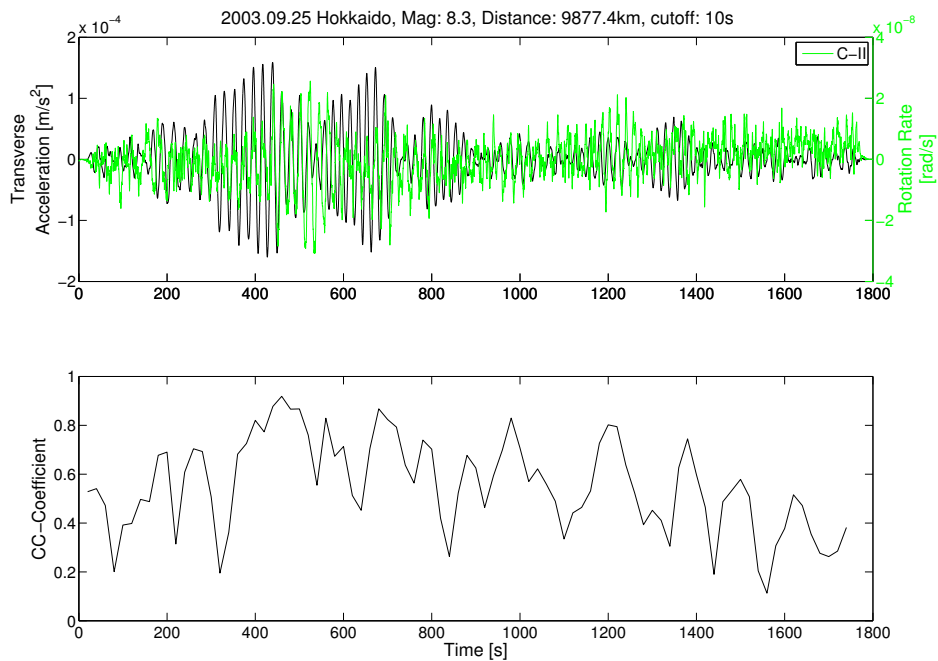
Figure E.8: 2003.09.25 Hokkaido event with a maximum CC-Coefficient of 0.9185.

Figure E.9: 2003.11.06 Vanuatu event with a maximum CC-Coefficient of 0.6117.
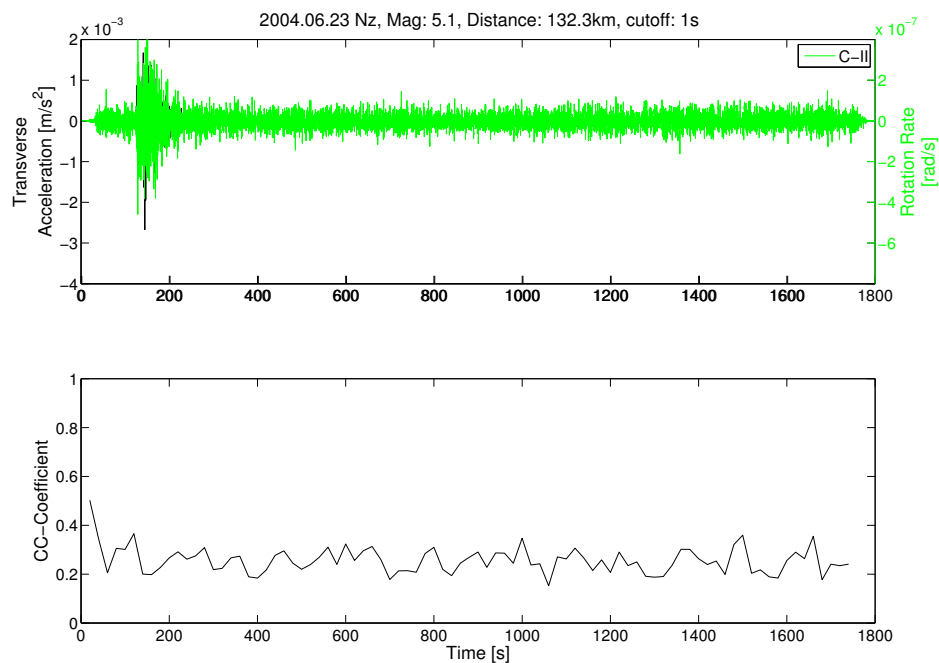
Figure E.10: 2004.06.23 Nz event with a maximum CC-Coefficient of 0.3658.
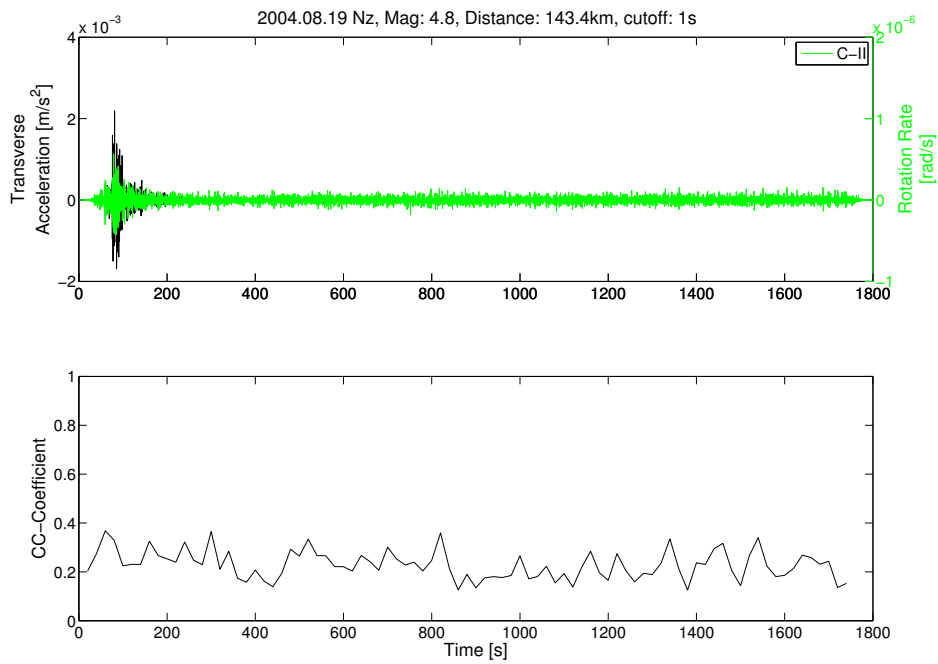
Figure E.11: 2004.08.19 Nz event with a maximum CC-Coefficient of 0.3680.
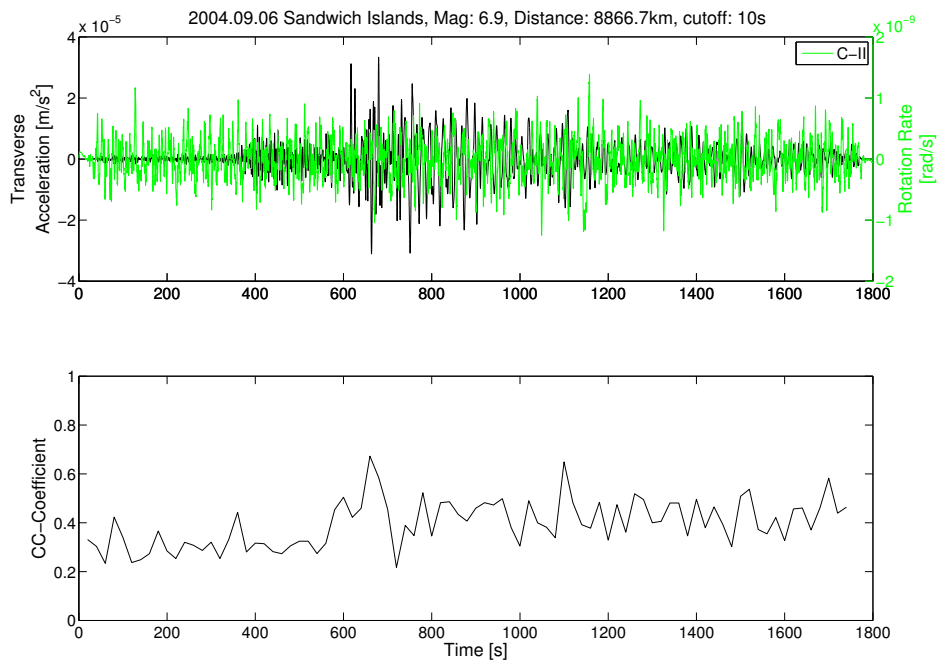
Figure E.12: 2004.09.06 Sandwich Islands event with a maximum CC-Coefficient of 0.6724.
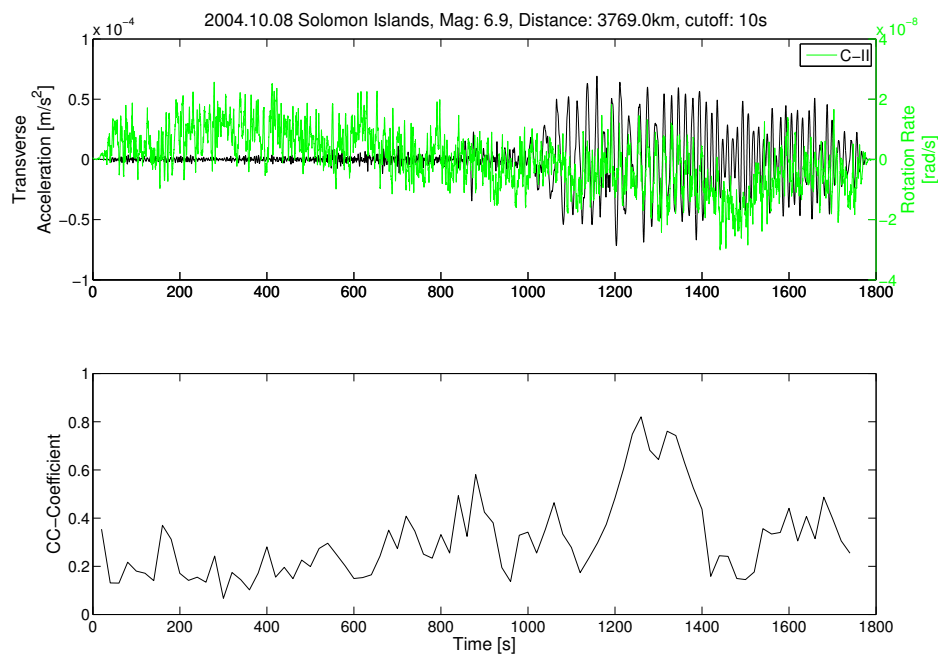
Figure E.13: 2004.10.08 Solomon Islands event with a maximum CC-Coefficient of 0.8204
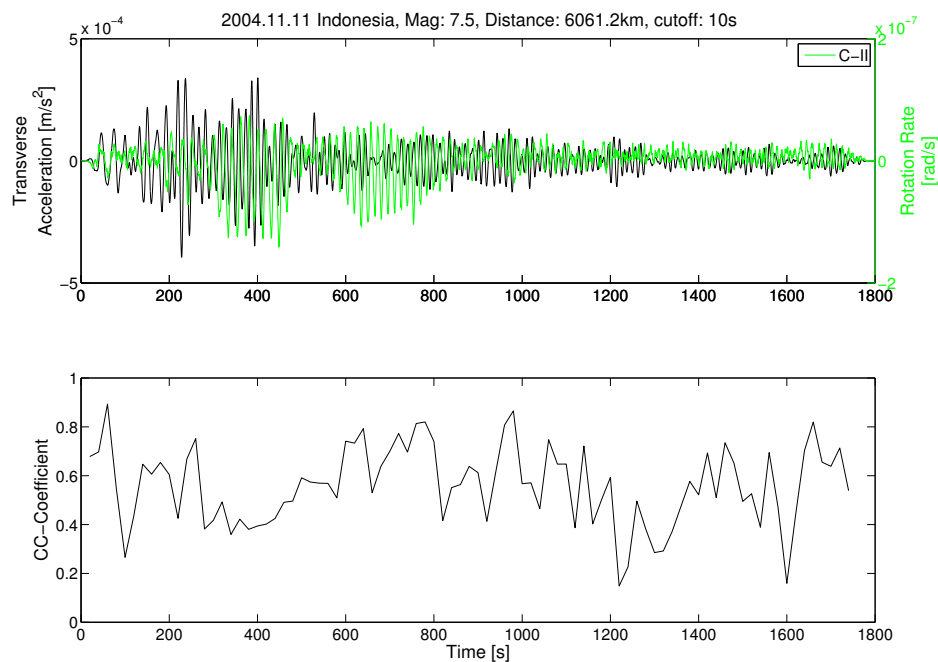
Figure E.14: 2004.11.11 Indonesia event with a maximum CC-Coefficient of 0.8934

Appendix F.

Superposition of Li tilt rate and horizontal rotation rate

The follwing pages offer the superposition plots of Li tilt rate and horizontal rotation rate observed by 'G0' in 2003 and 2004.

Additional assistance for the use of the provided figures:

Top: superposition of unfiltered Li tilt rate and unfiltered rotation rate in rad/s.

Middle: superposition of lowpass filtered data (cutoff period is 10 s).

Bottom: superposition of filtered data. The observed rotation rate was muliplied with a correction factor to fit the predictions.

The Li tilt in this case is only applicable in the Rayleigh wave section. Therefore, the the Rayleigh wave onset time is given for each event in the caption.

Figure F.1: 2003.03.11 Papua event with a Rayleigh wave onset at about 1159 s.
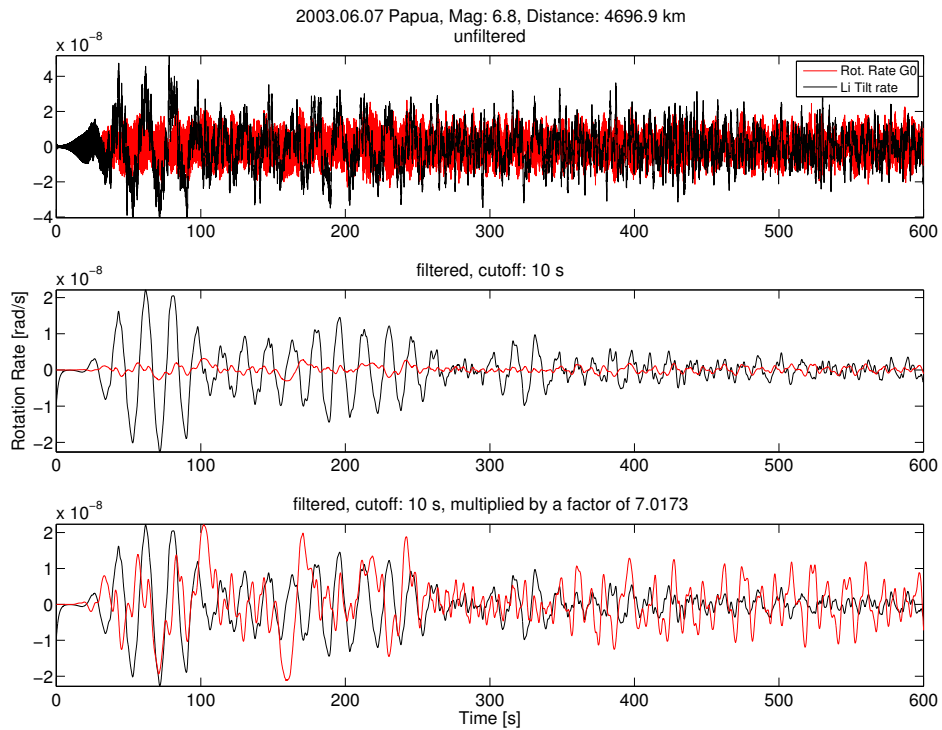
Figure F.2: 2003.06.07 Papua event with a Rayleigh wave onset before file start .
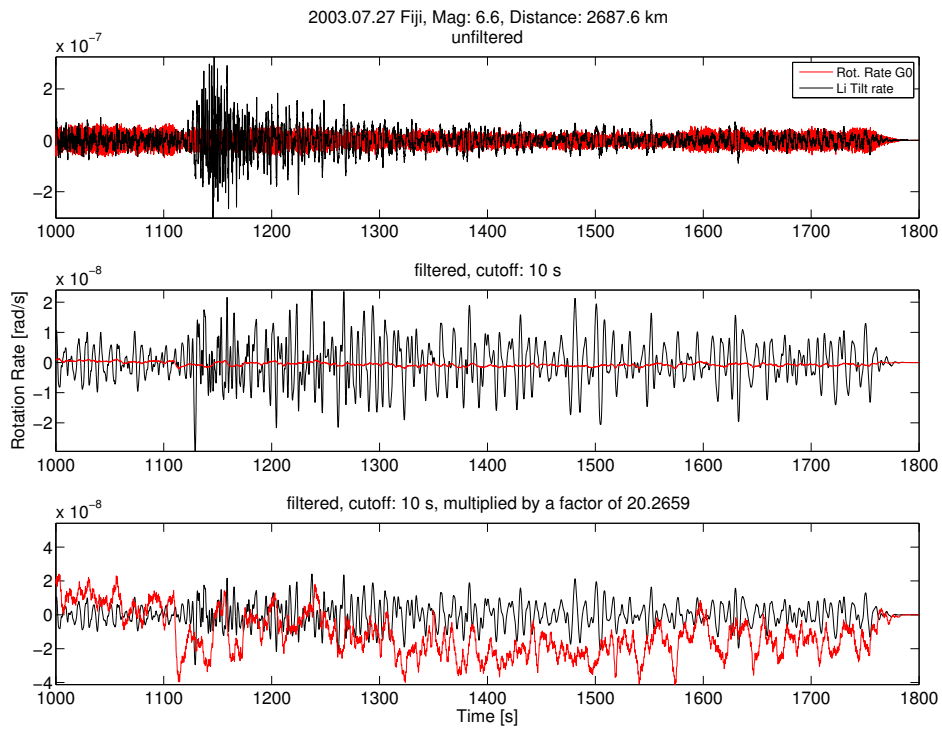
Figure F.3: 2003.07.27 Fiji event with a Rayleigh wave onset at about 1268 s.
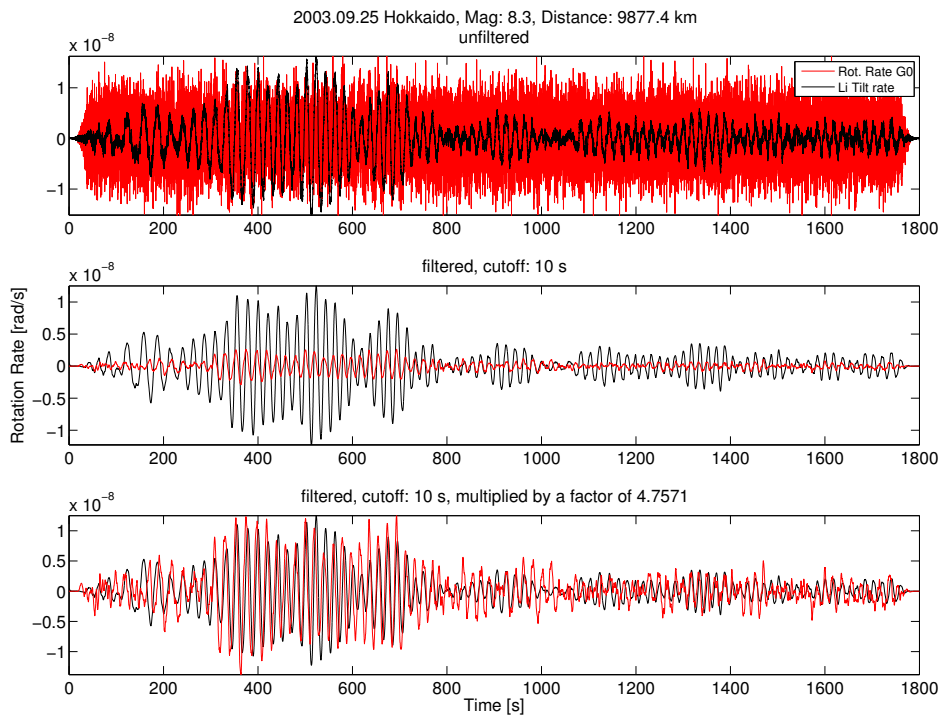
Figure F.4: 2003.09.25 Hokkaido event with a Rayleigh wave onset at about 116 s.

Figure F.5: 2003.11.06 Vanuatu event with a Rayleigh wave onset at about 747 s.
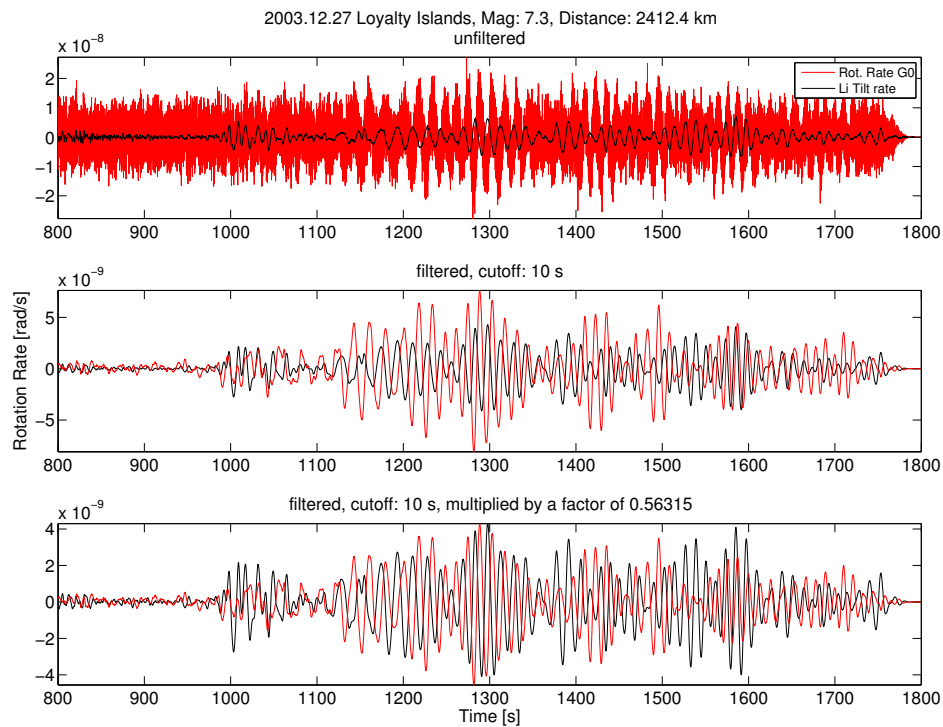
Figure F.6: 2003.12.27 Loyalty Island event with a Rayleigh wave onset at 1047 s.
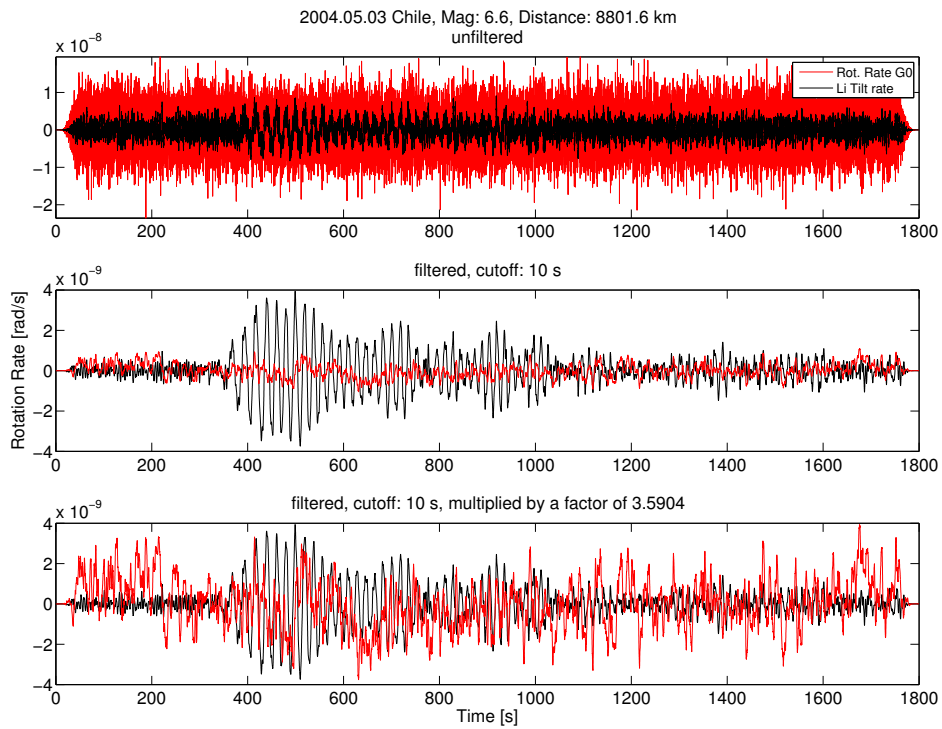
Figure F.7: 2004.05.03 Chile event with a Rayleigh wave onset at about 402 s.
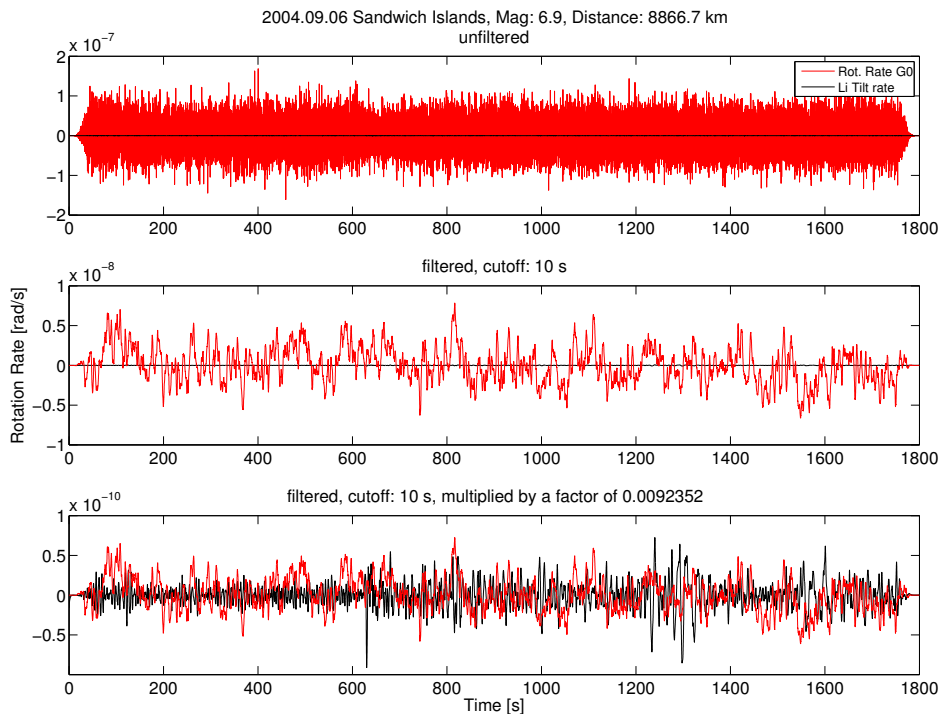
Figure F.8: 2004.09.06 Sandwich Island event with a Rayleigh wave onset 6 min later.

Figure F.9: 2004.11.09 Solomon Island event with a Rayleigh wave onset at 1231 s.
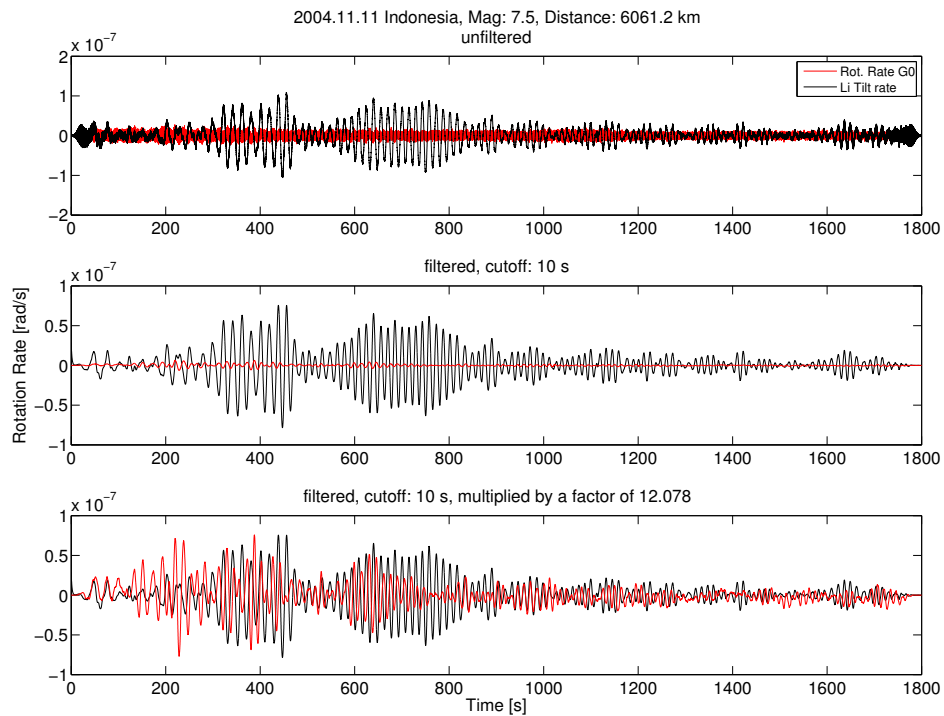
Figure F.10: 2004.11.11 Indonesia event with a Rayleigh wave onset at about 22 s.

Bibliography

Aki, K., Richards, P., 2002. Quantitative Seismology. University Science Books.

Bouchon, M. B., Aki, K., 1982. Strain, tilt, and rotation associated with strong ground motion in the vicinity of earthquake faults. BSSA 72, 1717–1738.

Cochard, A., Igel, H., Schuberth, B., Suryanto, W., Velikoseltsev, A., Schreiber, U., Wassermann, J., Scherbaum, F., Vollmer, D., 2006. Rotational motions in seismology: theory, observations, simulation. In: et al., T. (Ed.), Earthquake source asymmetry, structural media and rotation effects. Springer Verlag.

FESG, 2007. Forschungseinrichtung für Satellitengeodäsie, TU Munich, Fundamentalstation Wettzell hompage entered on 19.11.2007, http://www.wettzell.ifag.de/.

Flaws, A., 2003. Ring laser technology for seismic applications. Master's thesis, Department of Physics and Astronomy, University of Canterbury, Christchurch, New Zealand.

GNS, 2007. Institute of Geological and Nuclear Sciences homepage entered on 15.11.2007, http://www.gns.cri.nz/research/tectonics/map1.html.

GNS, Institute of Geological and Nuclear Sciences. hompage entered on 15.11.2007, http://www.gns.cri.nz/what/earthact/earthquakes/index.html.

Graizer, V. M., 2006. Tilts in Strong Ground Motion. BSSA 96, 2090–2102.

Güralp, Systems Limeted. hompage entered on 01.03.2008, http://www.guralp.com/.

Hart, G., DiJulio, R., Lew, M., 1975. Torsional response of high-rise buildings. ASCE, Journal of the Structural Division 101, 397–415.

Höling, B., 1990. Ein Lasergyroskop zur Messung der Erdrotation. Ph.D. thesis, MPI für Quantenoptik, Munich.

Huang, B., 2003. Ground rotational motions of the 1999 Chi-Chi, Taiwan earthquake as inferred from dense array observations. Geophysical Research Letters 30, 1307–1310.

Igel, H., Cochard, A., Wassermann, J., Flaws, A., Schreiber, U., Velikoseltsev, A., Dinh, N., 2007. Broad-band observations of earthquake-induced rotational ground motions. Geophysical Journal International 168 (1), 182–197.

Igel, H., Schreiber, U., Flaws, A., Schuberth, B., Velikoseltsev, A., Cochard, A., 2005. Rotational motions induced by the M8.1 Tokachi-oki earthquake, September 25, 2003. Geophys. Res. Lett. 32, L08309.

Jaroszewicz, L. R., Krajewski, Z., Solarz, L., Teisseyer, R., May 2006. Application of the fibre-optic Sagnac interferometer in the investigation of seismic rotational waves. Measurement Science and Technology 17, 1186–1193.

Kennett, B., Engdahl, E., Buland, R., 1995. Constraints on seismic velocities in the Earth from travel times. Geophysical Journal International 122, 108–124.

Li, H., Sun, L., Wang, S., 2001. Improved approach for obtaining rotational components of seismic motion .

Li, H., Sun, L., Wang, S., 2002. Frequency dispersion characteristics of phase velocities in surface wave for rotational components of seismic motion. Journal of Sound and Vibration 258(5), 815–827.

NEIC, 2007. National Earthquake Information Center of the United States Geological Survey hompage entered between 05. and 10.2007: http://earthquake.usgs.gov/regional/neic/.

Nigbor, R., 1994. Six degree- of - freedom ground - motion measurements. BSSA 84, 1665–1669.

Pancha, A., Webb, T., Stedman, G., McLeod, D., Schreiber, K., 2000. Ring laser detection of rotations from teleseimic waves. Geophysical Research Letters 27, 3553–3556.

Pham, D., Igel, H., Cochard, A., Schreiber, U., Velikoseltsev, A., unpublished. Tilt coupling on ring laser rotational signals, unpublished.

Refraction, Technology Inc. hompage entered on 01.03.2008, http://www.reftek.com/.

Scherbaum, F., 1996. Of Poles and Zeros - Fundamentals of Digital Seismology. Kluwer Academic Publishers.

Schott, AG. hompage entered on 01.03.2008, http://www.schott.com/optics_devices/english/products/zerodur/index.html.

Schreiber, K. U., Velikoseltsev, A., Rothacher, M., Klügel, T., Stedman, G., L., W. D., 2004. Direct measurement of diurnal polar motion by ring laser gyroscopes. J. Geophys. Res. 109, B06405.

Schreiber, U., 2000. Ringlasertechnologie für geowissenschaftliche Anwendungen. Verlag des Budesamtes für Kartographie und Geodäsie.

Schreiber, U., Klügel, T., Stedman, G., 2003. Earth tide and tilt detection by a ring laser gyroscope. Journal of Geophysical Research 108, 2132.

Schreiber, U., Stedman, G., Igel, H., Flaws, A., 2006. Ring Laser Gyroscopes as Rotation Sensors for Seismic Wave Studies. In: R., T., M., T., E., M. (Eds.), Earthquake source asymmetry, structural media and rotation effects. Springer Verlag.

Shearer, P., 1999. Introduction to Seismology. Cambridge University Press.

Solarz, L., Krajewski, Z., Jaroszewicz, L., 2004. Analysis of seismic rotations detected by two antiparallel seismometers: spline function approximation of rotation and displacement velocities. Acta Geophys. Pol 52, 197–217.

Spudich, P., Steck, L., Hellweg, M., Fletcher, J., Baker, L., 1995. Transient stresses at Parkfield, California, produced by the M7.4 Landers earthquake of June 28, 1992: Observations from UPSAR dense seismograph array. J. Geophys. Res. 100, 675–690.

Stedman, G., 2001. Ring laser tests of fundamental physics and geophysics. Rev. Progr. Phys. 60, 615–688.

Stedman, G., Li, Z., Rowe, C., McGregor, A., Bilger, H., 1995. Harmonic analysis in a large ring laser with backscatter-induced pulling. Physical Review A 51, 4944–4958.

Suryanto, W., Wassermann, J., Igel, H., Cochard, A., Vollmer, D., Scherbaum, F., Velikoseltsev, A., Schreiber, U., dec 2006. First comparison of seismic array derived rotations with direct ring laser measurements of rotational ground motion. Bull. Seism. Soc. Am. 96 (6), 2059–2071.

Takeo, M., 1998. Ground rotational motions recorded in near-source region of earthquakes. Geophysical Research Letters 25, 789–792.

Teisseyre, R., Suchcicki, J., K.P., T., Wiszniowski, J., Palagio, P., 2003. Seismic rotation waves: basic elements of theory and recording. Annals. of Geophys. 46, 671–685.

UC, 2007. University of Canterbury, Christchurch, New Zealand hompage entered on 19.11.2007, http://www.phys.canterbury.ac.nz/research/laser/ring_c2.shtml.

USGS, 2007. United States Geological Survey hompage entered on 20.11.2007, http://earthquake.usgs.gov/regional/world/new_zealand/seismicity.php.

Velikoseltsev, A., Schreiber, U., 2005. Observing Earth from Space. The GEOsensor Project. Sensor Documentation.

Acknowledgements

This study was mainly developed with:
LabView 6.1, Matlab 7.4, PITSA 5.0, and kile 1.7.

118

Erklärung/Declaration

Hiermit versichere ich, die vorliegende Arbeit selbständig verfasst und keine anderen als die von mir angegebenen Hilfsmittel verwendet zu haben.

I hereby declare that this thesis has been written by myself and that I have only utilised resources as stated.

. . . .
Susanne Lehndorfer
München, March 2008